DEPARTMENT OF THE INTERIOR

U.S. GEOLOGICAL SURVEY

ANALYSES OF RECORDED RESPONSES OF A UNIQUE BUILDING IN LOS ANGELES TO MOTIONS CAUSED BY WHITTIER NARROWS, CALIFORNIA, EARTHQUAKE OF OCTOBER 1, 1987

by

M. Çelebi[1], E. Şafak[1] and N. Youssef[2]

OPEN-FILE REPORT 89–542

[1]U.S. Geological Survey
345 Middlefield Road
Menlo Park, CA 94025

[2]A.C. Martin and Associates
Los Angeles, CA 90017

December 1989

TABLE OF CONTENTS

1.0 INTRODUCTION

1.1 Background Information

Strong-motion instrumentation of the 1100 Wilshire Finance Building (the Building) in Los Angeles, California, was completed in 1986 as a joint project between the owner and the United States Geological Survey (USGS). The instrumentation scheme, discussed later in this report, was designed and implemented during the construction of the Building. A year later, during the Whittier Narrows earthquake ($M_s = 5.6$), a complete set of acceleration responses at different levels of the building was recorded. This accomplishment is part of the USGS project on strong-motion instrumentation of structures.

1.2 Objective

The purpose of this report is to:

- discuss the general objectives of strong-motion instrumentation of structural systems,
- discuss specifically the instrumentation scheme of the 1100 Wilshire Finance Building in Los Angeles,
- discuss the strong-motion response records obtained from the building during the October 1, 1987 Whittier Narrows earthquake,
- discuss detailed analyses of these records.

1.3 Instrumentation Program of USGS

The main objective of any seismic instrumentation program for structural systems is to improve the understanding of the behavior, and potential for damage, of structures under seismic loading. The acquisition of structural response data during earthquakes is essential to confirm and develop methodologies used for analysis and design of earthquake-resistant structural systems. This objective can best be realized by selectively instrumenting structural systems (buildings, components, lifeline structures, etc.) to acquire data on the response to strong ground motion. As a long-term result one may expect design and construction practices to be modified to minimize future earthquake damage [1].

Various local and national codes in effect in the United States recommend different quantities and schemes of instrumentation. The Uniform Building Code (UBC) [2] recom-

mends for Seismic Zones 3 and 4 a minimum of three accelerographs be placed in every building over six stories in height with an aggregate floor area of 60,000 square feet or more, and in every building over 10 stories in height regardless of floor area. The City of Los Angeles adopted this recommendation in 1966—thus enabling numerous sensors in buildings to record the motions during the 1971 San Fernando Earthquake. Experience from past earthquakes as well as the 1971 San Fernando Earthquake show that the instrumentation guidelines given by the UBC code, although providing sufficient data for the limited analyses projected at the time, do not provide sufficient data to perform the model verifications and structural analyses now demanded by the engineering profession. In 1983, the City of Los Angeles changed the requirement of three accelerographs to only one—to be placed at the top of buildings meeting the above criteria.

On the other hand, valuable lessons have been derived from the study of data obtained from a well instrumented structure, the Imperial County Services Building, during the moderate-magnitude Imperial Valley earthquake ($M_s = 6.5$) of October 15, 1979 [3].

It is expected that a well-instrumented structure for which a complete set of recordings has been obtained, would provide useful information to:

- check the appropriateness of the design dynamic model (both lumped mass and finite element) in the elastic range;
- determine the importance of non-linear behavior on the overall and local response of the structure;
- follow the spreading of the non-linear behavior throughout the structure as the response increases, and investigate the effect of the non-linear behavior on frequency and damping;
- correlate the damage with inelastic behavior;
- determine ground motion parameters that correlate well with building response and damage; and
- make recommendations to improve seismic codes.

To enhance the effort in instrumentation of structures within the United States, the USGS recently established several regional advisory committees comprised of professionals from universities, state, federal, and local government agencies, and private companies. The advisory committees are formed in regions of seismic activity and are requested to develop lists of structures for possible instrumentation. The first of these committees was formed in the San Francisco Bay Region [4]. The second committee was formed in San Bernardino County [5]. Other committees followed.

In the State of California, the most extensive program for the instrumentation of structures is being conducted by the California Division of Mines and Geology (CDMG), and the objective of the USGS program in California is to complement the CDMG program. This is readily accomplished, since the CDMG and the USGS programs for instrumentation of structures within the State of California have distinct objectives. The CDMG program is required by law to instrument typical buildings and structural systems, while the USGS structural instrumentation program concentrates on research studies of non-typical structures of special engineering interest. Typical structures that are not thoroughly instrumented by other programs are also considered. The USGS structural instrumentation program is in addition to the large USGS permanent network of ground stations.

A general description of the targeted regions for structural instrumentation is shown in the map in Figure 1.1. Current status of committees in the targeted regions and reports issued by the committees are summarized in Figure 1.2. The recommendations of the committes are being implemented as funds become available.

1.4 The Case for Los Angeles

The Los Angeles area is a seismically active region requiring earthquake hazard mitigation programs including those related to the investigation of strong shaking of structures.

Earthquake hazards in the Los Angeles region have been recently documented in detail in USGS Professional Paper (No. 1360) edited by Ziony [6]. While the San Andreas fault is considered potentially to be the major active fault with an average slip rate of 20–30 mm/yr, other active faults also affect the seismic hazard in Los Angeles. Of these, the most important are the San Jacinto fault (slip rate of 8–12 mm/yr), the Transverse

Ranges faults extending from Santa Barbara to San Bernardino (6 mm/yr), Palos Verdes faults (1 mm/yr) and the Newport–Inglewood fault (1 mm/yr) [7]. The San Andreas and San Jacinto faults generate earthquakes with magnitudes of 7.5–8.0 and recurrence intervals of approximately two hundred years [8-10].

Los Angeles is therefore threatened by both near earthquakes, as well as the distant effects of earthquakes that occur at distances of 50 miles or more. The 1971 San Fernando Earthquake (approximately 50 miles from downtown Los Angeles) caused considerable damage in the city. During this earthquake, a significant number of records were obtained from buildings instrumented according to the UBC recommendations [2].

As part of its earthquake hazard reduction planning, USGS identified the Los Angeles area as one of the regions for the implementation of a structural instrumentation program to further these studies. One of the buildings recommended for instrumentation by the USGS–Los Angeles Region instrumentation of structures committee is the 1100 Wilshire Finance Building [11].

2.0 THE STRUCTURE

2.1 General Description

A general view and sketch of the Wilshire Finance Building is seen in Figure 2.1. The height of the building is 483 ft. (147 meters) including the basements. The general in-plan dimensions of the four sides of the basement are approximately 177 ft. × 146 ft. × 176 ft. × 154 ft. (54 m × 44.5 m × 54 m × 50 m). Typical plan views are seen in Figures 2.2 and 2.3. There is approximately an 11 ft. (3.4 m) elevation difference between the ground level on one side and the parking garage entrance level on the other side of the building.

The building, also referred to as the "half building," because of its distinctive vertical irregularity, is indeed a unique structure. A triangular prism (23-story office tower triangle with a sapphire–blue glass curtain wall) stacked atop a rectangular (11-story square structure clad in granite chip precast concrete panels) parking garage is an unusual shape for the seismically active region, and one that requires structural engineers to make the two shapes behave as one in the event of an earthquake. The dual-shape provides the opportunity for structural engineers and others to learn more about how unusual shapes

might perform during earthquakes. The twelfth transitional floor has a roof garden. Underground are a commercial level and three more parking levels. At the 12th level, the building plan abrubtly changes from the nominally rectangular shape to a triangle.

One challenging aspect of construction was a 75-foot diameter, 70-foot high double-helix ramp for the above-grade garage levels. With one circumference of the ramp, there is a rise of 11 feet, a typical story height. The grid of the spiral is not an independent element because some of the columns run all the way up through the garage and into the office tower. These had to be positioned to avoid cutting down leaseable space by interfering with office layouts. Similarly, to avoid obstructing vehicle circulation in the three levels of parking below the ramp, some ramp columns are terminated and their loads transferred to others [12].

2.2 Foundation System

The building is founded on shale and sits on reinforced concrete basement walls and columns, supported by massive concrete footings resting on shale. Some footing pads are as large as 18 feet (5.5 meters) by 18 feet (5.5 meters) and 7 feet (2.1 meters) thick depending on the various loads dictated by the dual-shape structure with a maximum soil bearing stress of 24 psf [12].

Underground levels, which go down 53.5 feet, added to engineering problems because the front and one side of the building reaches the property line and the tower perimeter columns are close to the property line [12].

There is a ductile concrete frame below grade compatible with the ductile steel frame above grade. It consists of pilasters and beams with poured-concrete infill panel walls anchored into the pilasters. The pilasters distribute their loads into the continuous wall and footings [12].

2.3 Seismic Resisting System

After studying several framing schemes, a ductile moment frame along the perimeter of both the rectangular garage base and the triangular tower was selected by the designers. This frame was supplemented with a common rigid frame in the core that acts as a spinal cord to connect the two configurations. The spinal cord helps tune and control the dynamic response of the building and accommodates the radical change of mass and stiffness between the two shapes [12].

Both static and dynamic analyses were performed using the SAP6 computer program [13]. Inherent in the model formulation is the assumption that the floors are rigid in plane, thus allowing each floor to be idealized by three mass degrees of freedom located at the floor center of mass. Only the primary lateral force resisting system (perimeter moment frames and core frames) is modeled. The shear walls in the base structure are modeled using equivalent springs with stiffnesses equal to the calculated shear stiffness of the walls. The resultant design torsional forces of the office tower is governed by wind load more than earthquake forces [12].

In addition to the analyses, standard wind and wind-driven rain simulation tests were made, along with the seismic tests, to check curtain wall connections and glass gasketing for anticipated earthquake motion. For the wind related tests, a 42-foot high replica mock-up was built of the granite curtain wall of the most extreme angle at the southeast corner of the building [12].

2.4 Modal Analyses

Los Angeles city code specifies that a dynamic analysis is mandatory for any building having irregularities in shape or stiffness [14]. While gravity loads used in design and analysis were based on the City code, the lateral loads were specified in terms of seismic or wind loads. For the Building, the seismic loads were specified by performance criteria for two levels of earthquake excitation. First, for the maximum probable earthquake, defined as an event with 50% probability of being exceeded in a 50-year period, the structure must remain elastic. The spectrum for this level earthquake is anchored at 0.25 g zero-period acceleration. Second, from consideration of local geological conditions, the most

extreme earthquake that can be anticipated, defined as the maximum credible earthquake, will cause no failure mode mechanisms to develop in the structure and controlled elastic action will occur. The spectrum for this level earthquake is anchored at 0.50 g zero-period acceleration. The design response spectra for these two earthquakes are provided in Figures 2.4 and 2.5.

During the design process, modal analyses performed on the mathematical model shows de-coupled translational and torsional modes as summarized in Table 1.

Table 1. Building Periods (From Analysis).
(Courtesy A. C. Martin and Associates)

Modes	Period (Seconds)	Type
1st Mode	4.94	Translational N.E.
2nd Mode	4.29	Translational N.W.
3rd Mode	2.65	Torsional
4th Mode	2.11	Translational N.E.
5th Mode	1.78	Translational N.W.
6th Mode	1.29	Torsional

The above described first six modes are shown in Figures 2.6 to 2.11.

3.0 STRONG-MOTION RESPONSE DATA

3.1 The Earthquake

The October 1, 1987 Whittier Narrows, California earthquake (M_L = 5.9 - NEIS, Caltech) occurred at 1442 GMT (0742 PDT), had its epicenter at 34.058°N and 118.077°W and had a depth of 12 km. The earthquake was the strongest shaking that has occurred in the Los Angeles basin since the February 9, 1971 San Fernando earthquake (M_L = 6.4). The earthquake was followed by many small aftershocks and a M_L = 5.5 aftershock on

the morning of October 4. The location of the epicenters of the 1987 and the 1971 events as well as the faults are shown in Figure 3.1 [15-17].

The main shock caused at least 2 fatalities and a number of reported injuries. Several deaths after the main shock were also attributed to the earthquake. The $M_L = 5.5$ aftershock caused one additional death and injuries to several people. The loss of property was extensive in the township of Whittier and to a lesser extent throughout neighboring communities of Los Angeles County. Most of the severe structural damage was caused in old and unreinforced masonry buildings. This is not to say that damage in engineered structures was minor. Details of damage surveys of the earthquake have been extensively reported elsewhere and are beyond the scope of this report. However, the 1100 Wilshire Finance Building did not suffer any damage during this medium size earthquake. Extensive quantity of response records from structures and ground stations of the USGS strong-motion program are reported by Porcella, Etheredge and others [17], and from the CDMG stations are reported by Shakal and others [18,19].

3.2 Instrumentation of the Building

The strong-motion instrumentation scheme of the building is shown in Figure 3.2. There are a total of 21 channels. Three tri-axial strong-motion accelerographs (SMA–1s) with a total of nine channels are deployed at three corners of the lowest basement level. The remaining 12 channels, connected to a central recording system, are deployed at the ground level, club level (12th Floor) where the plan changes from rectangular shape into triangular, the restaurant level (13th Floor) which is the first floor with the triangular plan and the top floor (32nd Floor). At each of these levels, two force-balance accelerometers (FBA–11s) are deployed parallel to one another at nominal NW and SE corners (Figure 3.2) with orientations of 208° clockwise from north, and the third FBA–11 is deployed at nominal NW corner with orientation of 298° clockwise from north. These orientations are coincident with the orientations of the horizontal channels of the three SMA–1s at the basement. The perpendicular distance between the two parallel NW208 and SE208 accelerometers is 169.83 ft. (51.76 m).

3.2 Recorded Data

The unprocessed acceleration response records obtained during the Whittier Narrows earthquake from the instrumentation described in Figure 3.2 are shown in Figures 3.3 and 3.4.

At the basement, the recorded peak horizontal acceleration is 0.18 g and the peak vertical acceleration is 0.08 g. The peak horizontal acceleration for the superstructure is 0.26 g recorded by the NW208 accelerometer at the 13th floor. The peak horizontal acceleration at the top floor (32nd Floor) is 0.19 g recorded by the NW208 accelerometer.

4.0 ANALYSES OF PROCESSED DATA

4.1 Time Histories

The processed time histories of acceleration, velocity and displacement records, grouped and equiscaled according to their locations and orientations at different levels of the building, are provided in Figures 4.1 to 4.3 for acceleration, Figures 4.4 to 4.6 for velocity and Figures 4.7 to 4.9 for displacement. These plots are summarized in Figures 4.10 to 4.12 each showing the three components (NW208, NW298 and SE208 directions) of acceleration, velocity and displacement simultaneously along the height of the building. However, these plots do not include the vertical components and the remaining horizontal components in the basement. Time history and subsequent Fourier amplitude spectra plots are prepared using a program package written by Mueller [20].

4.2 Fourier Spectra: Records at Basement

The Fourier amplitude spectra (total record window) of the three-component acceleration response records at the three basement locations are provided in Figures 4.13 to 4.15 and are summarized in Figure 4.16. The peaks of the spectra vary showing incoming earthquake energy at different frequencies and levels. The Fourier amplitude spectra of the basement acceleration records (windowed beyond the peak) indicate peaks in the neighborhood of 1 Hz (but with smaller energy than those spectra with full record) as demonstrated in Figure 4.17. This is due to the effect of the structural response on the motions at the basement.

4.3 Fourier Spectra: Horizontal Records at All Levels

The Fourier amplitude spectra (total record window) obtained from the horizontal acceleration response records from the three accelerometers (NW208, NW298 and SE208 orientations) are provided in Figure 4.18 for the basement, in Figure 4.19 for the ground level, in Figure 4.20 for the 12th floor, in Figure 4.21 for the 13th floor and in Figure 4.22 for the 32nd floor, respectively. From these, we identify the dominant frequencies at the basement and the ground level as 1.5–2.0 Hz and at the 12th, 13th and 32nd levels as 0.7–0.8 Hz with clearly decreasing energy at higher frequencies. However, when the time windows are taken after the larger peaks, the dominant frequencies at the basement (Figure 4.23) are 1 Hz in the 208 direction and 1 and 2 Hz in the 298 direction. Repeating the process for the ground level, we see in Figure 4.24 (plotted between 0–2 Hz), dominant frequencies at 0.8 Hz and 1 Hz. At the 12th, 13th and 32nd floors (Figures 4.25–4.27), the dominant frequencies clearly are 0.8 Hz but there exists another frequency at approximately 0.7 Hz. We can attribute this to the fact that the dominant structural vibration frequency becomes more influential after the larger peaks of the ground motion.

4.4 Relative Accelerations and Displacements at Different Levels

The expected primary behavior of the building is one of torsion because of the configuration of the structure. In order to quantify torsional behavior of the structure, it is necessary to obtain relative accelerations (Figure 4.28) or relative displacements (Figure 4.29) between two parallel sensors at each instrumented level. This can be done, as in this case, when the records are synchronized. The relative acceleration at any level, divided by the distance between the two parallel sensors at that level, yields the rotational acceleration. Similarly, the rotational displacement is determined by dividing the relative displacement at any one level by the distance between the two parallel sensors. The relative accelerations will be used later to determine the torsional frequencies. From Figure 4.29, we determine the maximum relative displacement experienced at the top floor as 3.53 cm and therefore the maximum rotation as 6.82×10^{-4} radians or 0.039 degrees. The relative displacement plots in Figure 4.29 show that the sense of the rotation changes from 32nd floor to 13th or 12th floor. This is more clearly depicted in Figure 4.30 where the first 10

seconds of the relative displacement at the top three instrumented floors are enlarged to demonstrate the difference in the sense of the rotation at the 32nd floor when compared with the 13th and 12th floors. Clearly this is an indication of the second torsional mode for the triangular portion of the structure. Hence, we can state that only the second torsional mode is observed from analyses of the records. The other modes determined from analytical methods (Table 1) are not observed.

To further demonstrate the torsional behavior of the structure, we define "representative" angle of twist as the difference of relative displacement between two instrumented floor levels. The true angle of twist would be calculated by dividing the representative angle of twist by a constant that is equal to the difference in height of the respective floors. Figure 4.31 shows plots of "representative" angles of twist (for 32nd to 13th, 32nd to 12th, and 32nd to basement) and their respective Fourier amplitude spectra. We note here that the amplitude of the 32nd to basement plot is less than the others which is a clear indication that the sense of rotation is different at the 12th and 13th levels as compared to the 32nd level. The spectra in Figure 4.31 depict identical peak frequency at 0.8 Hz indicating that it belongs to same mode which, in this case is the second torsional mode.

It is seen in Figure 4.29 that the relative displacement plot for the basement level shows a slope in the beginning of the record that cannot be attributable to the nature of the ground motions or surface wave motions causing differential displacements at the basement level. We will not investigate this herein. However, we will show that the torsional energy at the basement is very low. Figures 4.32 and 4.33 show equiscaled Fourier amplitude spectra of horizontal accelerations at NW208 locations as compared to the relative horizontal accelerations (NW208–SE208) at each of the instrumented levels. Thus it is seen that the torsional frequencies from relative horizontal accelerations (NW208–SE208) are closely coupled and consistent at 0.7 and 0.8 Hz for the 12th, 13th and 32nd floor levels. Another torsional frequency at 1.25 Hz at the 32nd level practically disappears at the 13th and 12th levels. Furthermore, at the basement level, the level of energy at these frequencies becomes insignificant. This prompts us with the conclusion that the unique structure, expected to respond in a torsional mode, does so with a closely-coupled second torsional

mode. However, the apparent torsional response observed in the relative displacement plot for the basement is not due to a spatial variation of ground motion but rather due to the processing and integration errors.

4.5 Center of Rigidity

The center of rigidity of complex structures is difficult to assess particularly for a structure like the Wilshire Finance Building. Hand calculations based on rigidities of lateral force resisting members at any one story are possible and may be the only way for estimating the center of rigidity in the majority of cases. However, when response data of the type detailed for this structure is available, it is possible to determine the center of rigidity at a level of the structure by a procedure that minimizes the coherence between the relative accelerations (as representative torsional accelerations) recorded by two parallel sensors at a level and the translational acceleration (Şafak and Çelebi) [21]. The procedure starts with an assumed center of rigidity. The horizontal records are transferred to this center in terms of two translations and a rotation. Then, the coherence functions between the torsional and each horizontal component of motion are calculated. The measure of total coherence is determined as the area under the coherence function, termed as the coherence area. By changing the location of the center of rigidity, the variation of the coherence area is noted. The location that gives the minimum coherence area becomes the estimated center of rigidity.

In Figure 4.34, the recorded motions at NW (208 and 298 directions) and SE (208 direction) of the 32nd floor and corresponding Fourier spectra are shown. The coherence areas plotted against the horizontal coordinates (x,y) of the assumed center of rigidity in Figure 4.35 for the 32nd floor provide the minimum at 1.90 meters and 42.25 meters which are the coordinates of the estimated center of rigidity according to the defined reference axis system also shown in the figure. In Figure 4.36, the two translational components of motion and the rotational motion at the center of rigidity, obtained by transforming the recorded motions, as well as their corresponding Fourier spectra are provided. These translational components at the center of rigidity are theoretically decoupled from the torsional component. The rotational contribution of the motions recorded by the three

sensors (as the differences between the recorded motions and the translational motions at. the center of rigidity) and corresponding Fourier spectra are shown in Figure 4.37. Note that the spectra and the dominant frequency for the torsional motion at center of rigidity (Figure 4.36) and the rotational components to the motions in NW208, NW298 ans SE208 (Figure 4.37) are all alike. Furthermore, the frequencies of the two translational components (Figure 4.36) and torsional components are same and have values at 0.7-0.8 Hz. This provides a unique exhibition of closely (0.7-0.8 Hz) coupled (translational and torsional) modes.

A summary of the estimated centers of rigidity using the above described procedure is provided in Table 2.

Table 2. Estimated Centers of Rigidity (refer to reference axes system).

	X_G (m)	Y_G (m)
32nd Floor	1.90	42.25
13th Floor	3.80	45.10
12th Floor	1.70	30.50
Ground Level	12.35	27.10
Basement	9.20	25.40

4.6 System Identification

In order to reconfirm the modal frequencies and to quantify modal damping percentages, amplitude spectra of the recorded accelerations at the 32nd and 13th floors were recalculated by using the system identification algorithm described in Şafak [22]. The algorithm is based on the maximum entropy spectral estimation technique. Each record is considered as the output of a recursive filter subjected to a white-noise input with unit variance, and the filter parameters are determined by using the prediction error method. The

transfer function of the filter, when evaluated on the unit circle in the complex plane, gives the spectrum of the record. The advantages of this approach over the Fourier approach are that the estimated spectrum is less influenced by noise, and is available in analytical form, such that all the modes (*i.e.,* modal frequencies, dampings, and participation factors) that exist in the record can be calculated analytically. The number of modes that can be extracted from a given record is determined by observing the variation of the total estimation error of the identification algorithm with the number of modes. The number of modes beyond which the estimation error does not decrease significantly is the optimum number of modes.

During this process, 20 seconds of the acceleration records (windowed between 5-25 seconds) were used to obtain the estimated spectra. These were compared with the spectra of the filtered (band-pass filter between 0.1–5.0 Hz) motion. For each component of motion recorded at the 32nd and 13th floors, the Fourier spectra and estimated spectra are shown in Figures 4.38 to 4.43. For the sixth mode (as determined by mathematical model) or the second torsional mode (as determined by the analyses of the records) the procedure yields modal damping values of approximately 6–7%.

5.0 CONCLUSIONS AND FUTURE WORK

We conclude that the performance of the unique Building during the 1 October 1987 Whittier Narrows earthquake was as expected. In particular the following summary of conclusions are drawn:

- The building is unique in its dynamic response. Higher modes are excited.
- The building responds in a second torsional mode at closely-coupled frequency identified from records to be 0.7–0.8 Hz. The motions at the basement have frequencies between 1.0–2.0 Hz. The other modes determined from analytical methods are not observed.
- The modal analyses performed during the design/analyses processes identifies the second torsional mode (at 1.29 seconds or 0.78 Hz) as the sixth mode. This compares well with the frequency determined from the records.

- The center of rigidities estimated from the records exhibit substantial variation at different levels.
- The modal damping is estimated to be 6–7% by using a system identification approach.
- A question is raised about the definition of fundamental mode as defined by modal analyses. We observe herein that the mode of vibration of this particular structure will always be a coupled mode (torsional and translational) and never pure translational nor pure torsional. Therefore, in complex structures such as this Building, it would be necessary to determine coupled modes rather than uncoupled modes.

For the future, comparison of design response spectra with the spectra of basement motions would be very useful to assess the actual site specific response characteristics including the influence of the presence of the tall structure. This may be significant in light of the important contribution of the higher modes as described in this report. As a follow-up, time-history or response spectrum analysis would provide comparison of estimated and measured displacements and relative displacements. This would further facilitate evaluation of the mathematical model and related assumptions.

REFERENCES

[1.] Çelebi, M., Şafak, E., Brady, G., Maley, R., and Sotoudeh, V., 1985, Integrated Instrumentation Plan for Assessing the Seismic Response of Structures–A Review of the Current USGS Program, USGS Circular **947**.

[2.] Uniform Building Code, *International Conference of Building Officials*, Whittier, CA, 1970, 1973, 1976, 1979, 1982, 1985, 1988 editions.

[3.] Rojahn, C. and Mork, P. N., 1982, An analysis of strong motion data from a severely damaged structure—The Imperial County Services Building, El Centro, California, *in* The Imperial Valley, California, earthquake of October 15, 1979: *U. S. Geol. Surv. Prof. Pap.* **1254**.

[4.] Çelebi, M. (Chairman) *et al.*, 1984, Report on recommended list of structures for seismic instrumentation in the San Francisco Bay region: *U. S. Geol. Surv. Open-File Rep.* **84–488**.

[5.] Çelebi, M. (Chairman), *et al.*, 1985, Report on recommended list of structures for seismic instrumentation in San Bernardino County, California: *U. S. Geol. Surv. Open-File Rep.* **85–583**.

[6.] Ziony, J. I.(editor), 1985, Evaluating Earthquake Hazards in the Los Angeles Region—An Earth-Science Perspective, *U. S. Geol. Surv. Prof. Pap.* **1360**.

[7.] Ziony, J. I. and Yerkes, R. F., 1985, Evaluating Earthquake Potential and Surface-Faulting Potential, *in* Evaluating Earthquake Hazards in the Los Angeles Region—An Earth-Science Perspective, edited by J. I. Ziony, *U. S. Geol. Surv. Prof. Pap.* **1360**.

[8.] Joyner, W. B. and Fumal, T. E., 1985, Predictive Mapping of Earthquake Ground Motion, *in* Evaluating Earthquake Hazards in the Los Angeles Region—An Earth-Science Perspective, edited by J. I. Ziony, *U. S. Geol. Surv. Prof. Pap.* **1360**.

[9.] Dieterich, J. H., et. al., 1988, Probabilities of Large Earthquakes Occurring in California on the San Andreas Fault, (Report of the Working Group on California Earthquake Probabilities), *U. S. Geol. Surv. Open-File Rep.* **88—398**.

[10.] Lindh, A., G., 1983, Preliminary Assessment of Long-Term Probabilities of Large Earthquakes Along Selected Fault Segments of the San Andreas Fault System in California, *U. S. Geol. Surv. Open-File Rep.* **83—63**.

[11.] Çelebi, M. (compiler), 1988, Report on Recommended List of Structures for Seismic Instrumentation in the Los Angeles Region, *U. S. Geol. Surv. Open-File Rep.* **88–277**.

[12.] *Private Communication from A. C. Martin and Associates*, Los Angeles, Ca.,1989.

[13.] SAP6: A Structural Analysis Program for Static and Dynamic Analysis, Users Manual, SAP Users Group, Structural Mechanics Computer Laboratory, University of Southern California, Los Angeles, California, January 1981.

[14.] City of Los Angeles Building Code, 1980, Building News, Inc., 3055 Overland Avenue, Los Angeles, California.

[15.] Çelebi, M., Brady, G., and Krawinkler, H., 1987, Preliminary Evaluation of Structures: Whittier Narrows Earthquake of October 1, 1987, *U. S. Geol. Surv. Open-File Rep.* **87-621**.

[16.] Mueller, C., et. al., 1988, Digital Recordings of Aftershocks of the 1 October 1987 Whittier Narrows, California, Earthquake, *U. S. Geol. Surv. Open-File Rep.* **88-688**.

[17.] Etheredge, E. and Porcella, R., 1987, Strong-motion data from the October 1, 1987 Whittier Narrows earthquake, *U. S. Geol. Surv. Open-File Rep.* **87–616**.

[18.] Shakal, A. F., Huang, M. J., Ventura, C. E., Parke, D. L., Cao, T. Q., Sherburne, R. W., and Blasquez, R., CSMIP Strong-Motion Records from the Whittier, California Earthquake of 1 October 1987, Report No. OSMS 87–05, October 31, 1987.

[19.] Huang, M., Ventura, C., and Shakal, A., 1989, Strong-motion records from Buildings, PROC., ASCE Structures Congress, San Fransisco, Ca., May 1989.

[20.] Mueller, C., 1989, Computer Programs for Analyzing Digital Seismic Data, *U. S. Geol. Surv. Open-File Rep. (in preparation).*

[21.] Şafak, E., and Çelebi, M., 1989, A Method to Estimate Center of Rigidity Using Vibration Recordings, in print, *ASCE Journal of Structural Division.*

[22.] Şafak, E., 1988, Analysis of Recordings in Structural Engineering: Adaptive Filtering, Prediction and Control, *U. S. Geol. Surv. Open-File Rep.* **88–667**, October 1988.

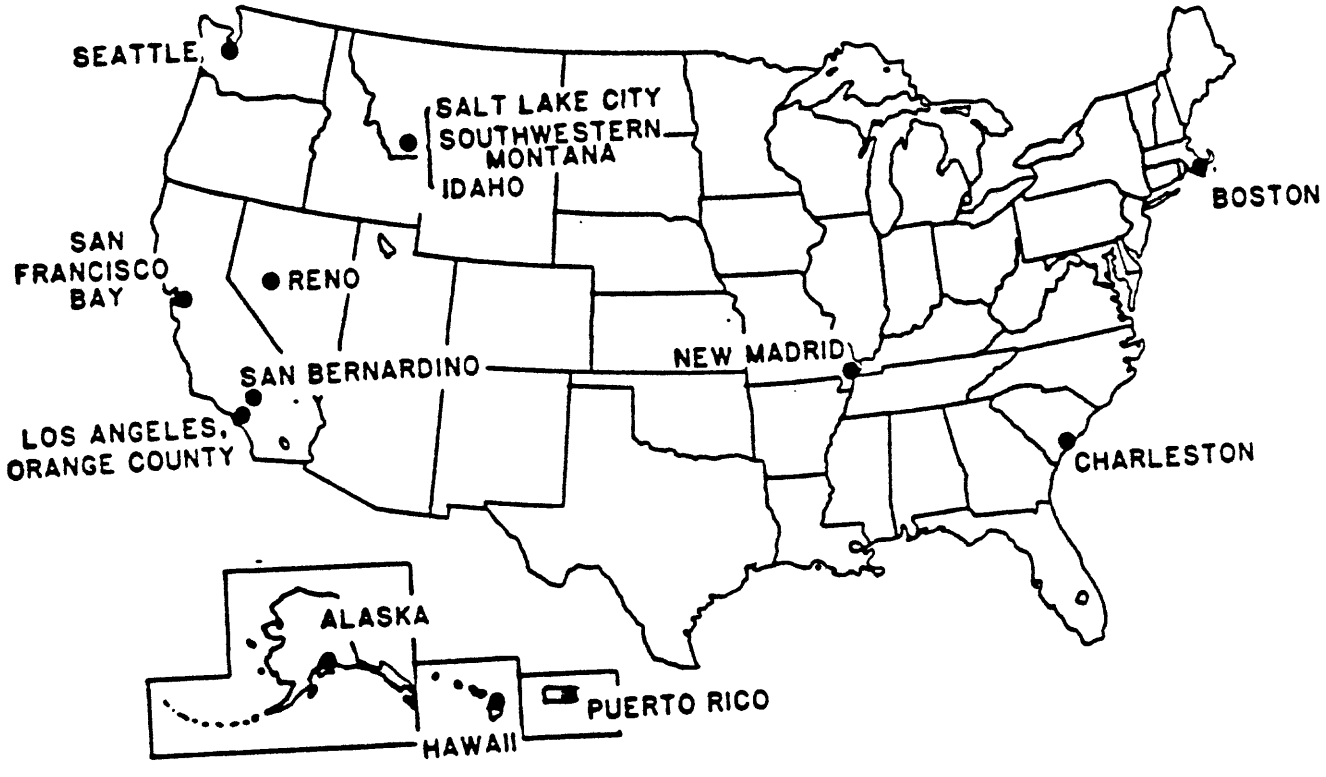

Figure 1.1. Targeted seismic regions for USGS instrumentation of structures program.

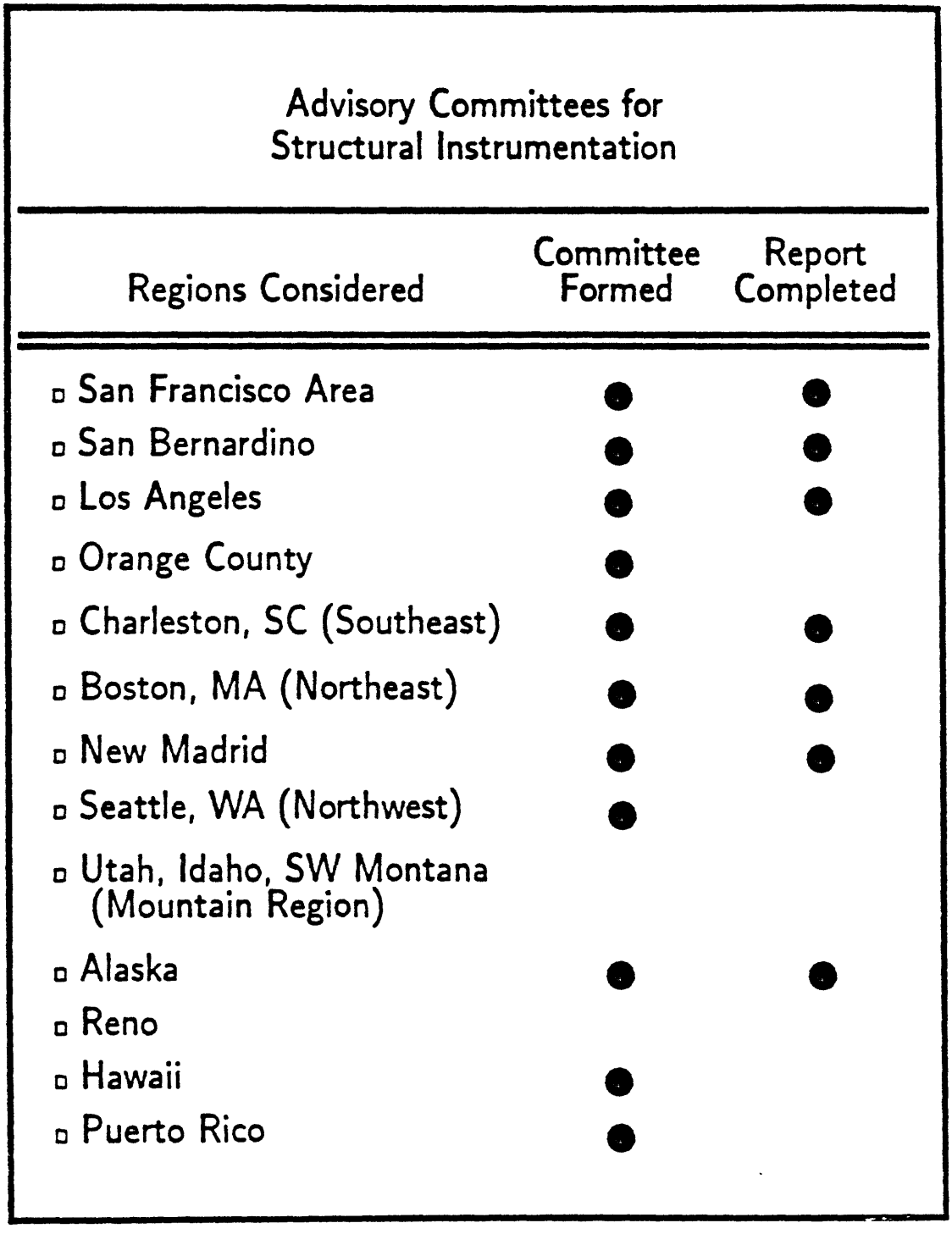

Figure 1.2. Status of USGS Structural Instrumentation Advisory Committees.

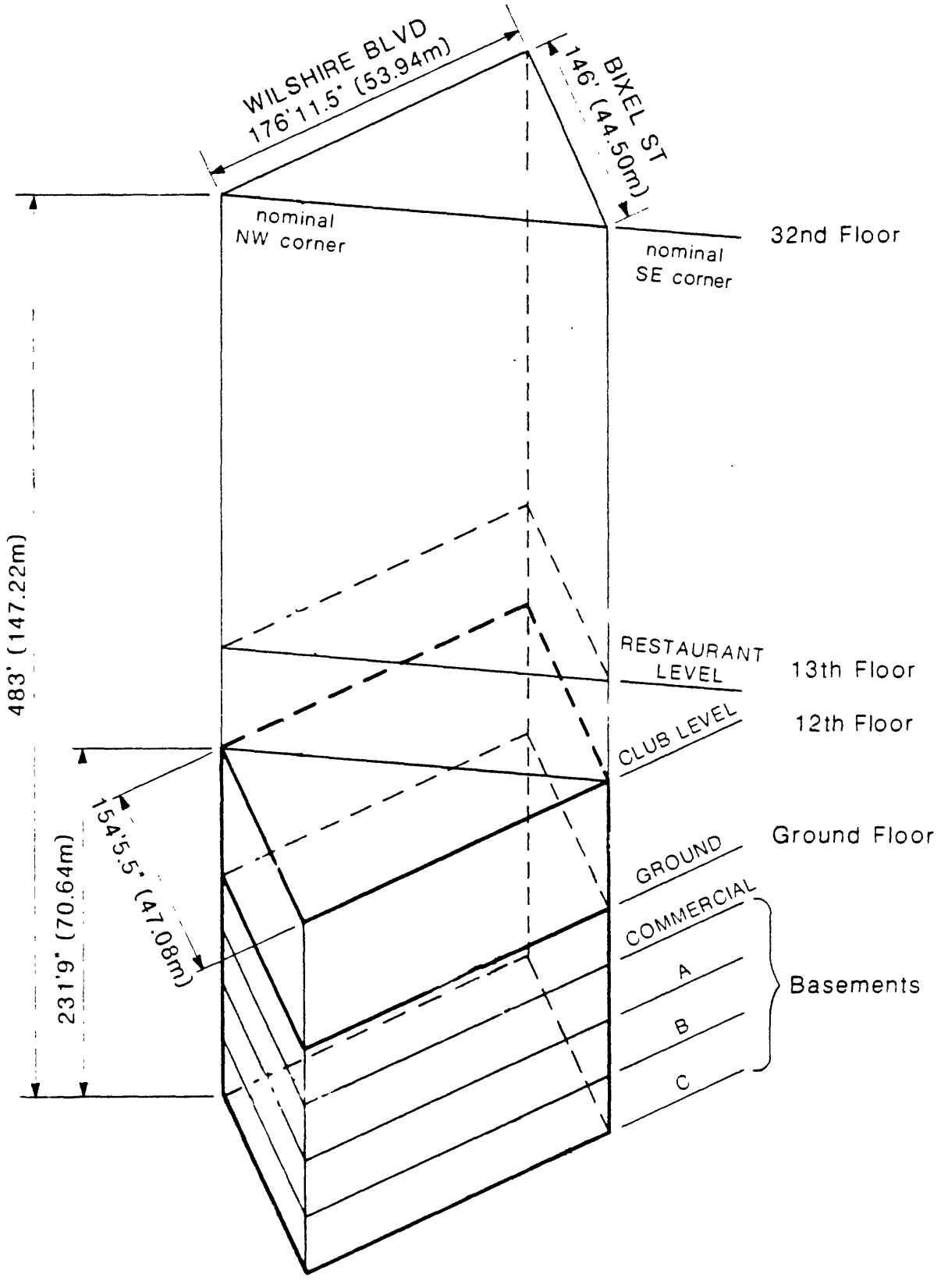

Figure 2.1. General three-dimensional sketch of the Wilshire Finance Building.

CLUB LEVEL

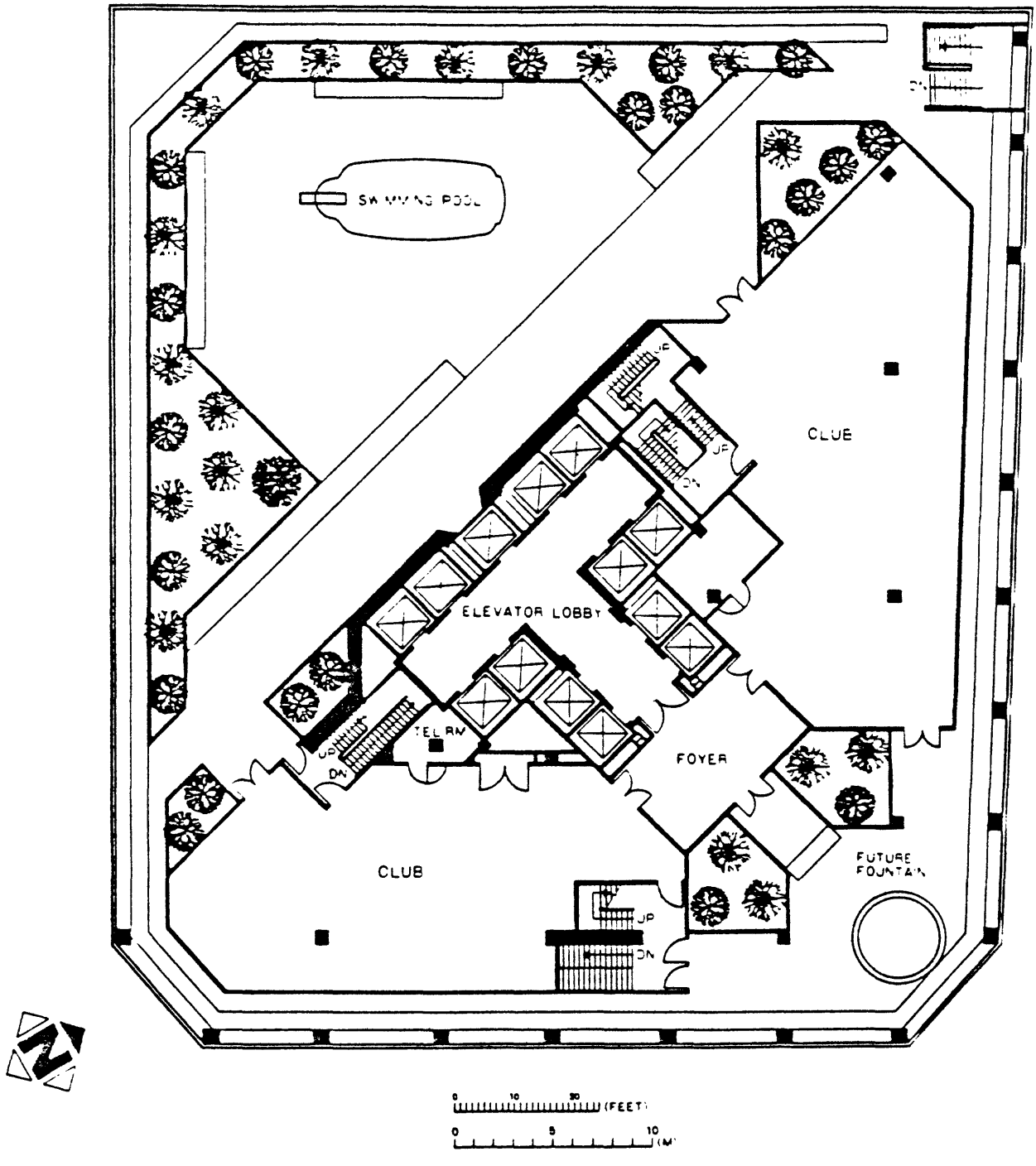

Figure 2.2. Plan view of the Building (Club Level).

TYPICAL HIGH RISE(22Nd THRU 32Nd FLR.)

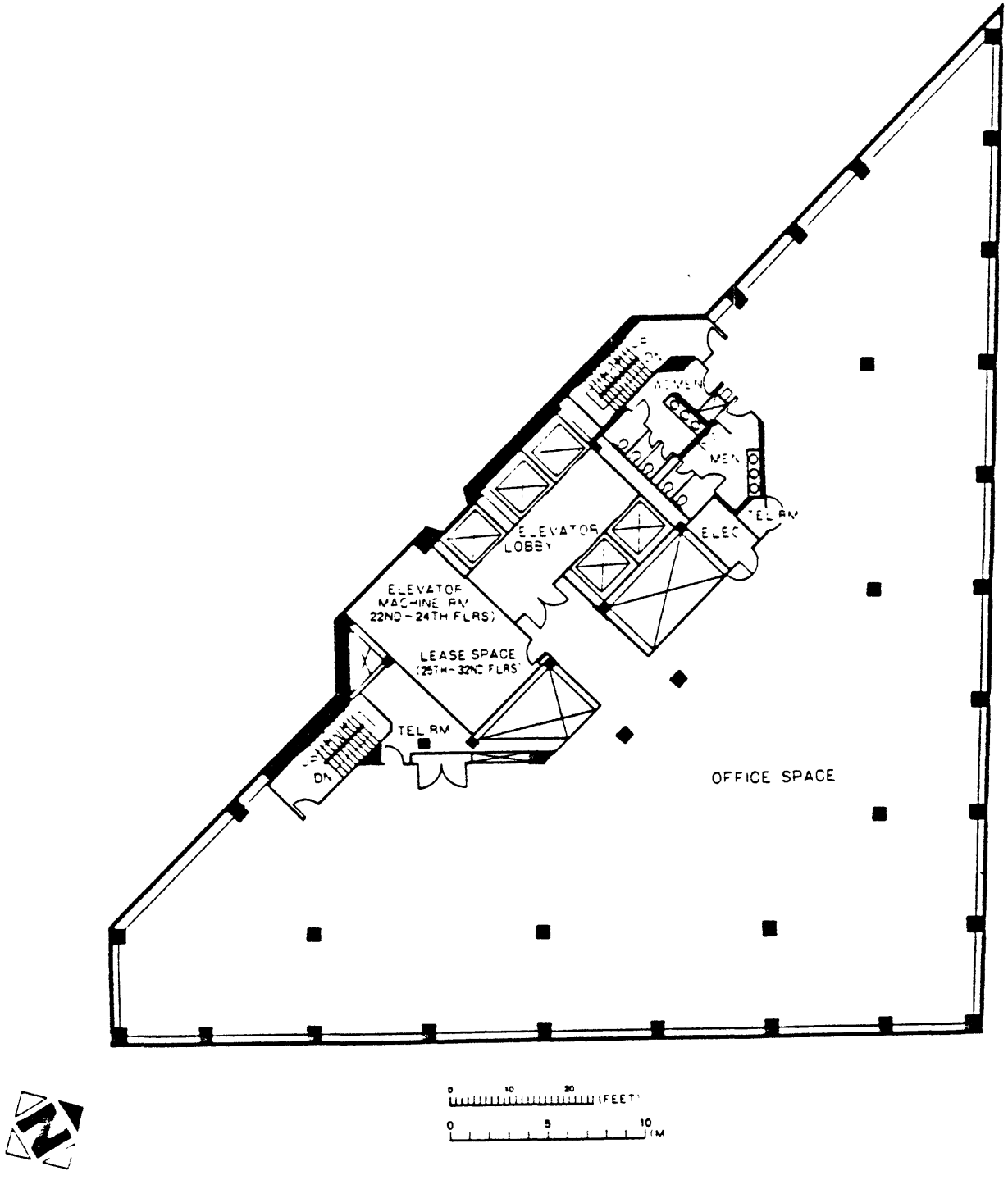

Figure 2.3. Typical Plan view of the high-rise part of the building.

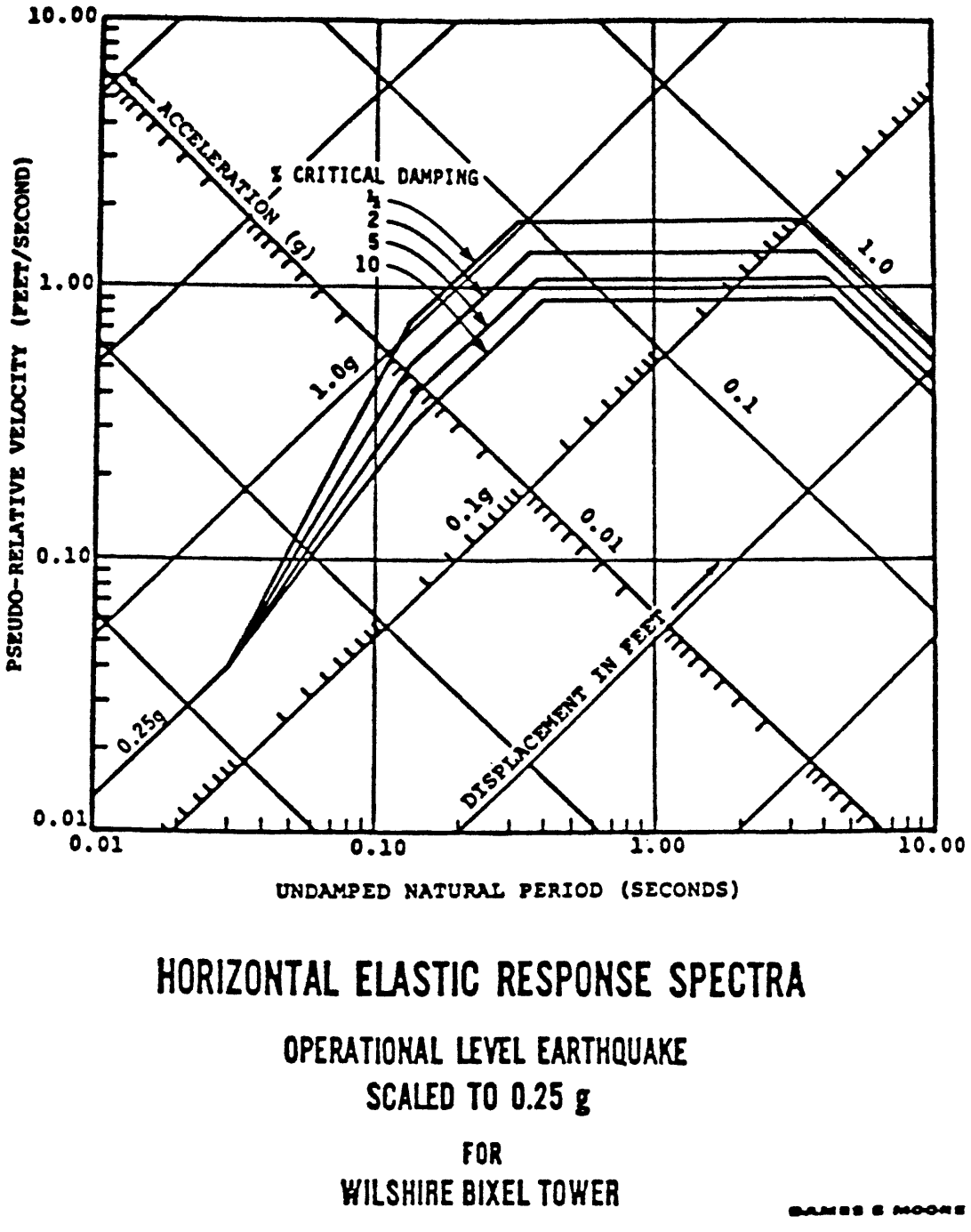

Figure 2.4. Horizontal Elastic Design Response Spectra for Wilshire Finance Building (Operational Level Earthquake).

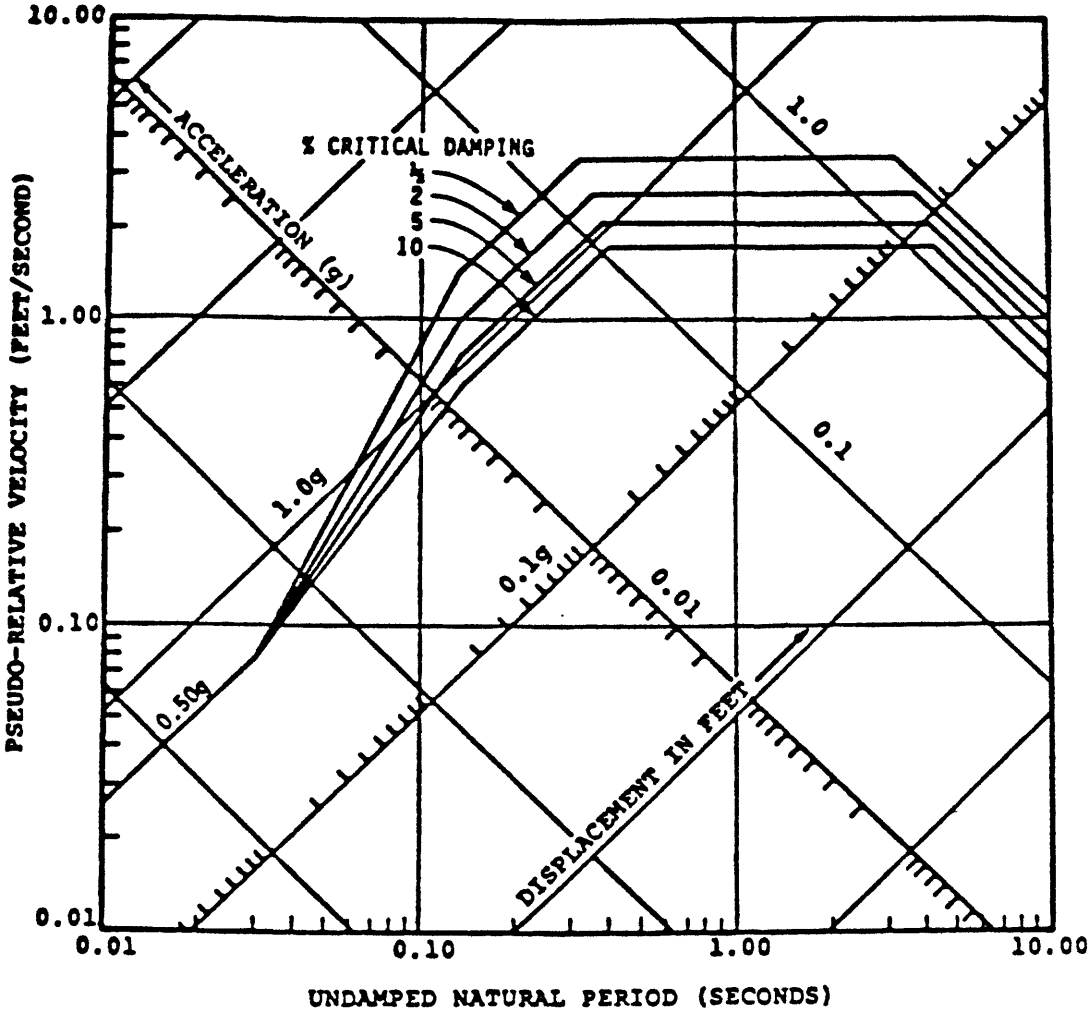

Figure 2.5. Horizontal Elastic Design Response Spectra for Wilshire Finance Building (Contingency Level Earthquake).

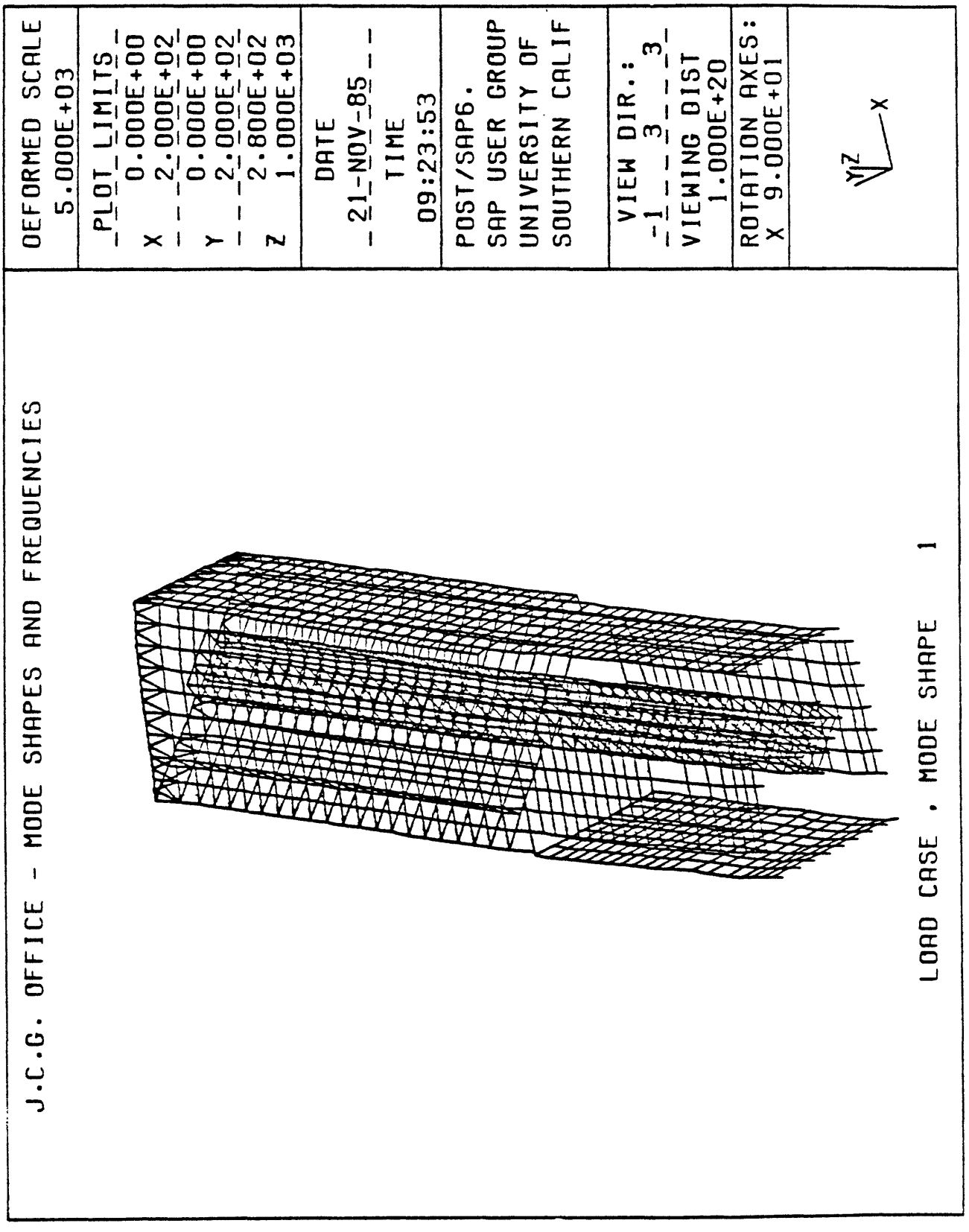

Figure 2.6. First Mode Shape of the Building (from Modal Analysis—courtesy A. C. Martin and Associates).

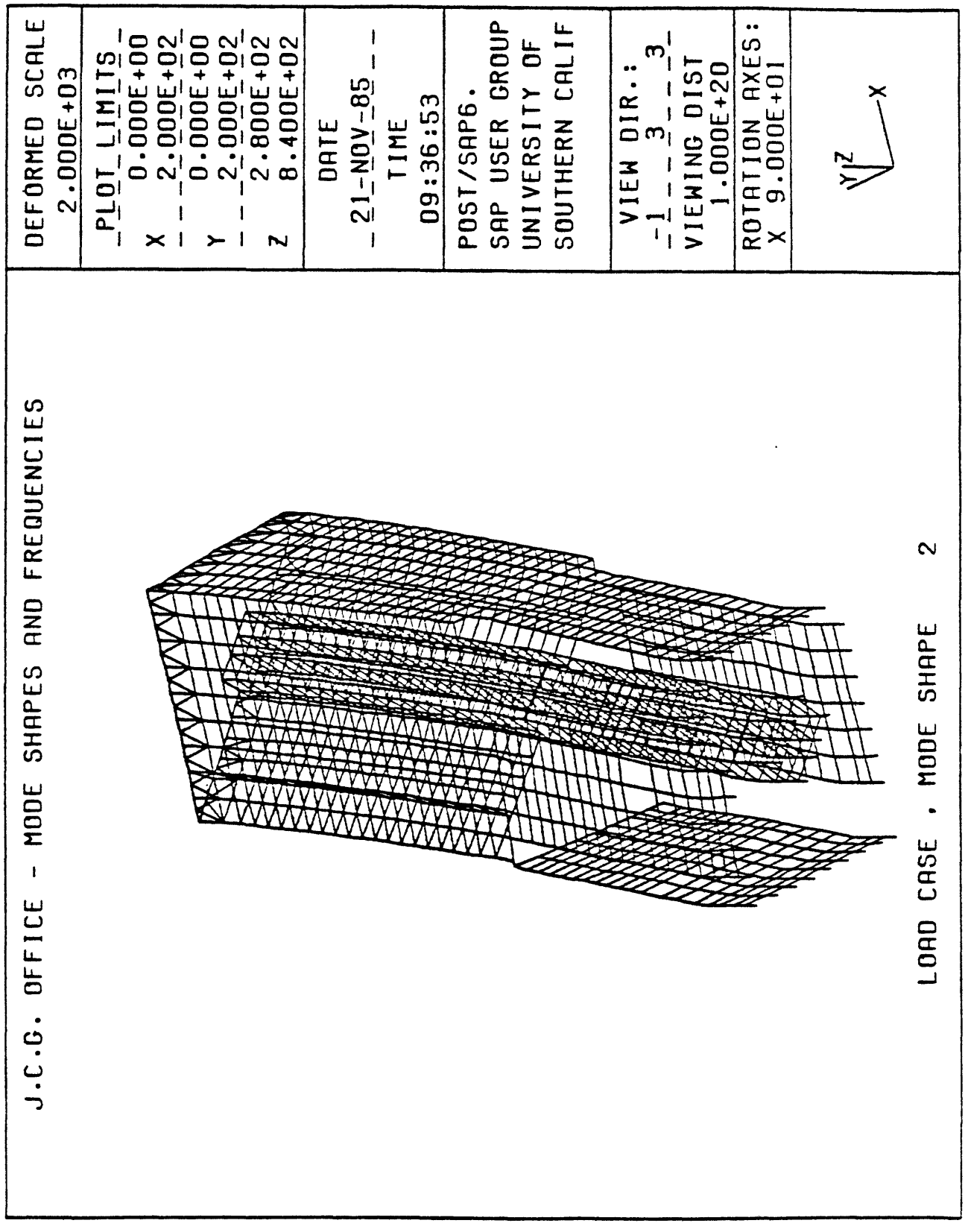

Figure 2.7. Second Mode Shape of the Building (from Modal Analysis—courtesy A. C. Martin and Associates).

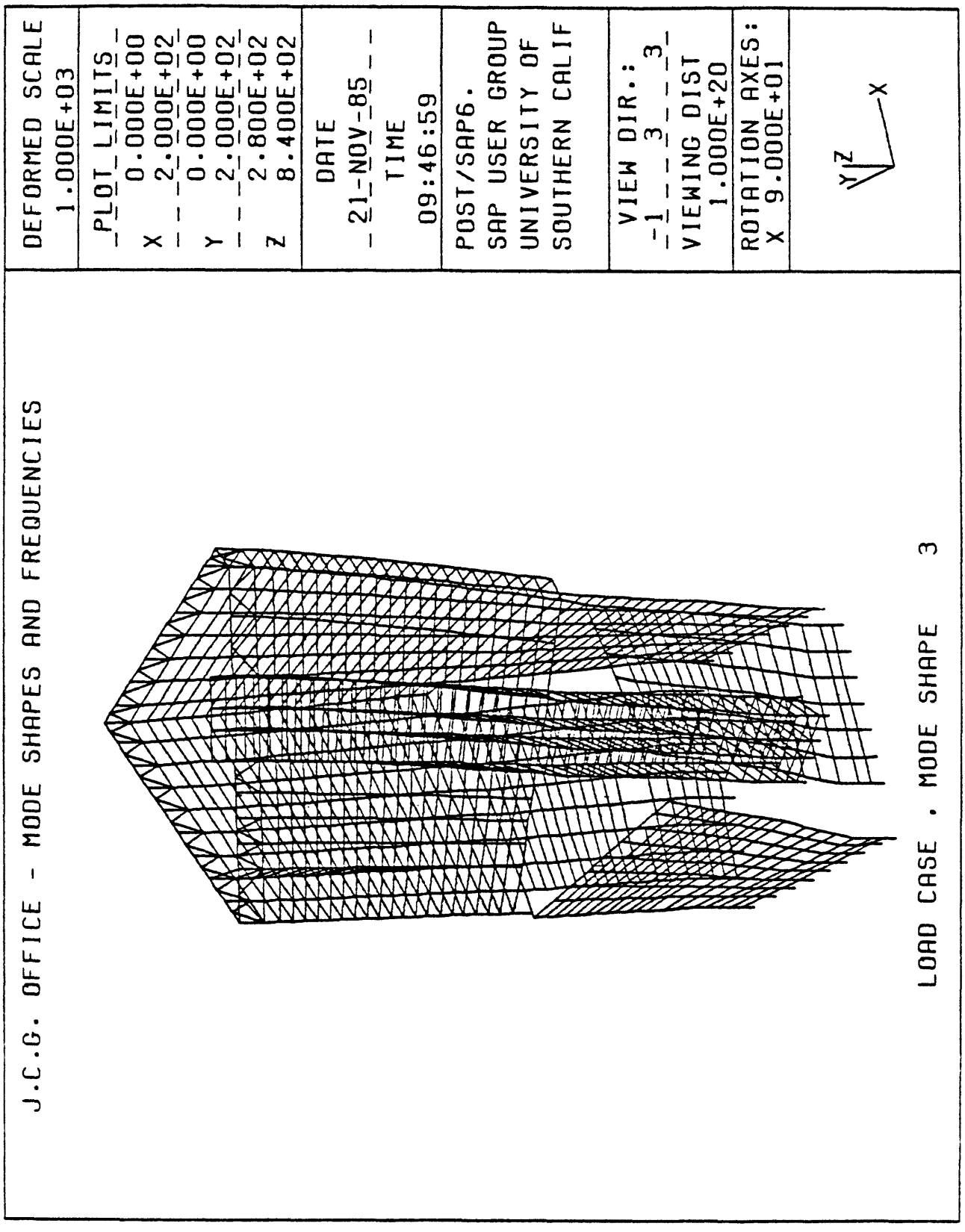

Figure 2.8. Third Mode Shape of the Building (from Modal Analysis—courtesy A. C. Martin and Associates).

Figure 2.9. Fourth Mode Shape of the Building (from Modal Analysis—courtesy A. C. Martin and Associates).

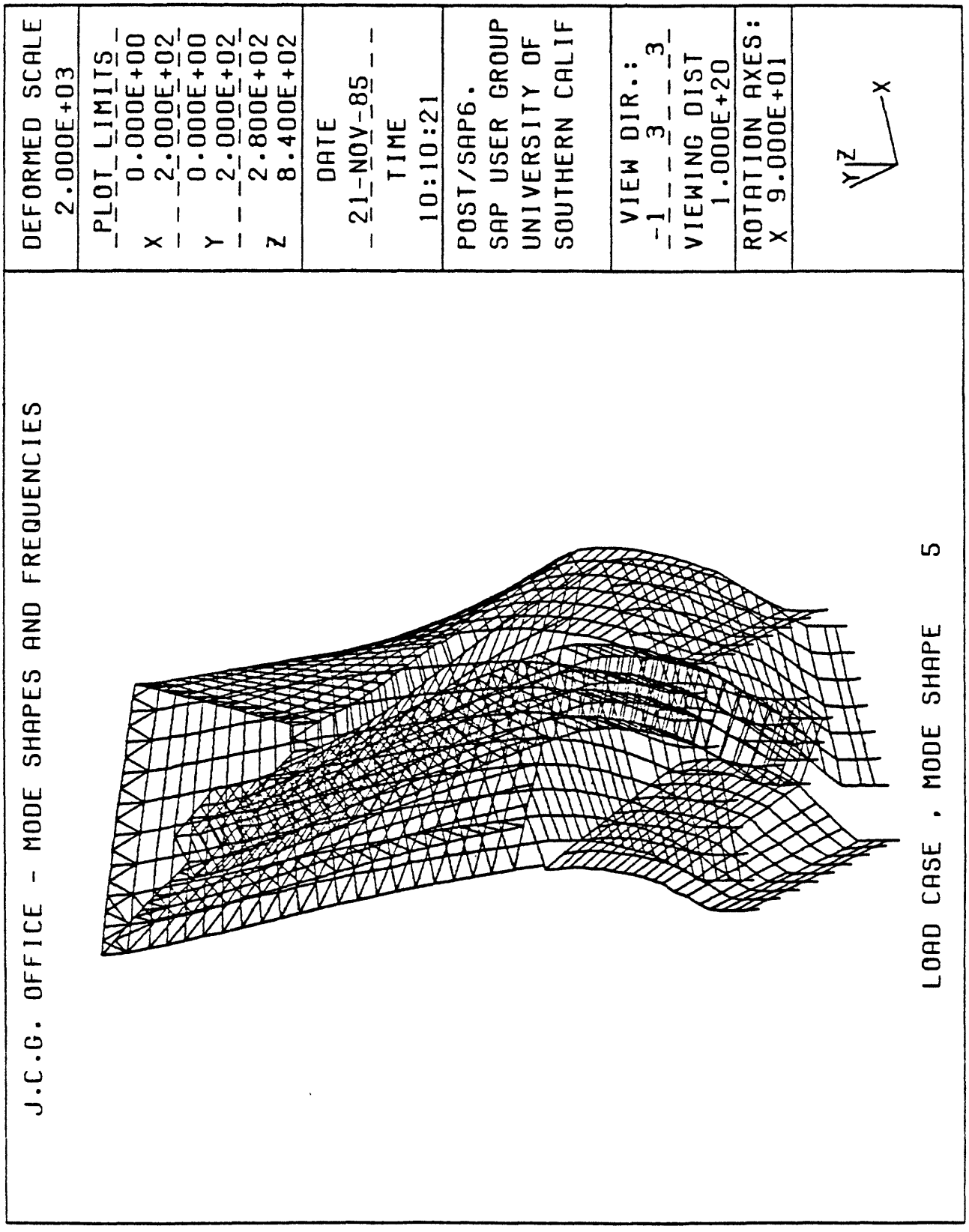

Figure 2.10. Fifth Mode Shape of the Building (from Modal Analysis-courtesy A. C. Martin and Associates).

Figure 2.11. Sixth Mode Shape of the Building (from Modal Analysis—courtesy A. C. Martin and Associates).

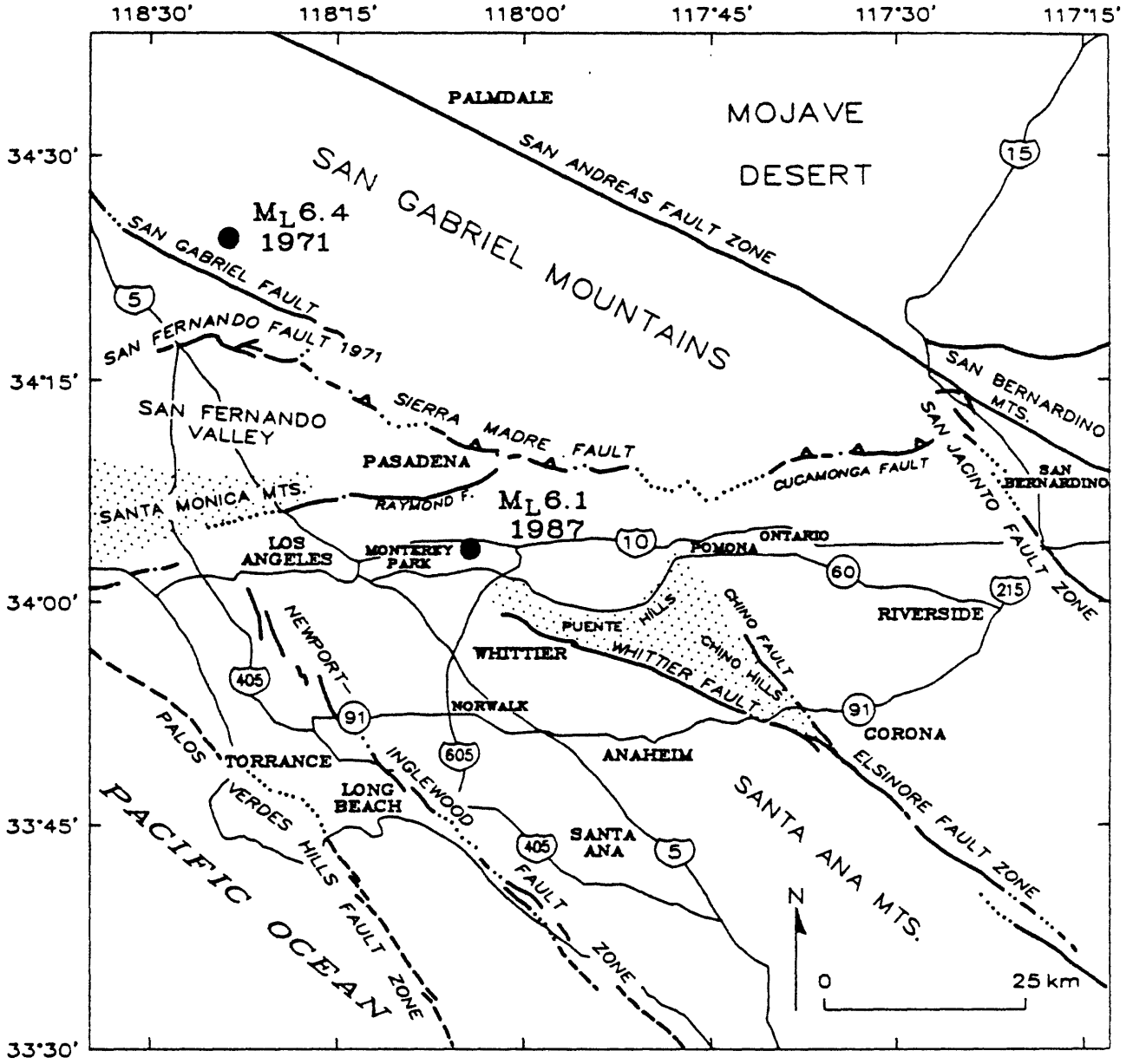

Figure 3.1. The location of the epicenters of the 1985 and 1987 events and the known fault systems in the Los Angeles basin.

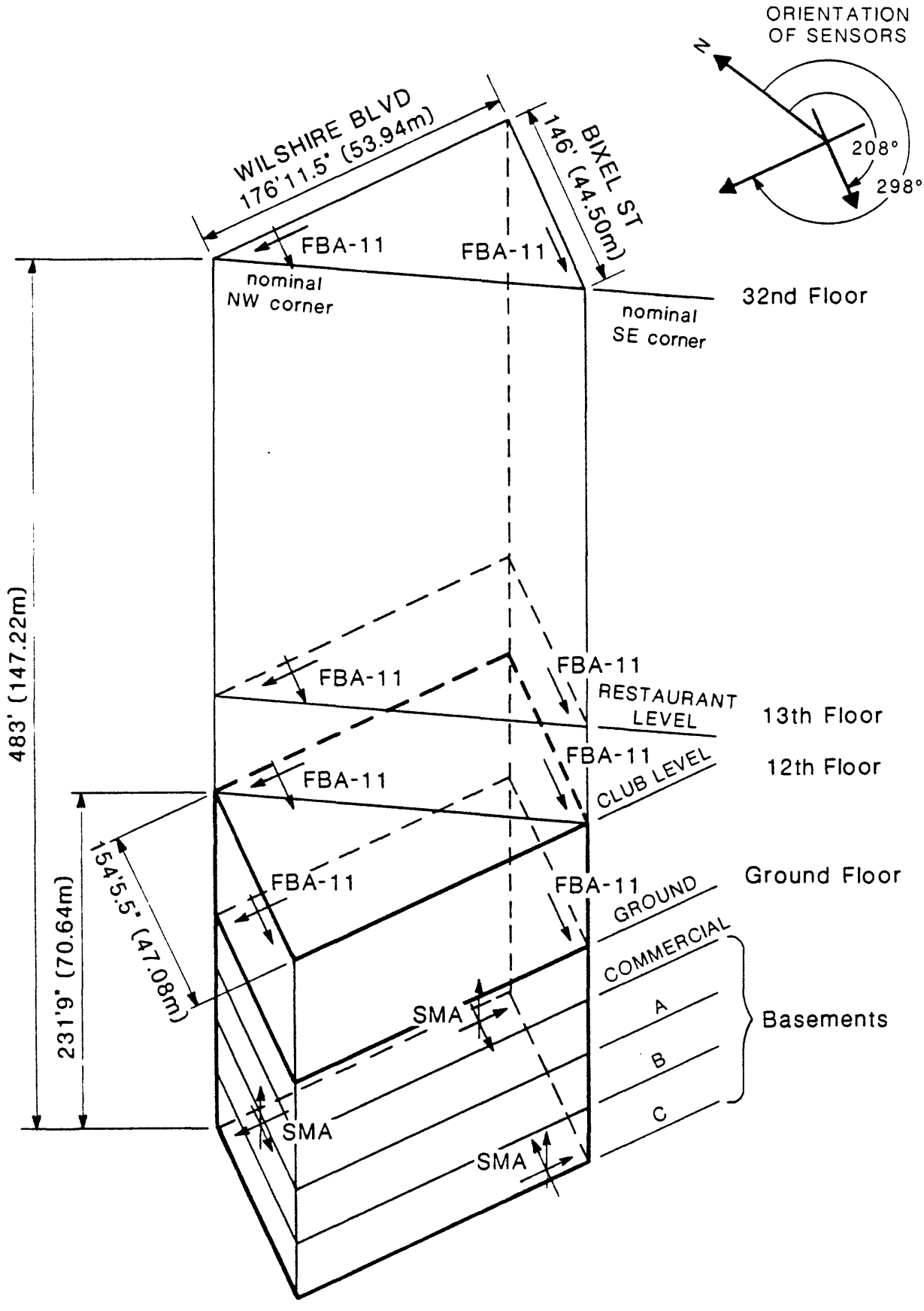

Figure 3.2. Instrumentation scheme and orientation of sensors.

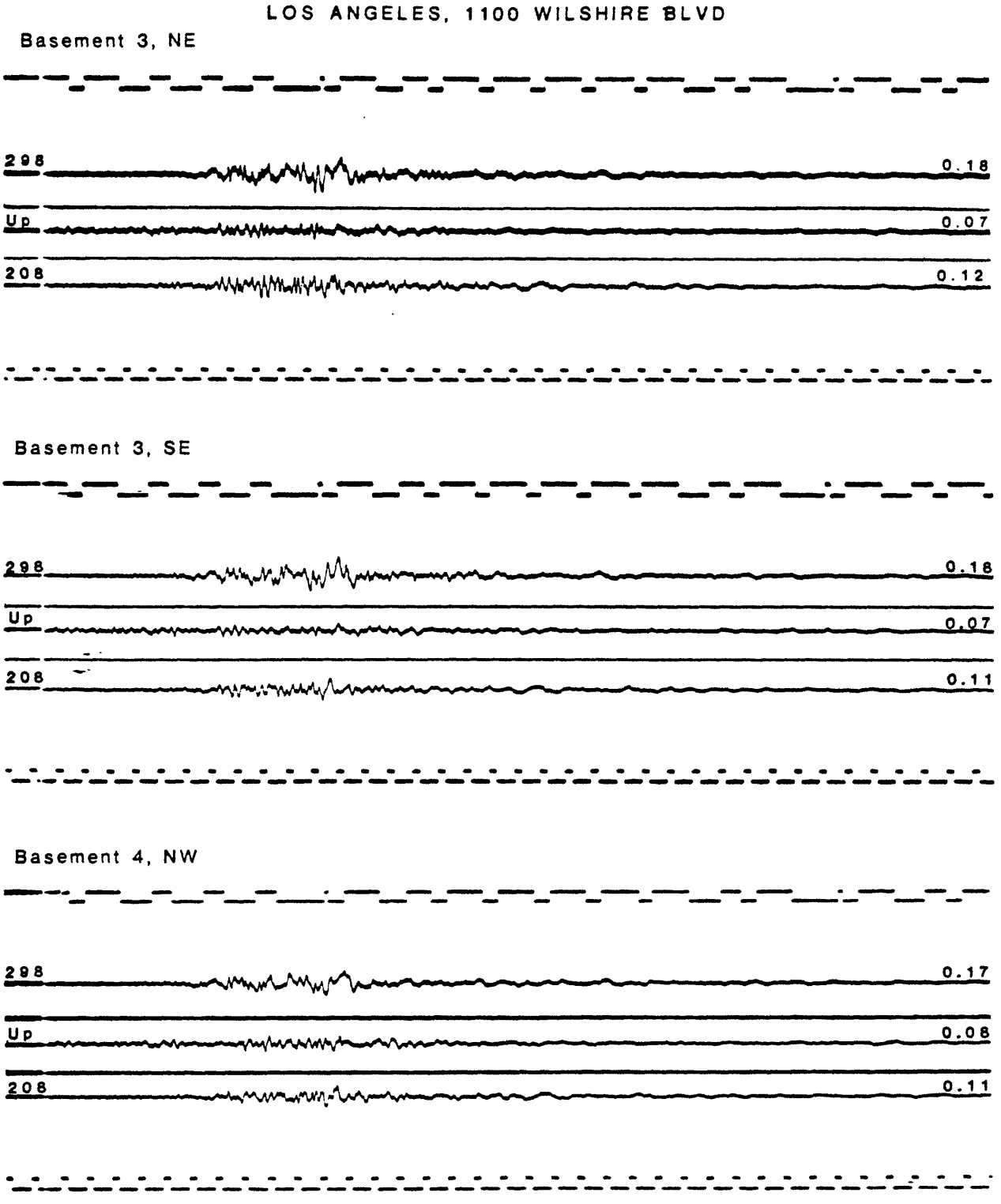

Figure 3.3. Unprocessed Acceleration Records of the Basement Motions.

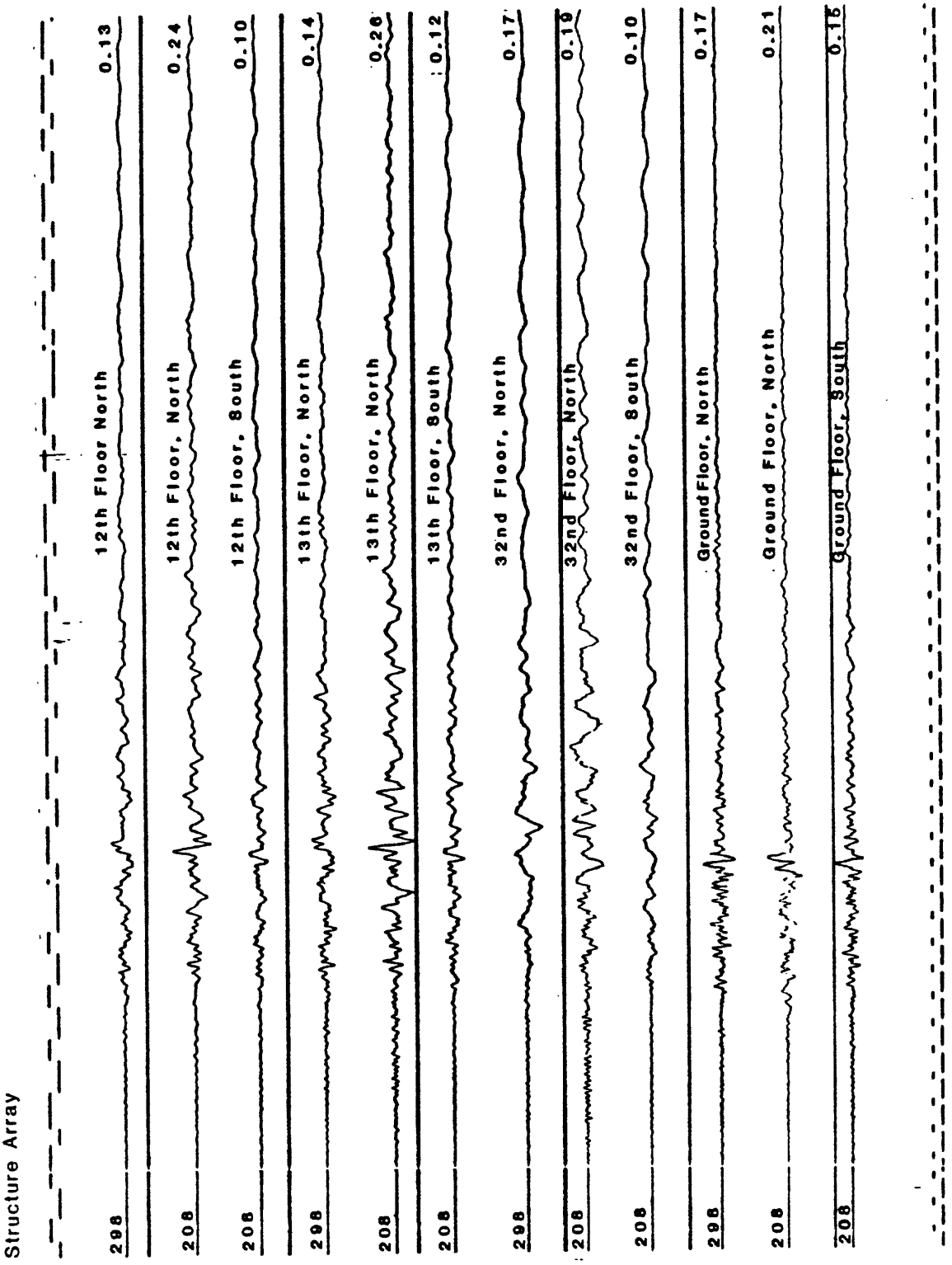

Figure 3.4. Unprocessed Acceleration Records of Motions at different levels.

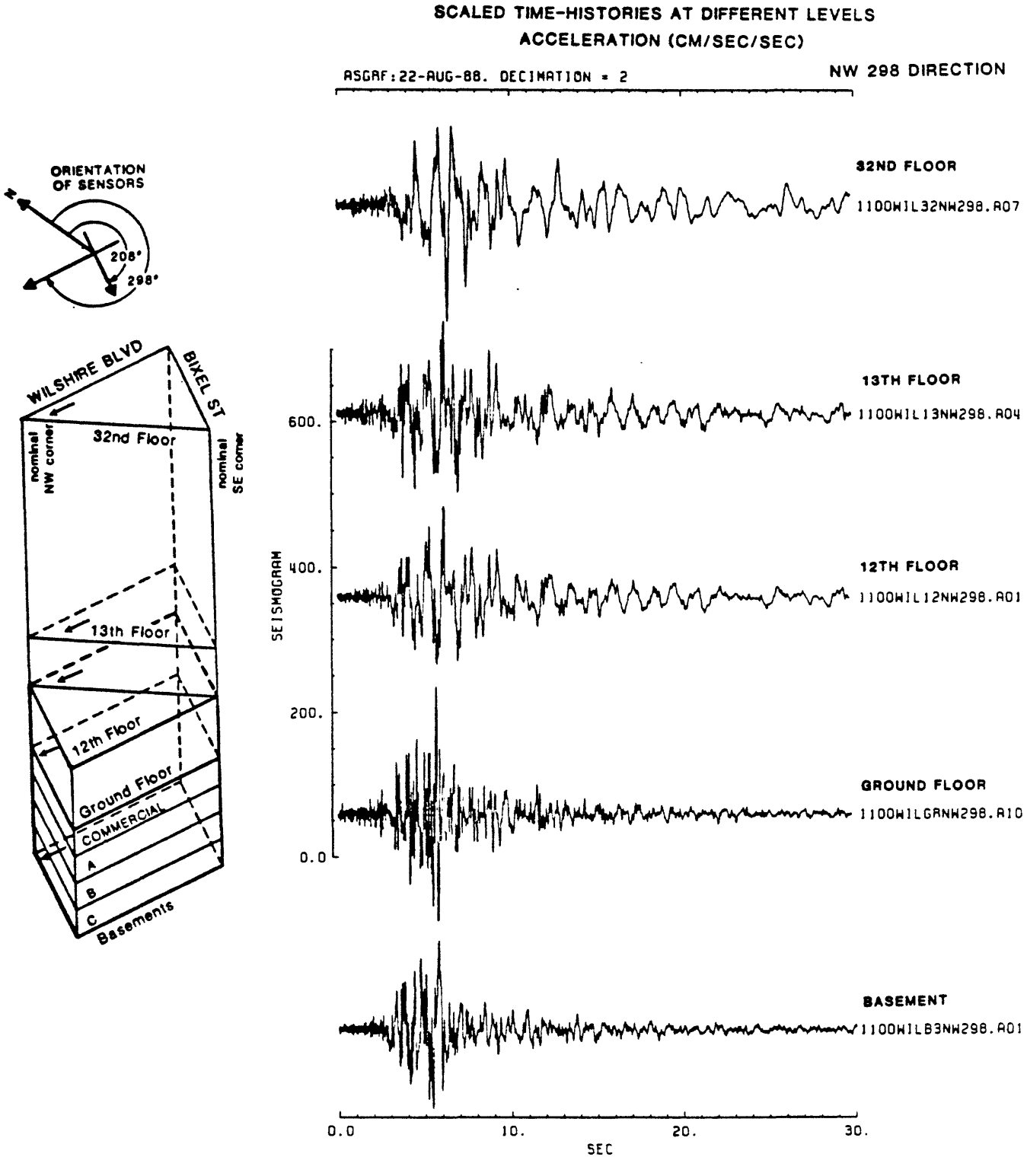

Figure 4.1. Equiscaled plots of acceleration records grouped according to their orientations (NW298 direction).

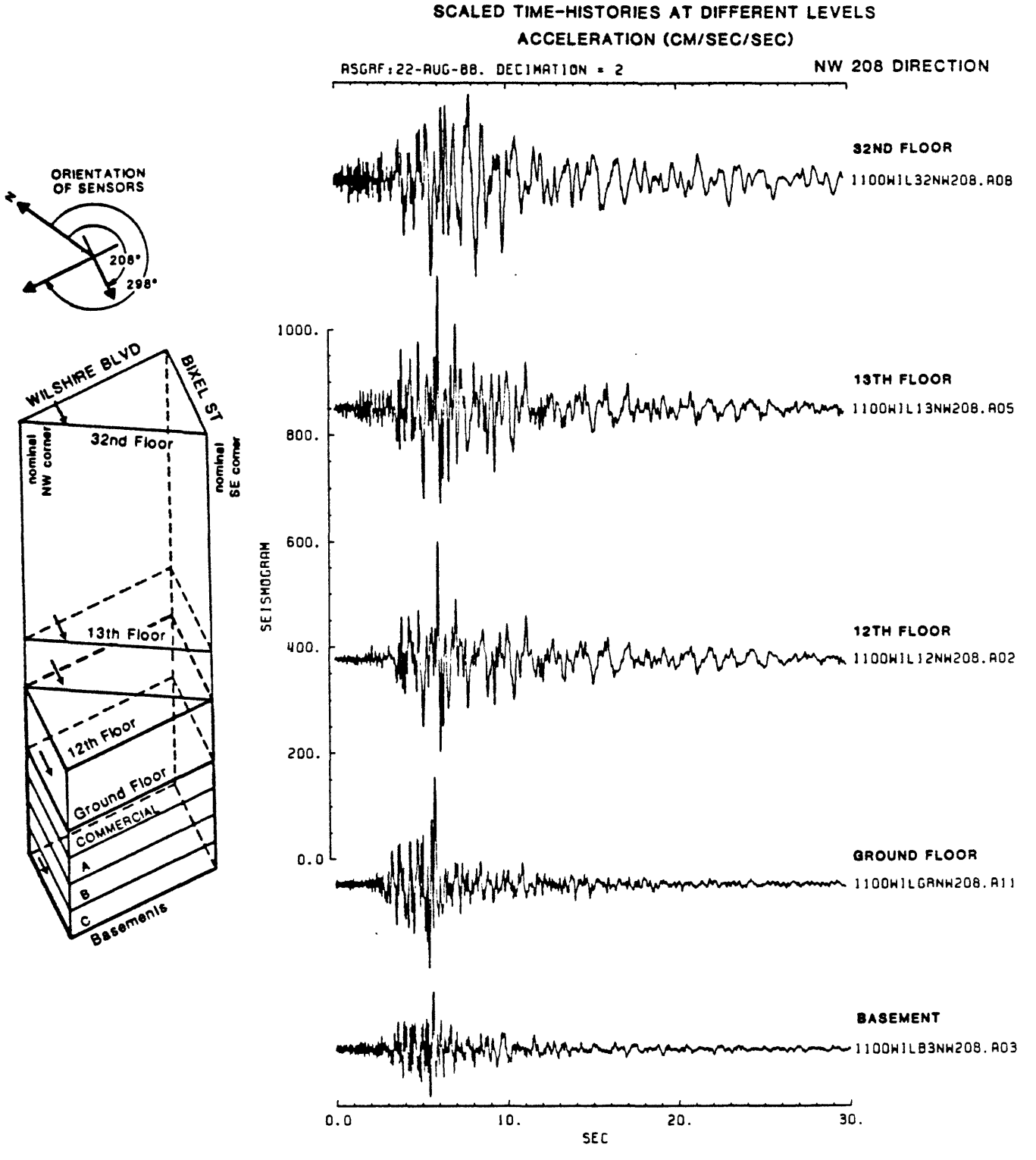

Figure 4.2. Equiscaled plots of acceleration records grouped according to their orientations (NW208 direction).

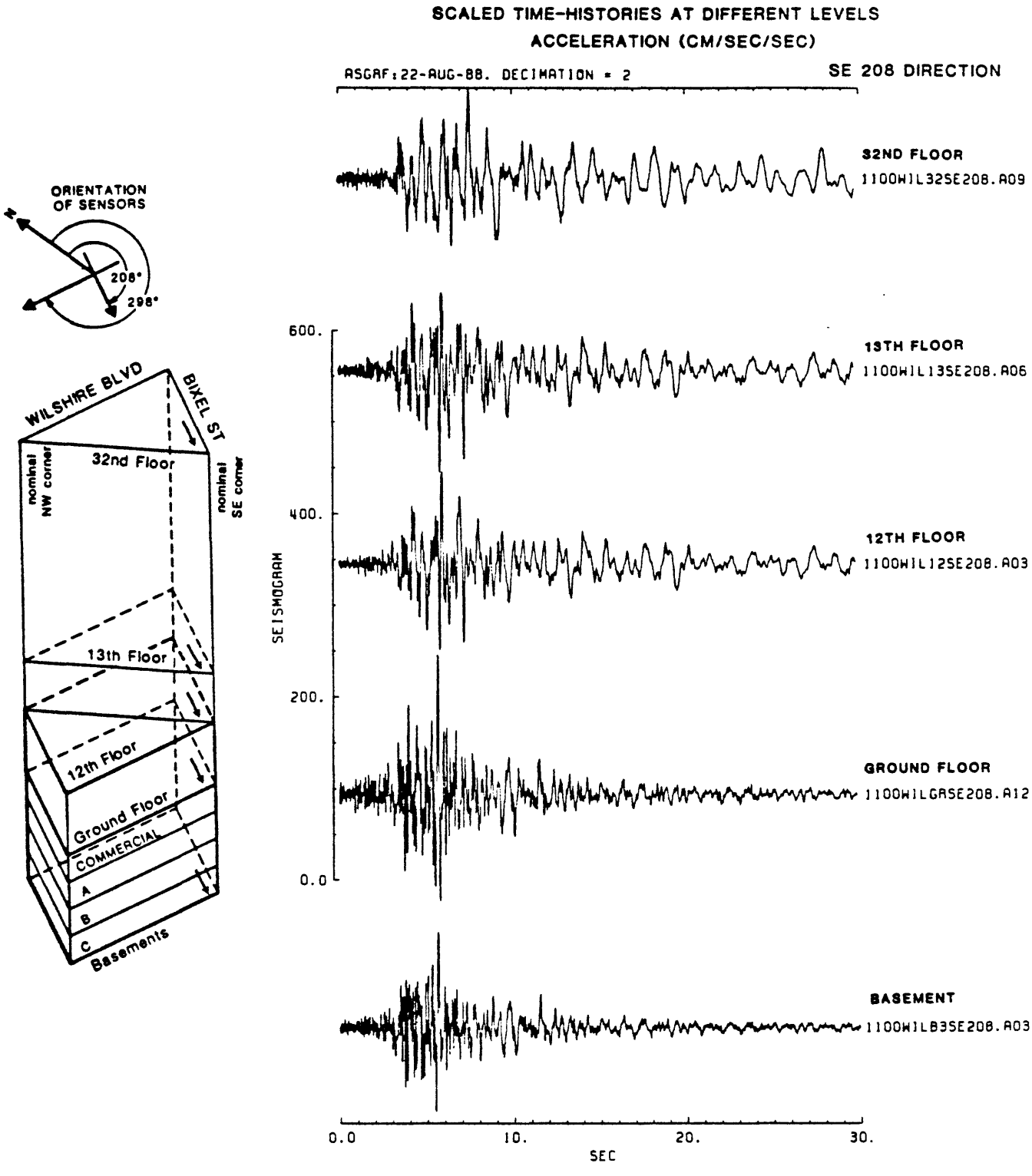

Figure 4.3. Equiscaled plots of acceleration records grouped according to their orientations (SE208 direction).

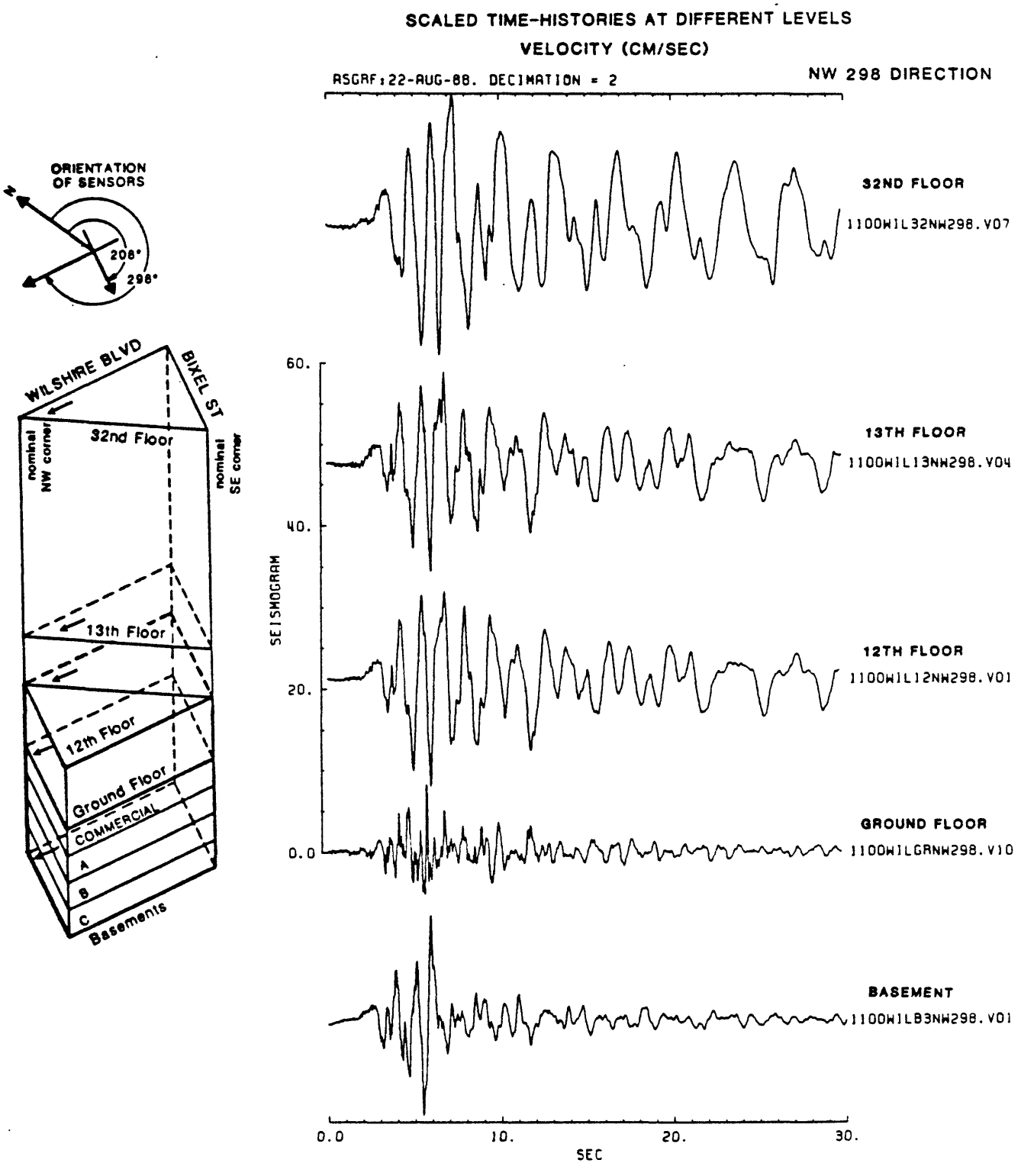

Figure 4.4. Equiscaled plots of velocity records grouped according to their orientations (NW298 direction).

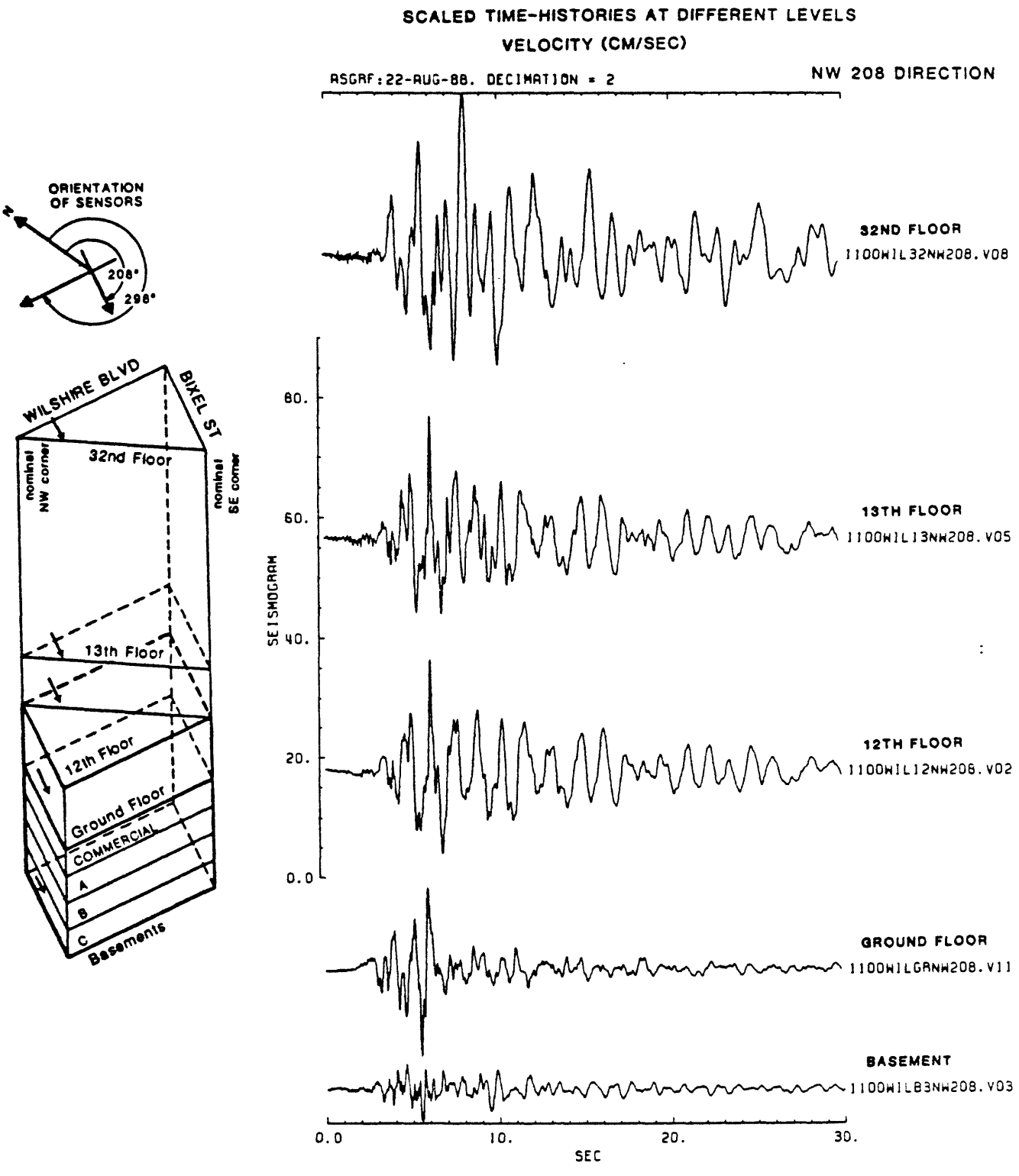

Figure 4.5. Equiscaled plots of velocity records grouped according to their orientations (NW208 direction).

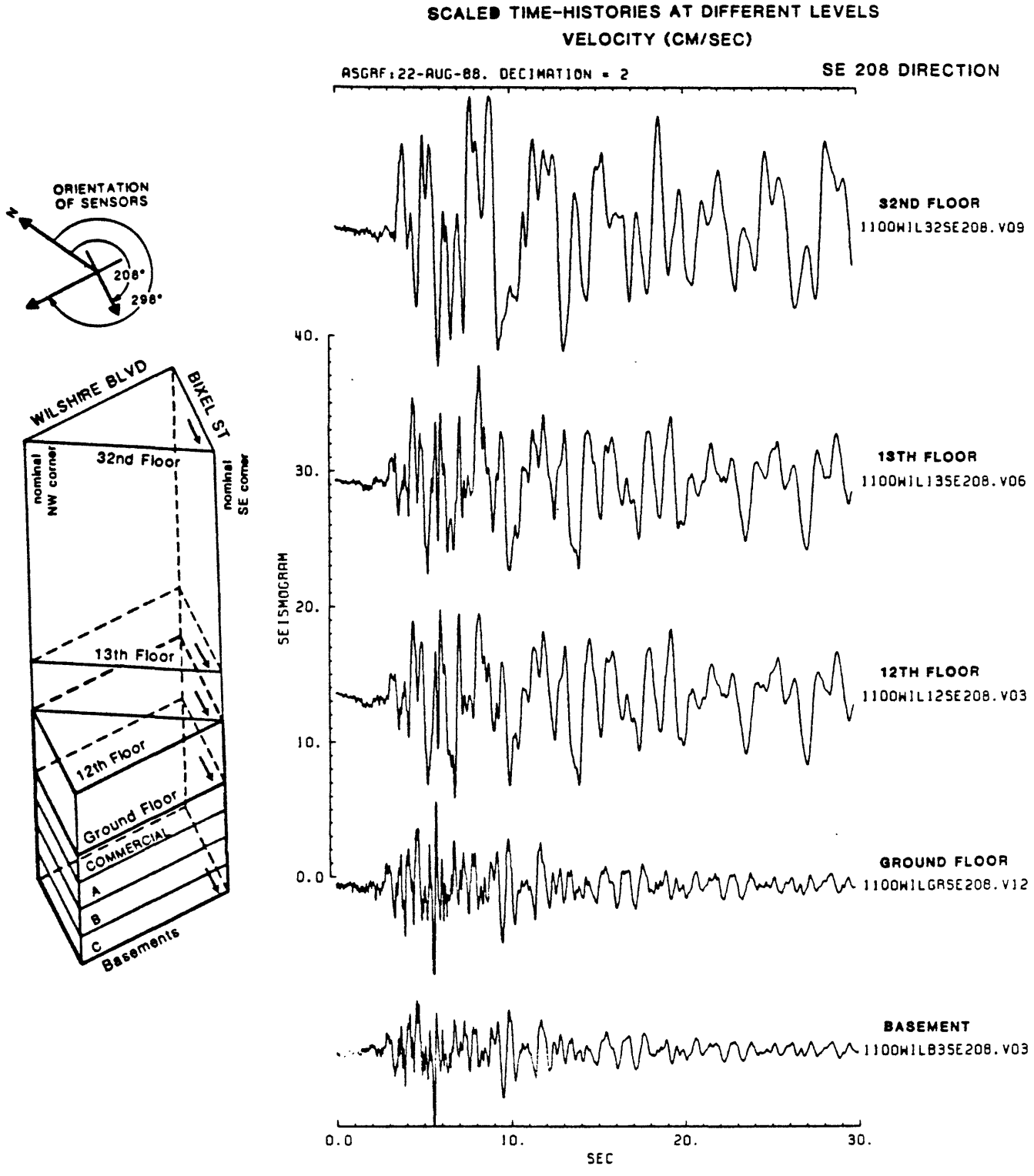

Figure 4.6. Equiscaled plots of velocity records grouped according to their orientations (SE208 direction).

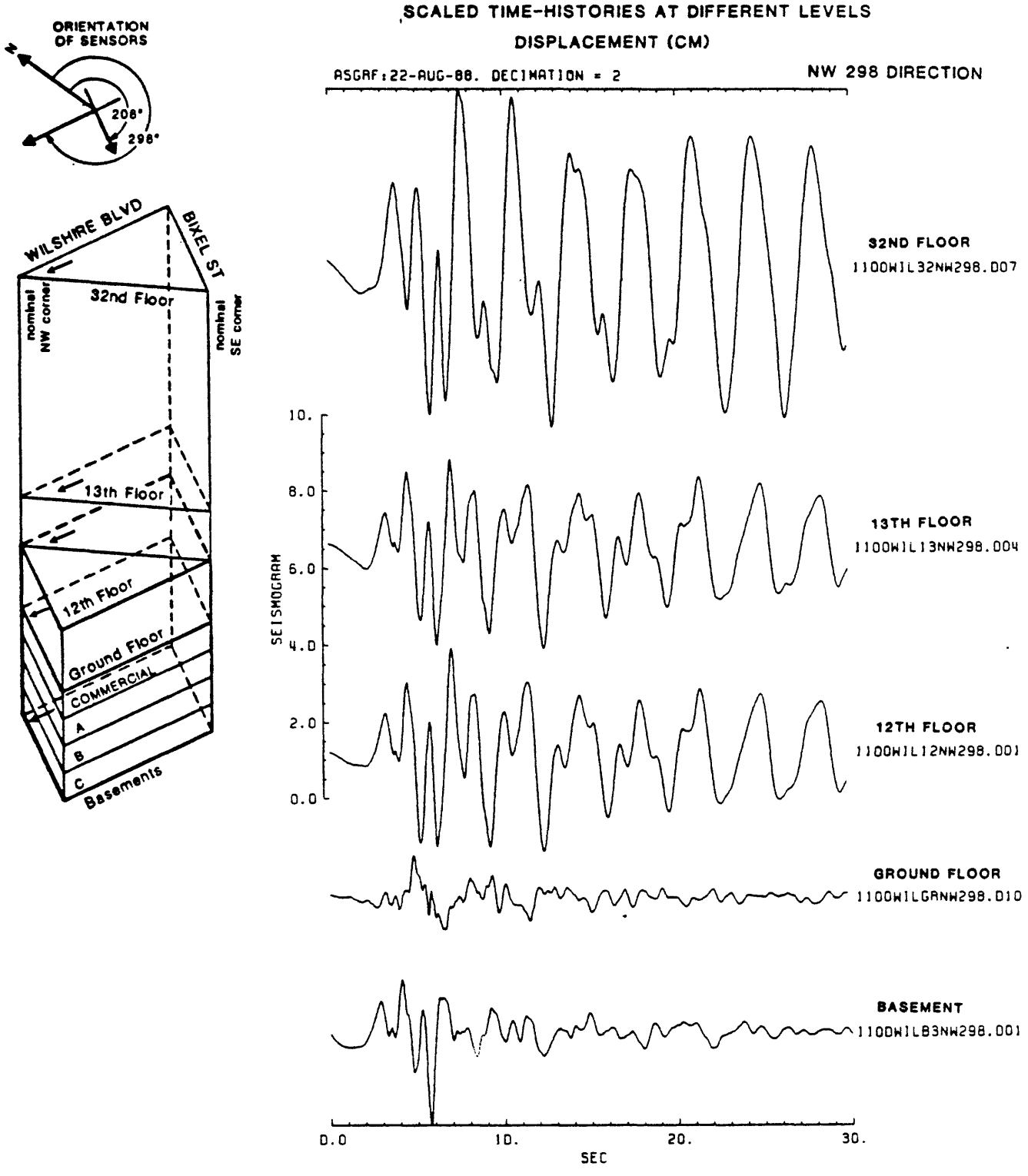

Figure 4.7. Equiscaled plots of displacement records grouped according to their orientations (NW298 direction).

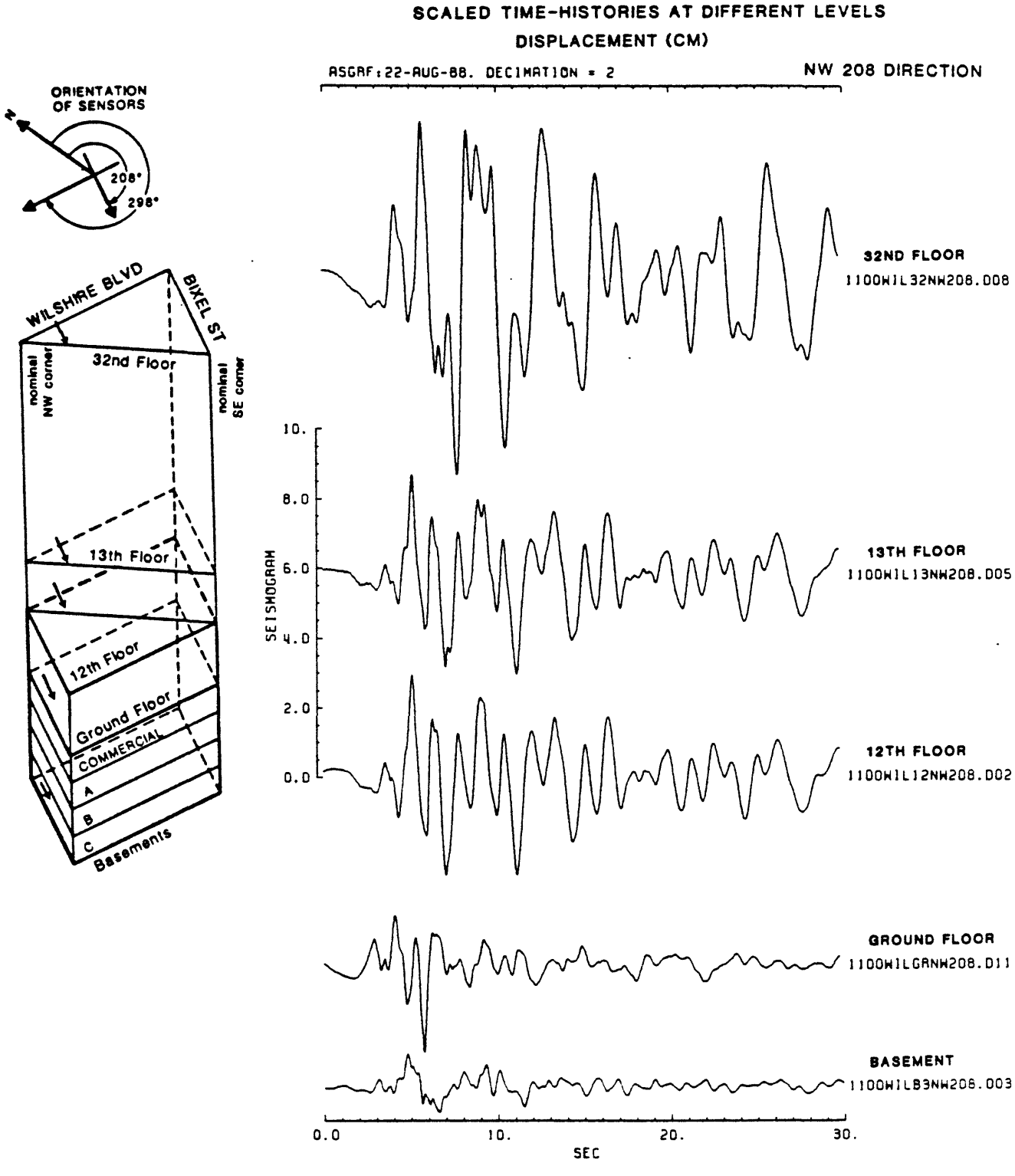

Figure 4.8. Equiscaled plots of displacement records grouped according to their orientations (NW208 direction).

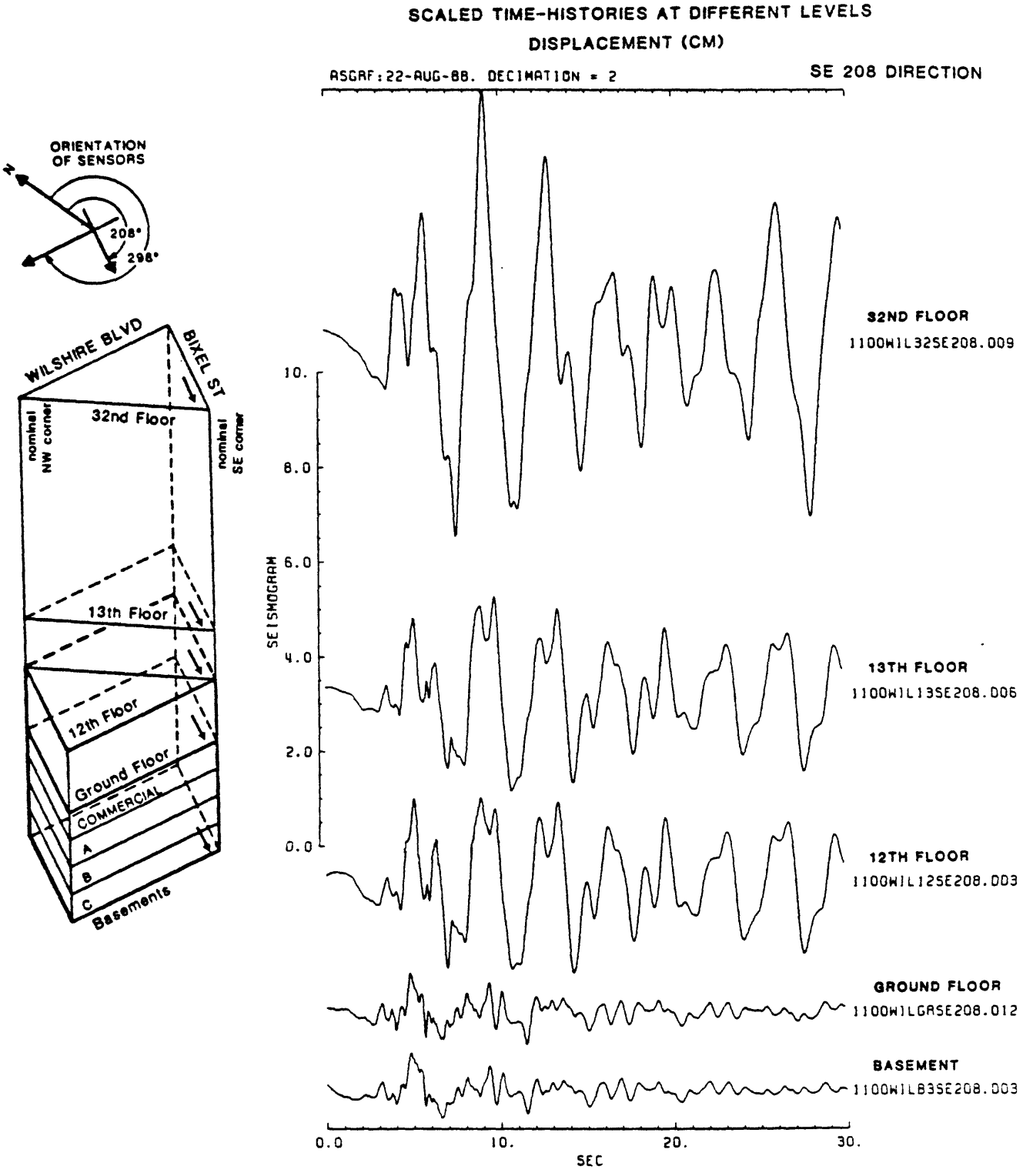

Figure 4.9. Equiscaled plots of displacement records grouped according to their orientations (SE208 direction).

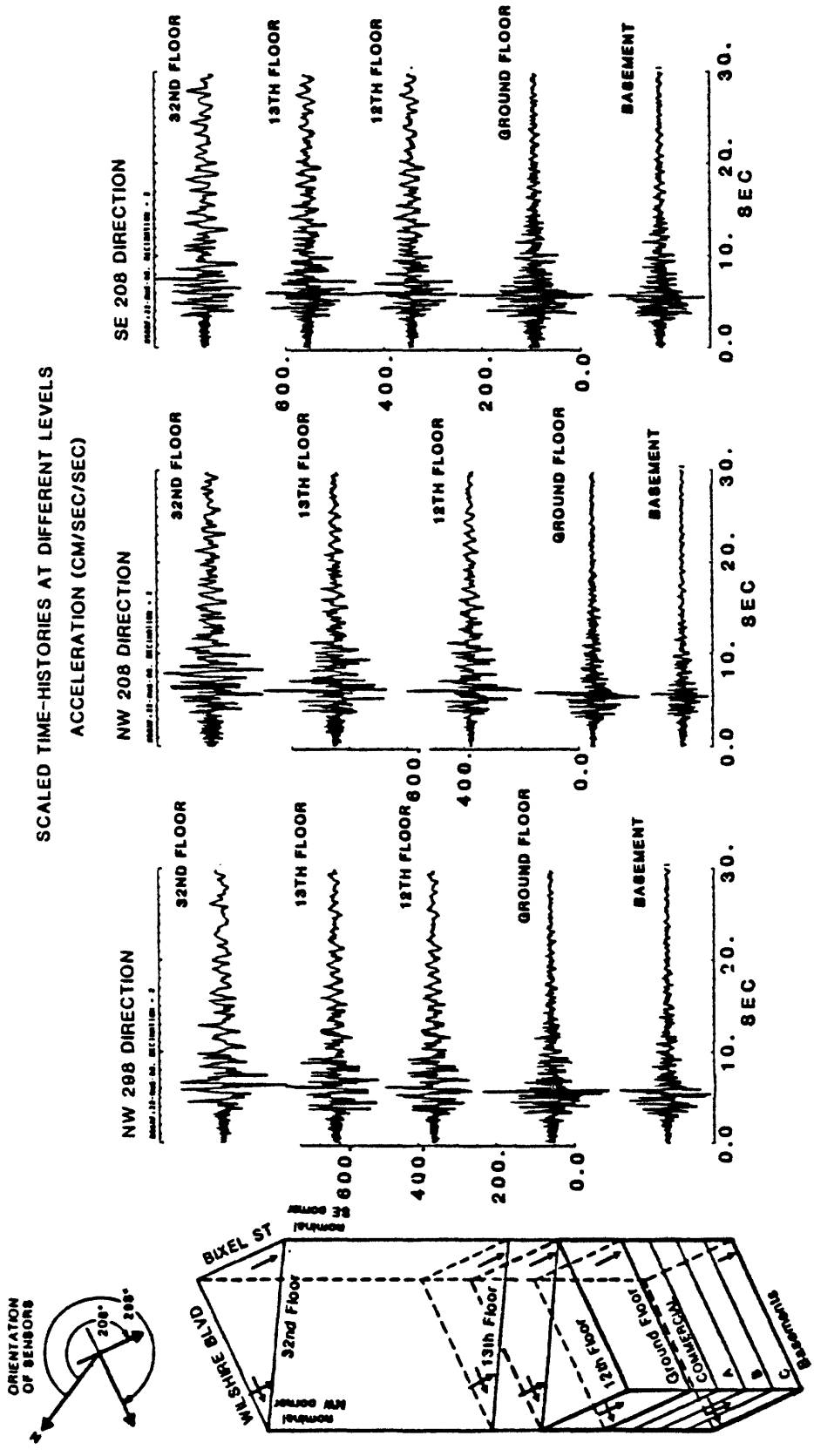

Figure 4.10. Summary equiscaled plots of acceleration records grouped according to their orientations (NW298, NW208 and SE208 directions).

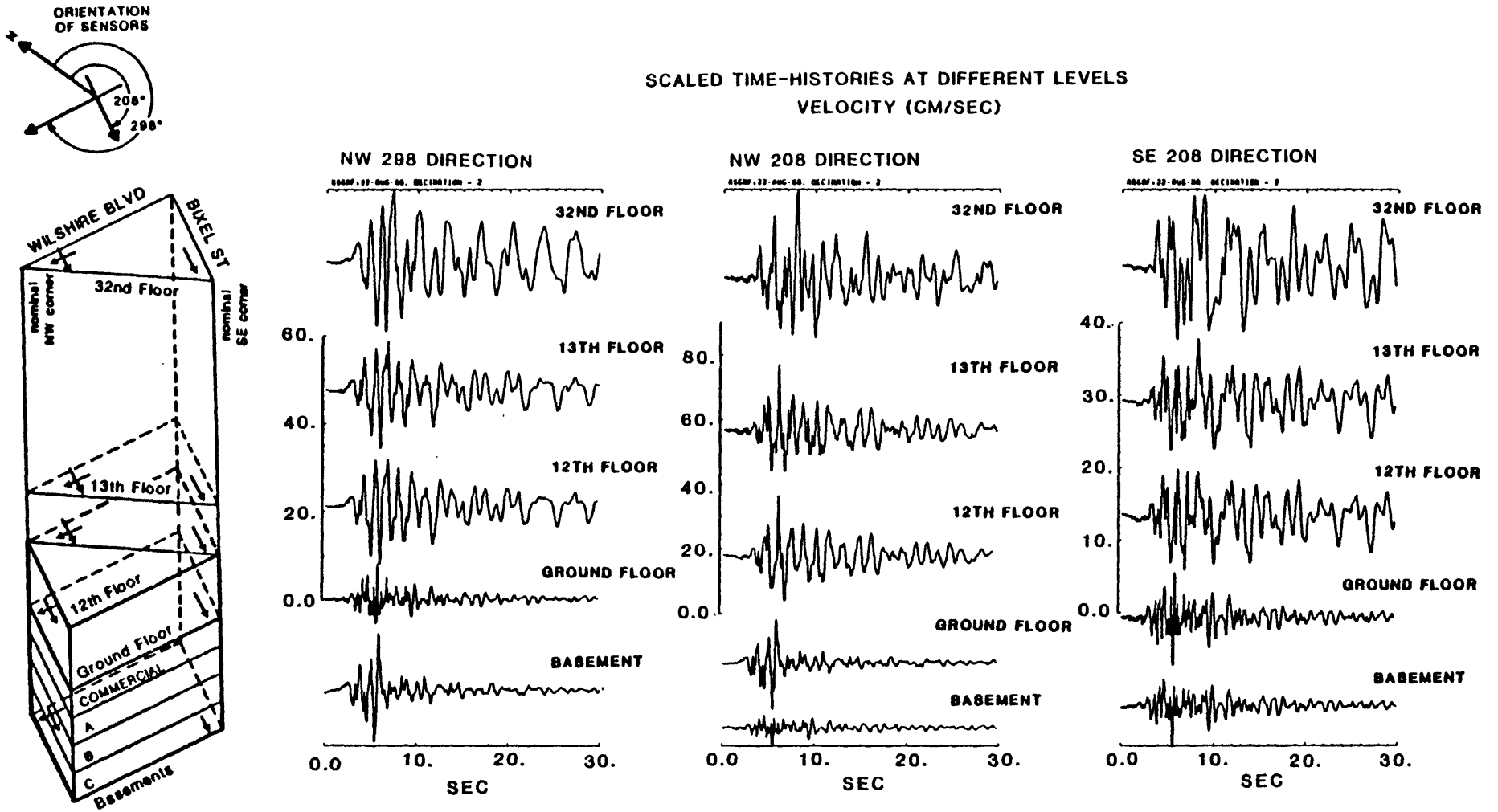

Figure 4.11. Summary equiscaled plots of velocity records grouped according to their orientations (NW298, NW208 and SE208 directions).

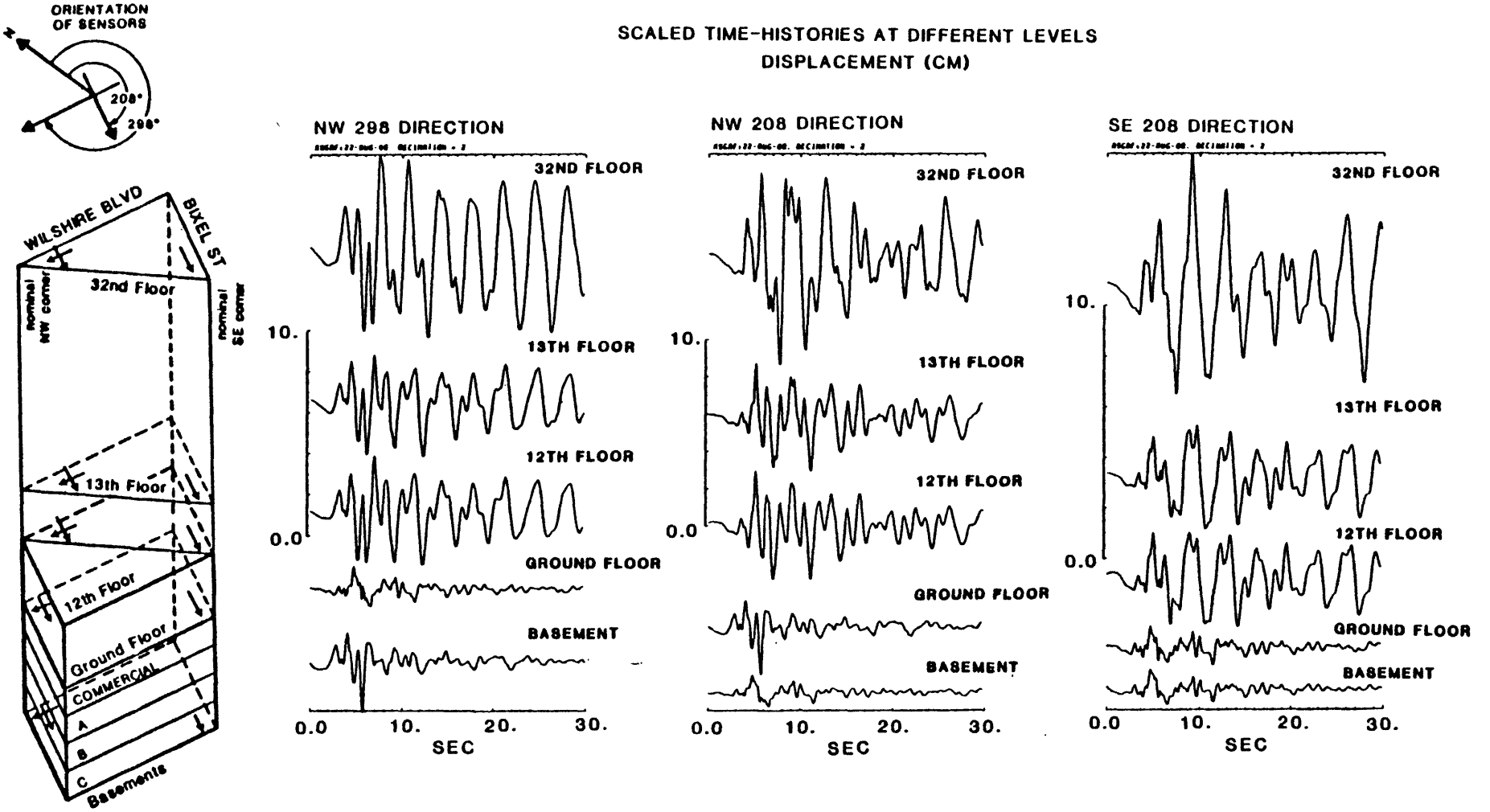

Figure 4.12. Summary equiscaled plots of displacement records grouped according to their orientations (NW298, NW208 and SE208 directions).

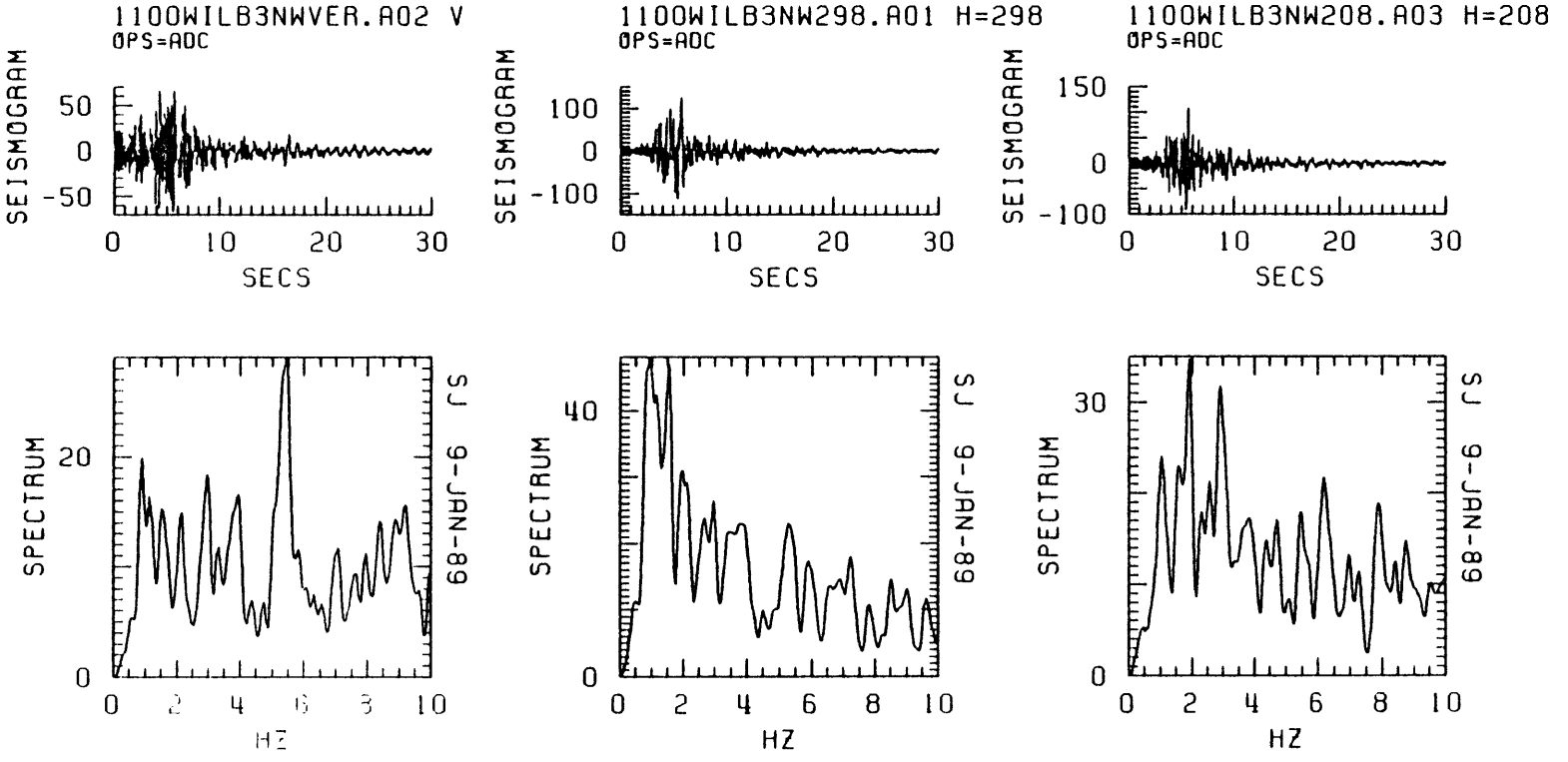

Figure 4.13. Acceleration seismograms from the tri-axial accelerograph at the NW location of the basement. Vertical, NW298 and NW208 components and their Fourier amplitude spectra are shown.

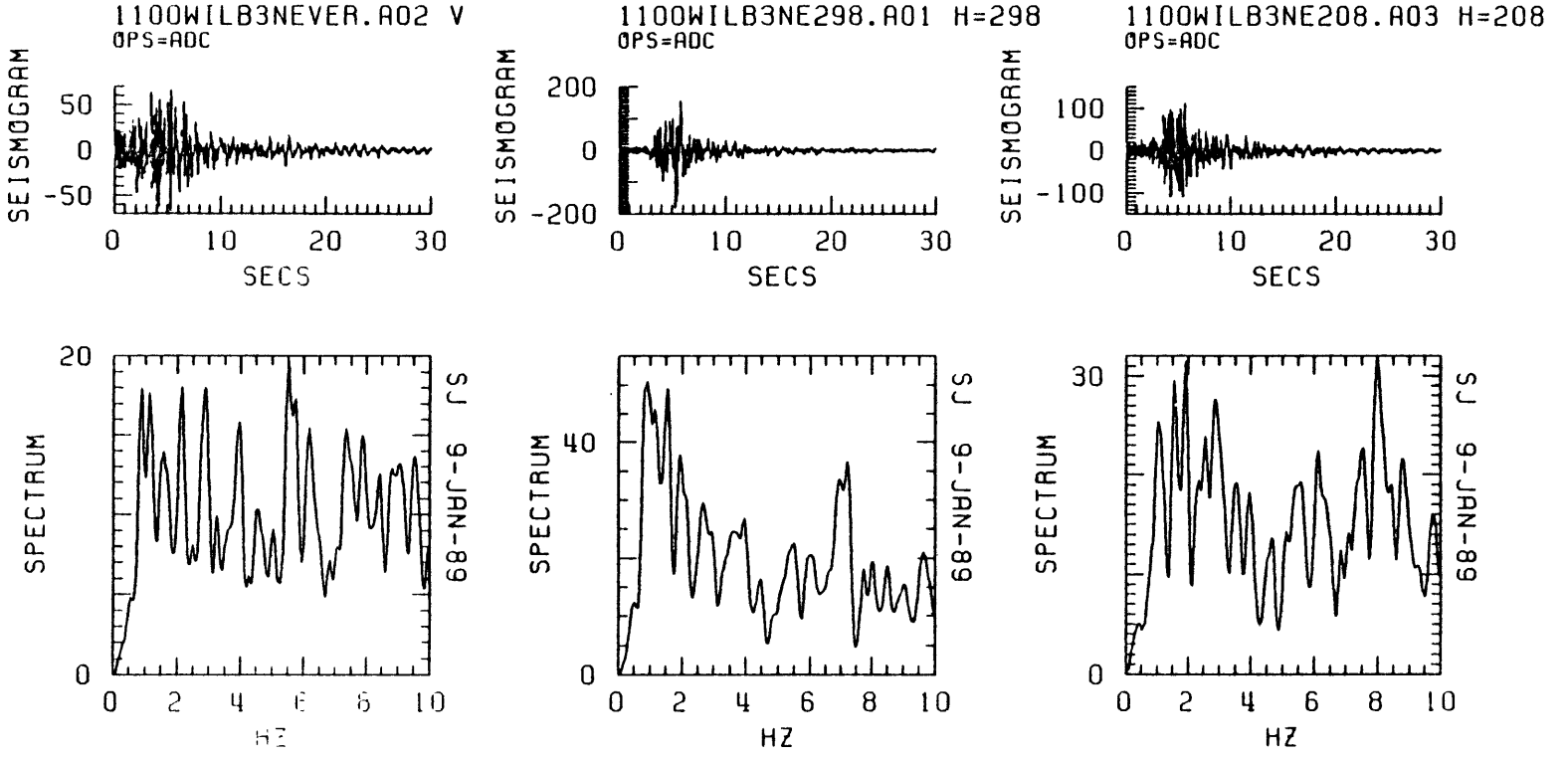

Figure 4.14. Acceleration seismograms from the tri-axial accelerograph at the NE location of the basement. Vertical, NE298 and NE208 components and their Fourier amplitude spectra are shown.

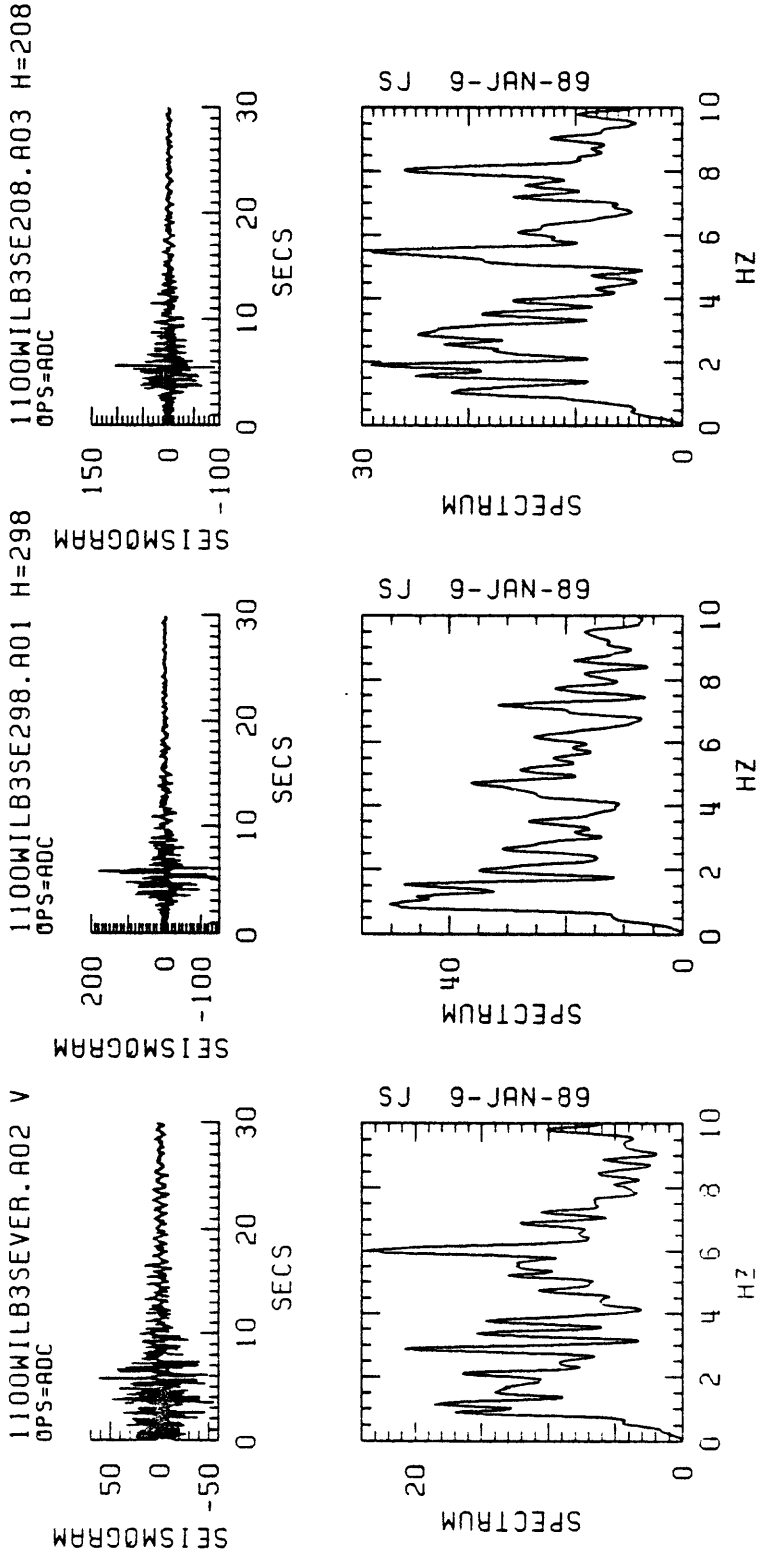

Figure 4.15. Acceleration seismograms from the tri-axial accelerograph at the SE location of the basement. Vertical, SE298 and SE208 components and their Fourier amplitude spectra are shown.

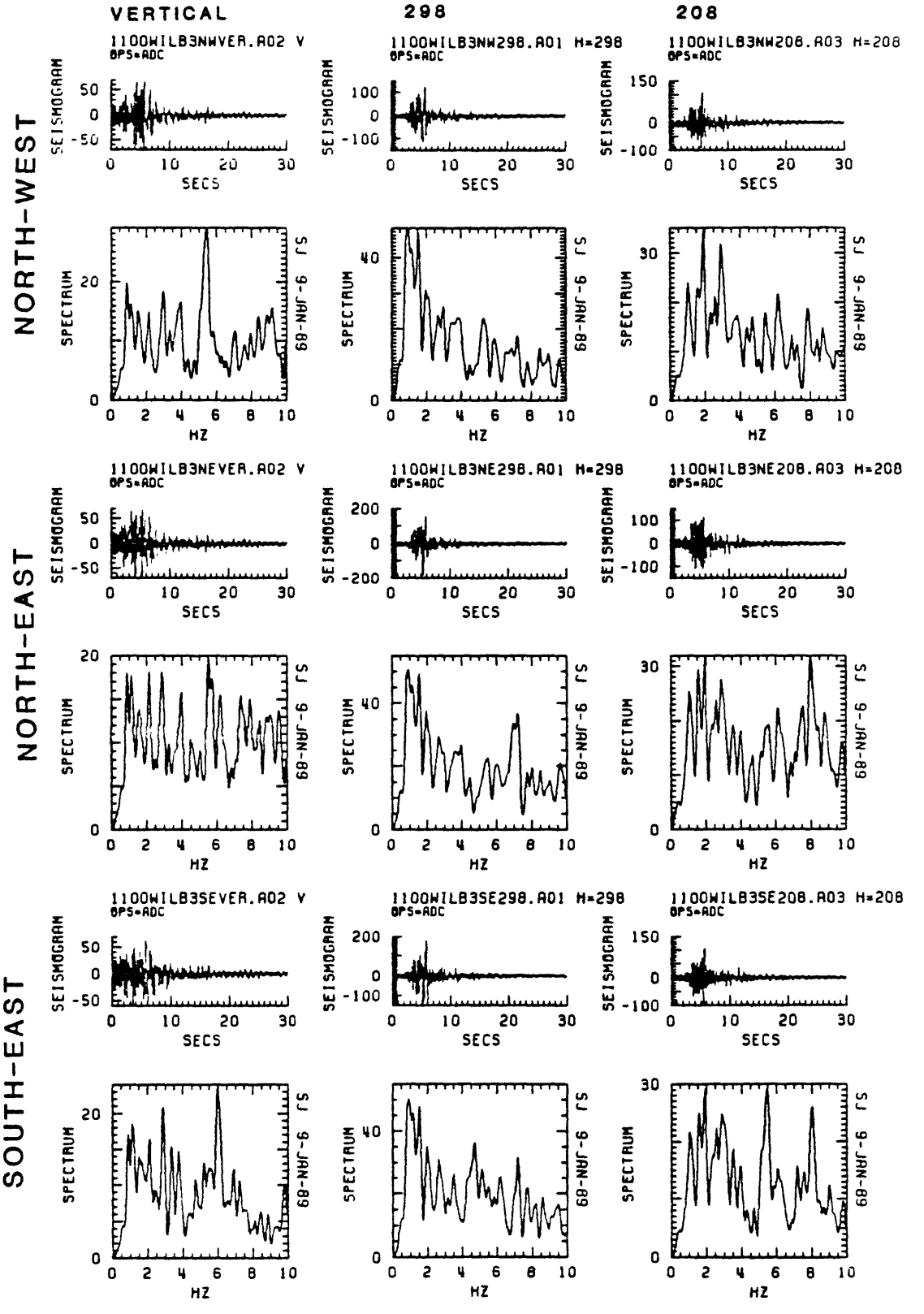

Figure 4.16. Acceleration seismograms from the tri-axial accelerographs at the three locations of the basement (NW, NE and SE). Fourier amplitude spectra are derived with total record window.

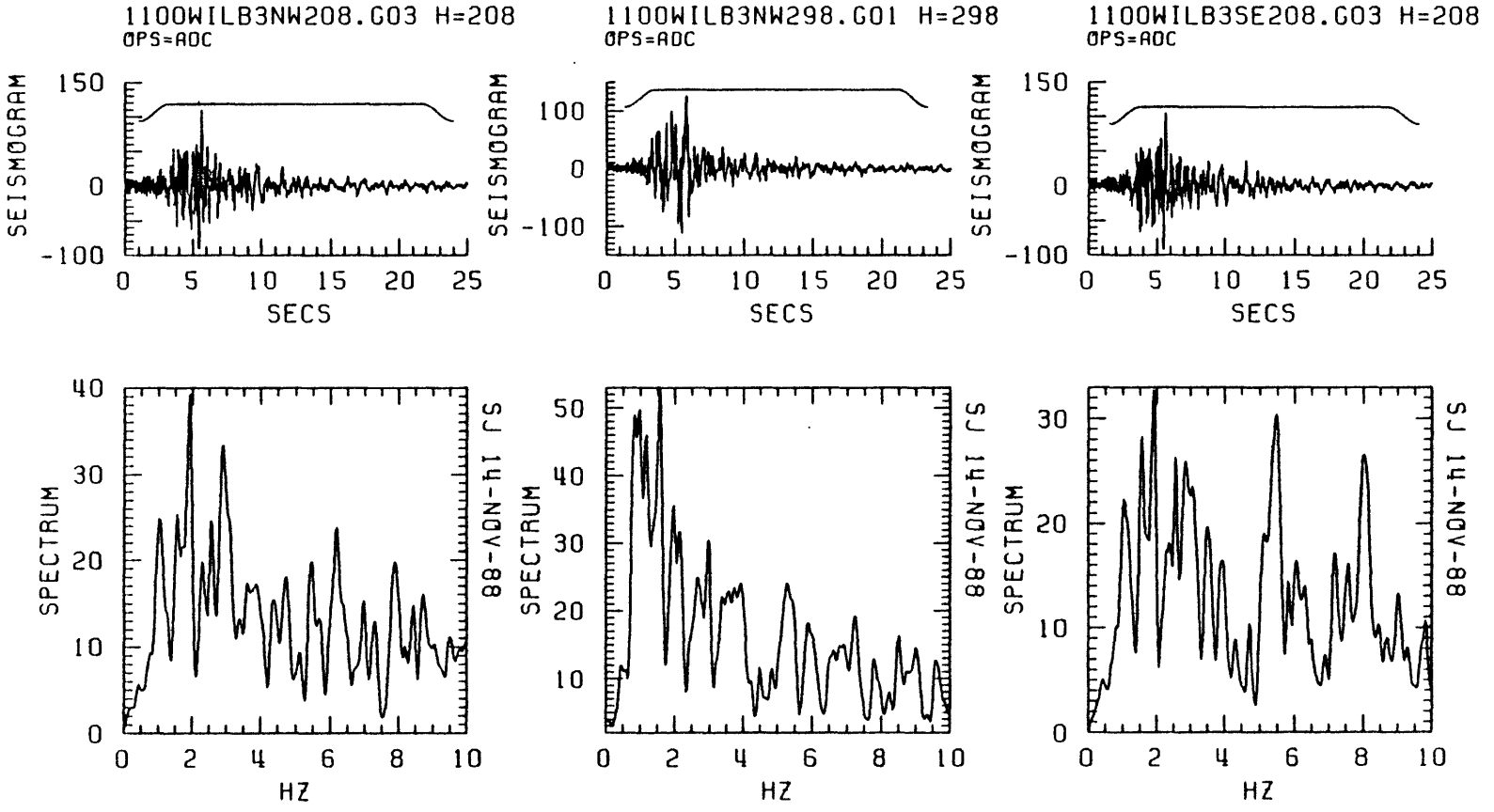

Figure 4.18. Total record duration window of acceleration seismograms from the basement (NW208, NW298 and SE208) locations and corresponding Fourier amplitude spectra.

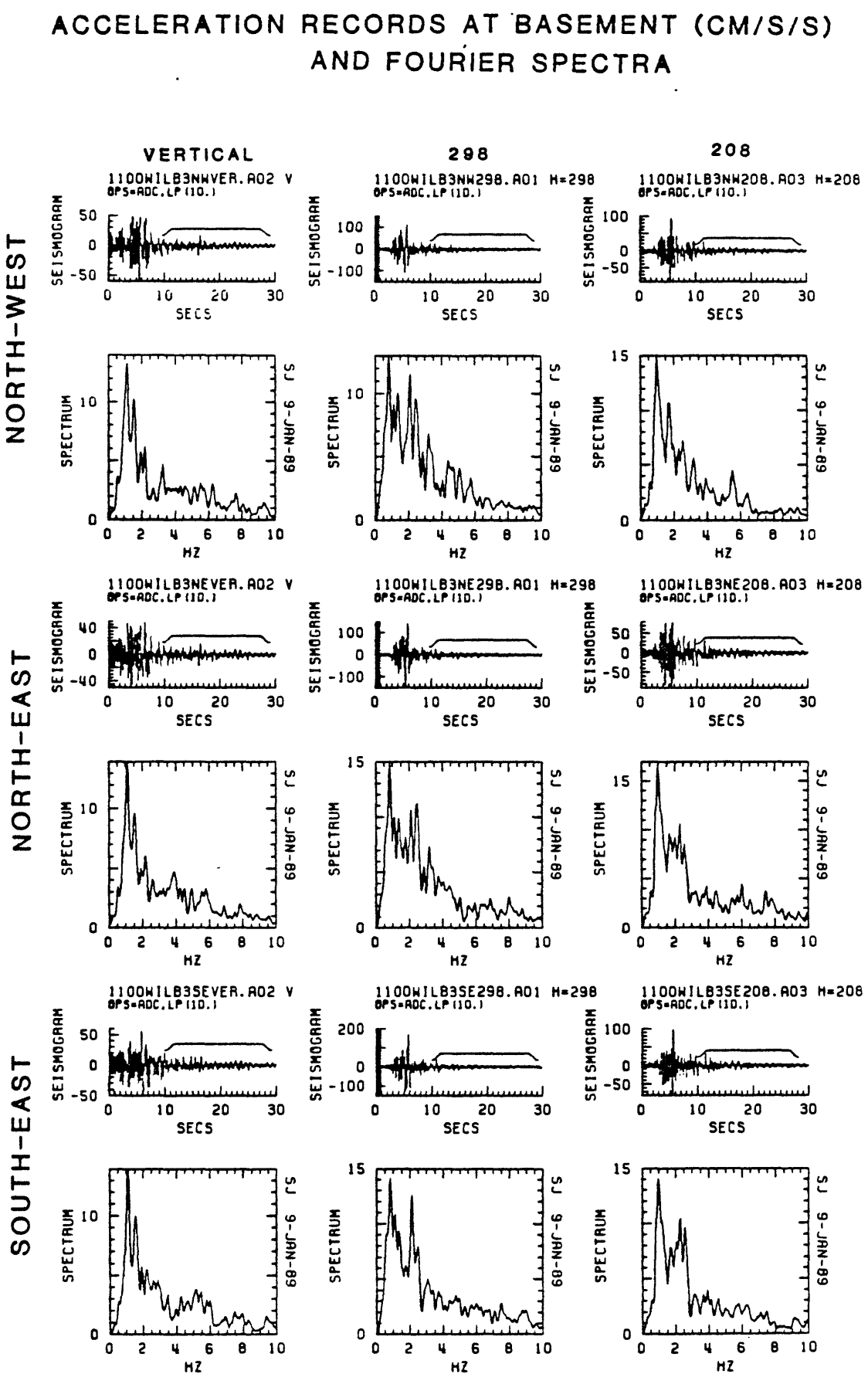

Figure 4.17. Acceleration seismograms from the tri-axial accelerographs at the three locations of the basement (NW, NE and SE). Windows of the records used to derive the Fourier amplitude spectra are shown.

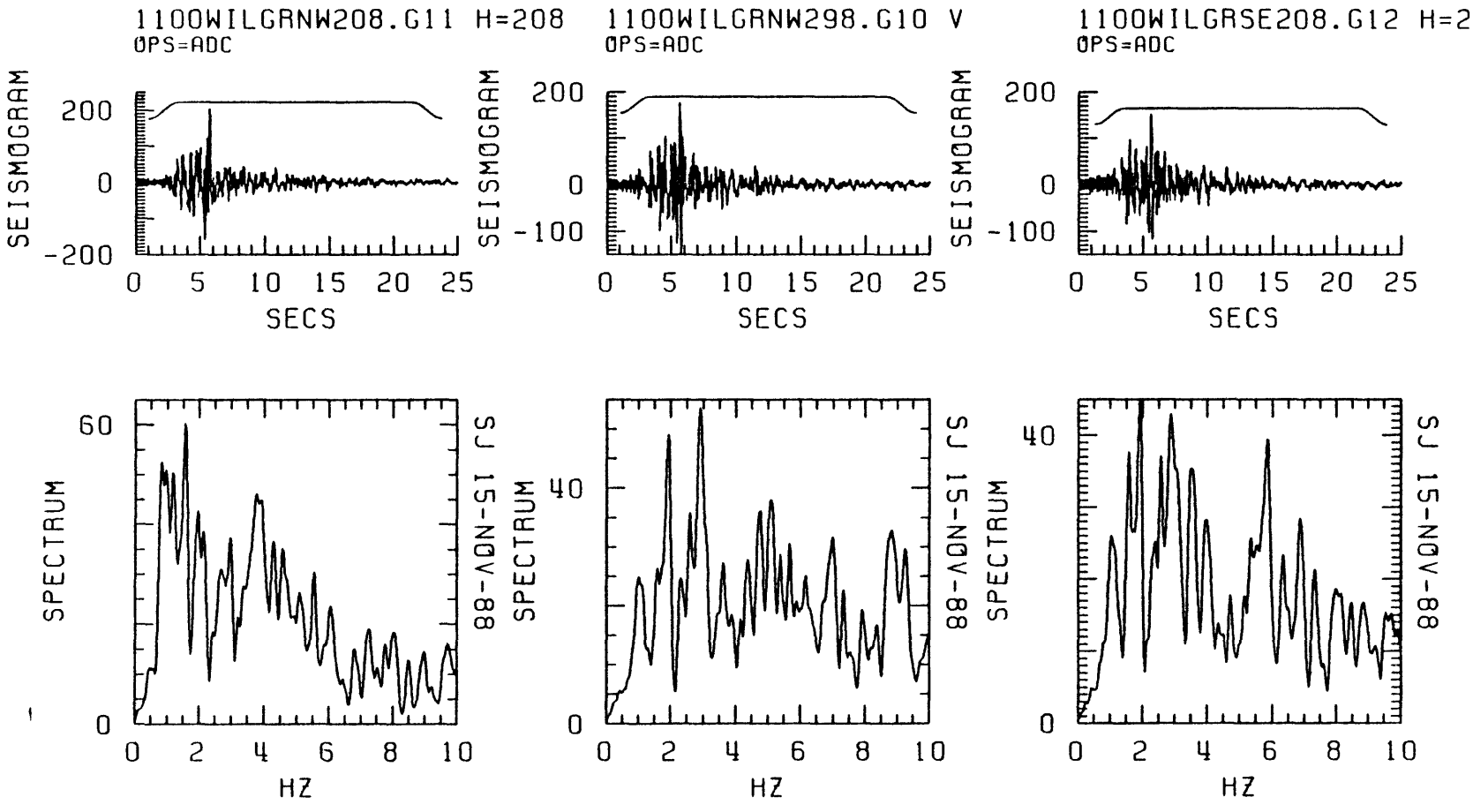

Figure 4.19. Total record duration window of acceleration seismograms from the ground level (NW208, NW298 and SE208) locations and corresponding Fourier amplitude spectra.

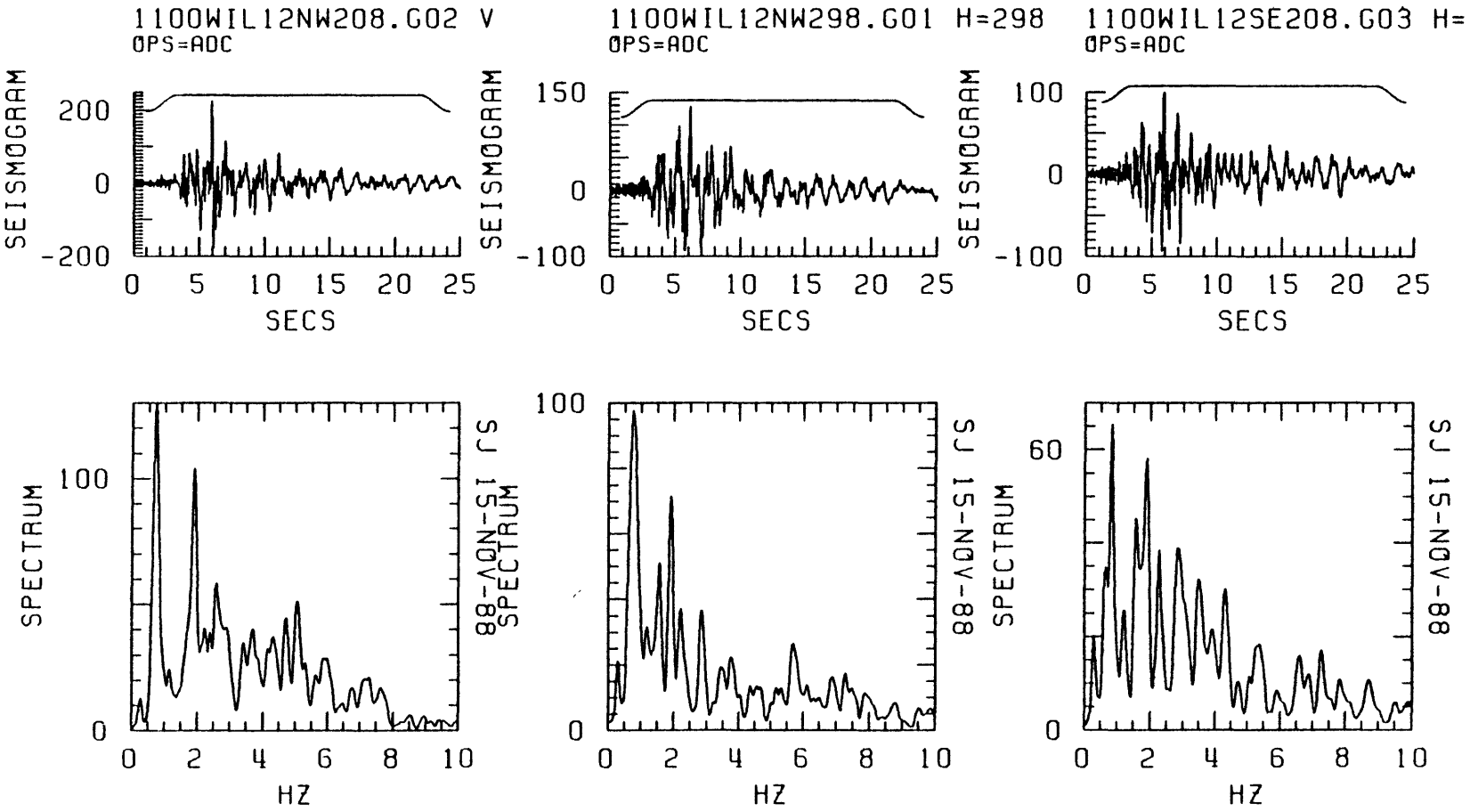

Figure 4.20. Total record duration window of acceleration seismograms from the 12th floor (NW208, NW298 and SE208) locations and corresponding Fourier amplitude spectra.

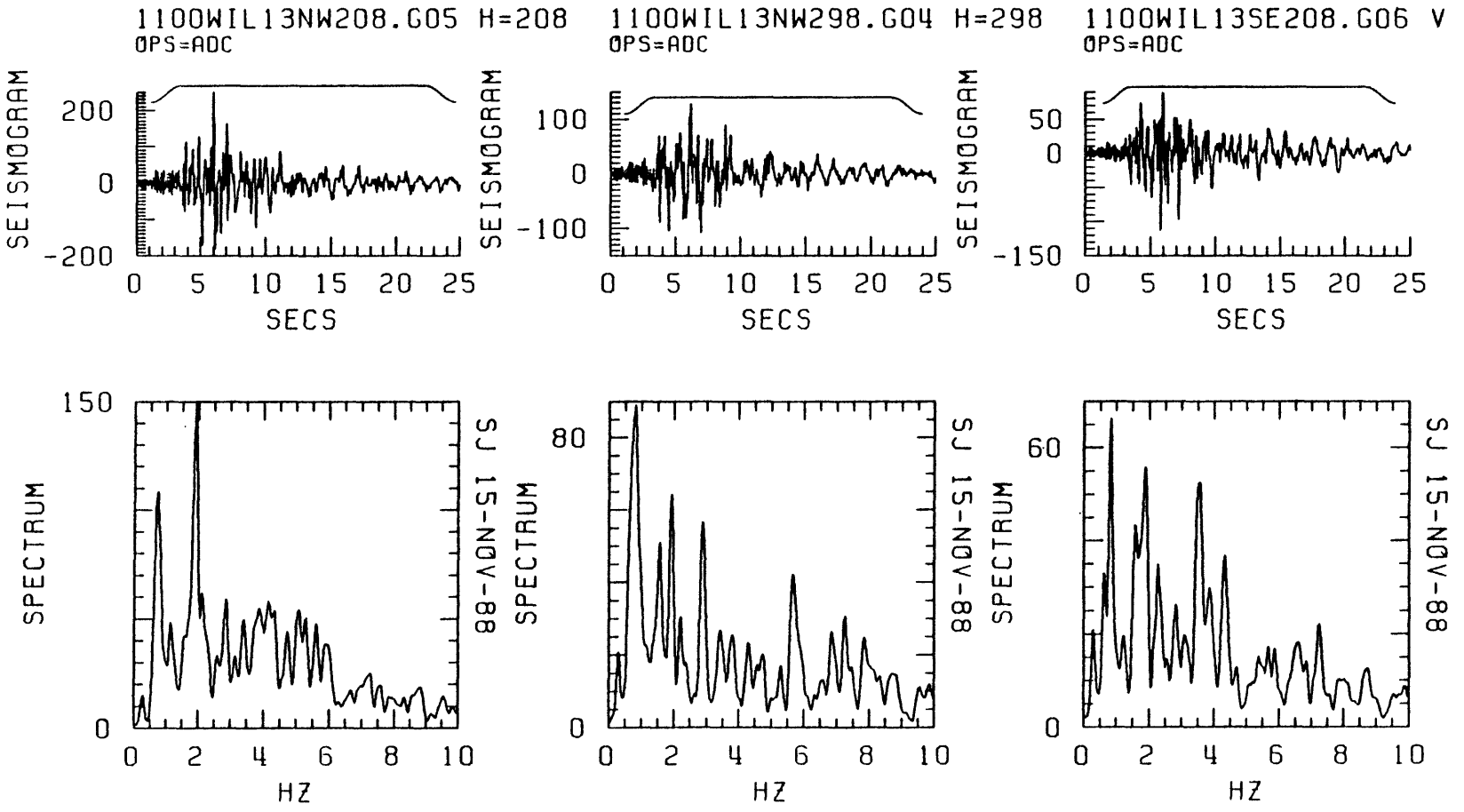

Figure 4.21. Total record duration window of acceleration seismograms from the 13th floor (NW208, NW298 and SE208) locations and corresponding Fourier amplitude spectra.

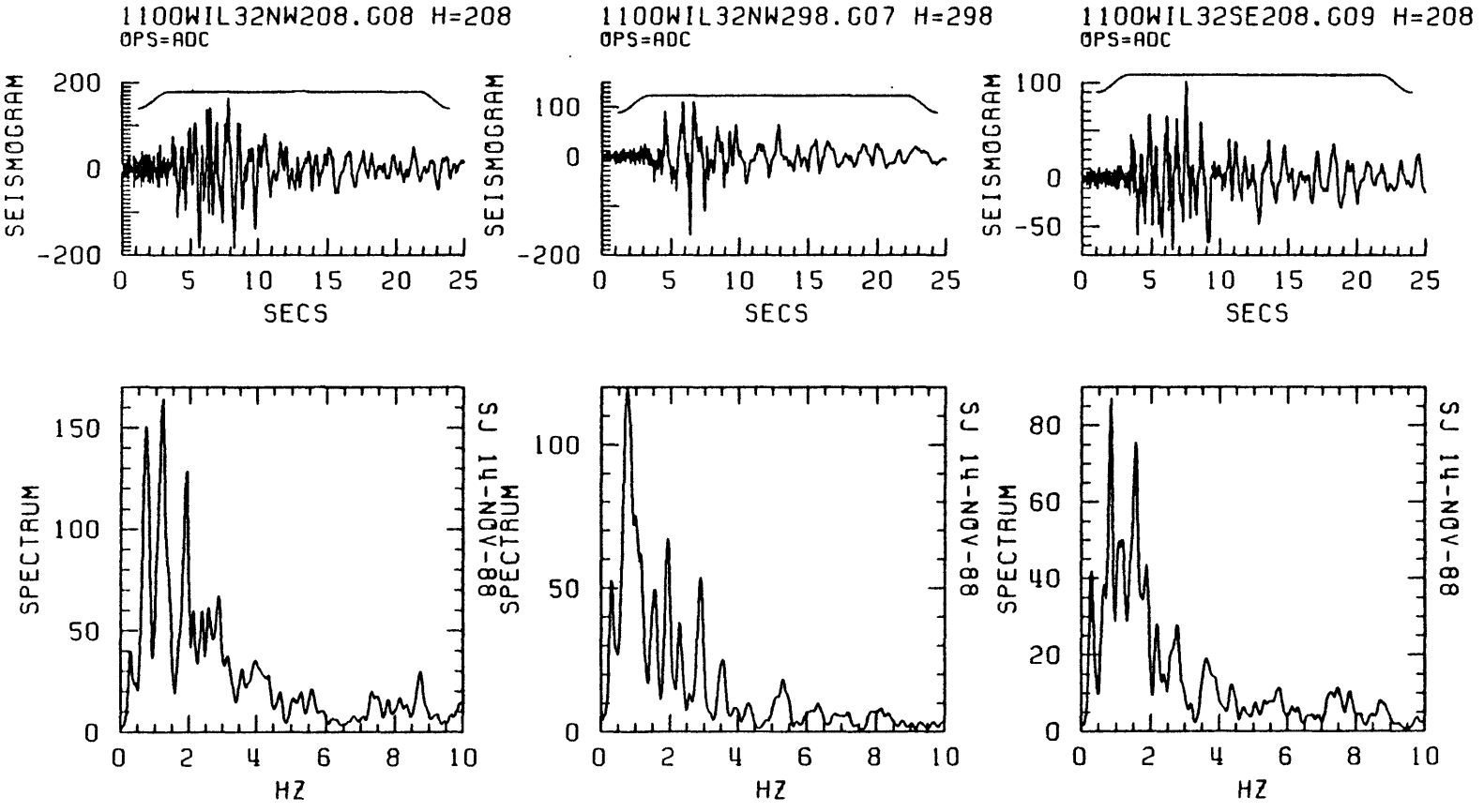

Figure 4.22. Total record duration window of acceleration seismograms from the 32nd floor (NW208, NW298 and SE208) locations and corresponding Fourier amplitude spectra.

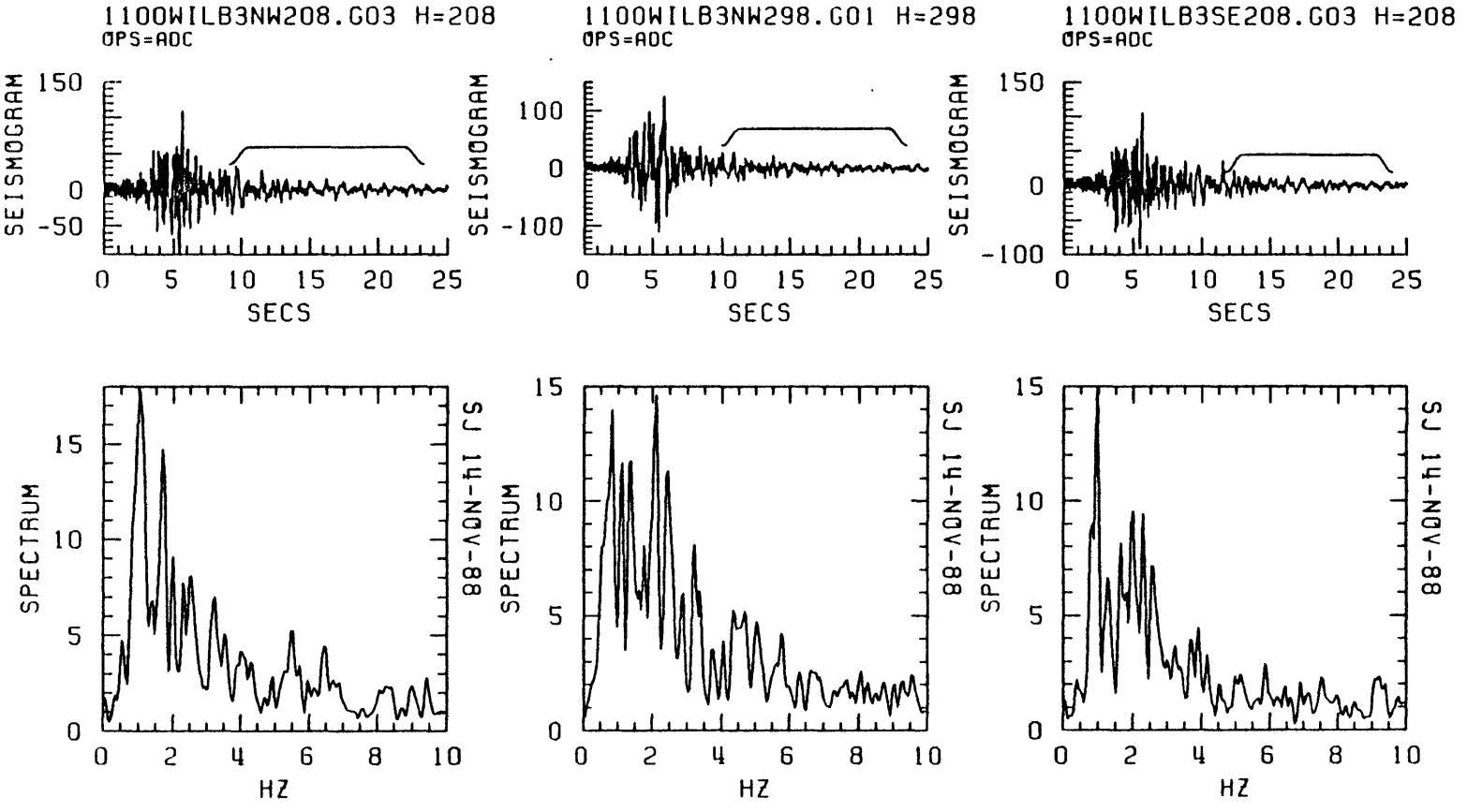

Figure 4.23. Acceleration seismograms with time windows beyond the peaks of the records from the basement (NW208, NW298 and SE208) locations and corresponding Fourier amplitude spectra.

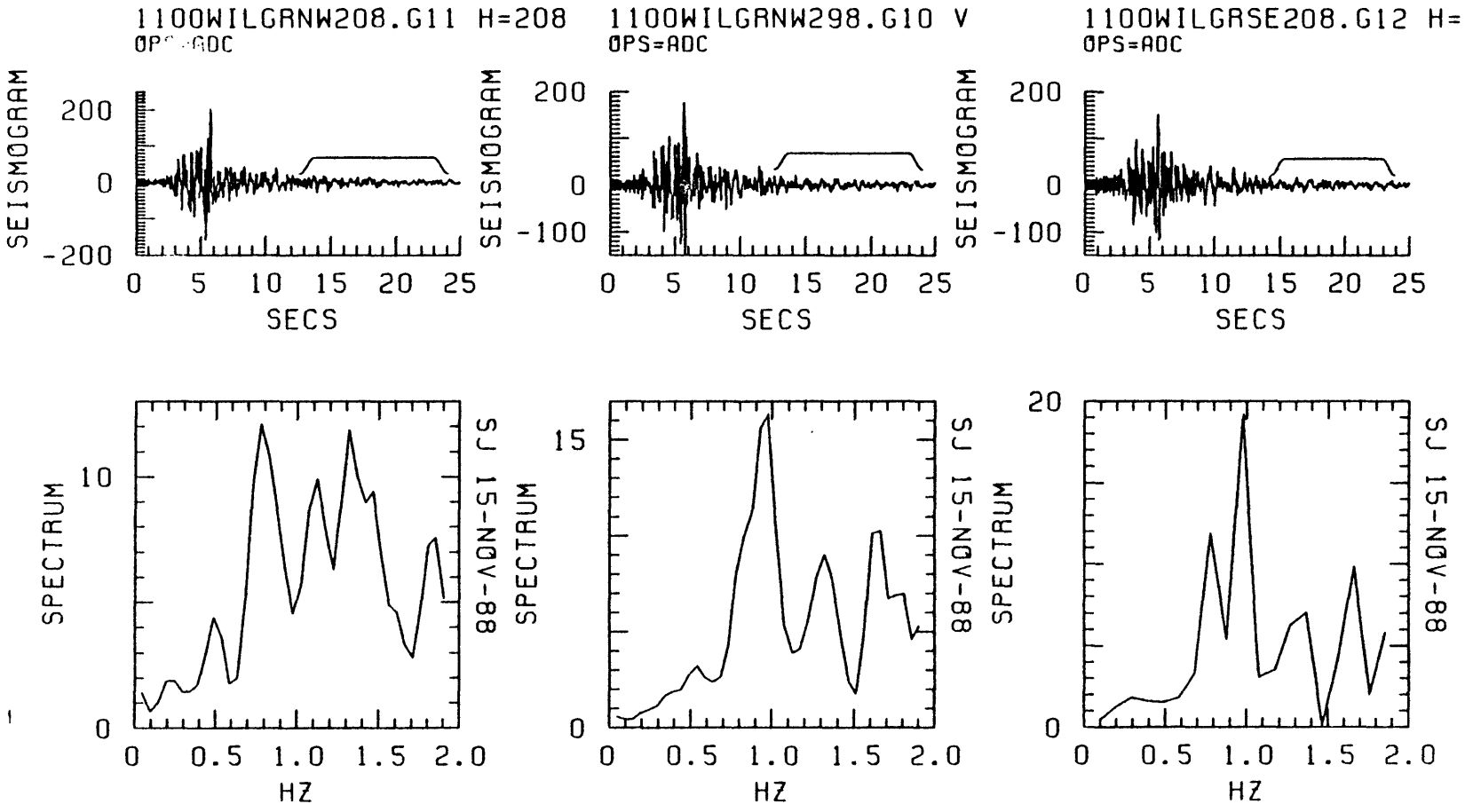

Figure 4.24. Acceleration seismograms with time windows beyond the peaks of the records from the ground level (NW208, NW298 and SE208) locations and corresponding Fourier amplitude spectra.

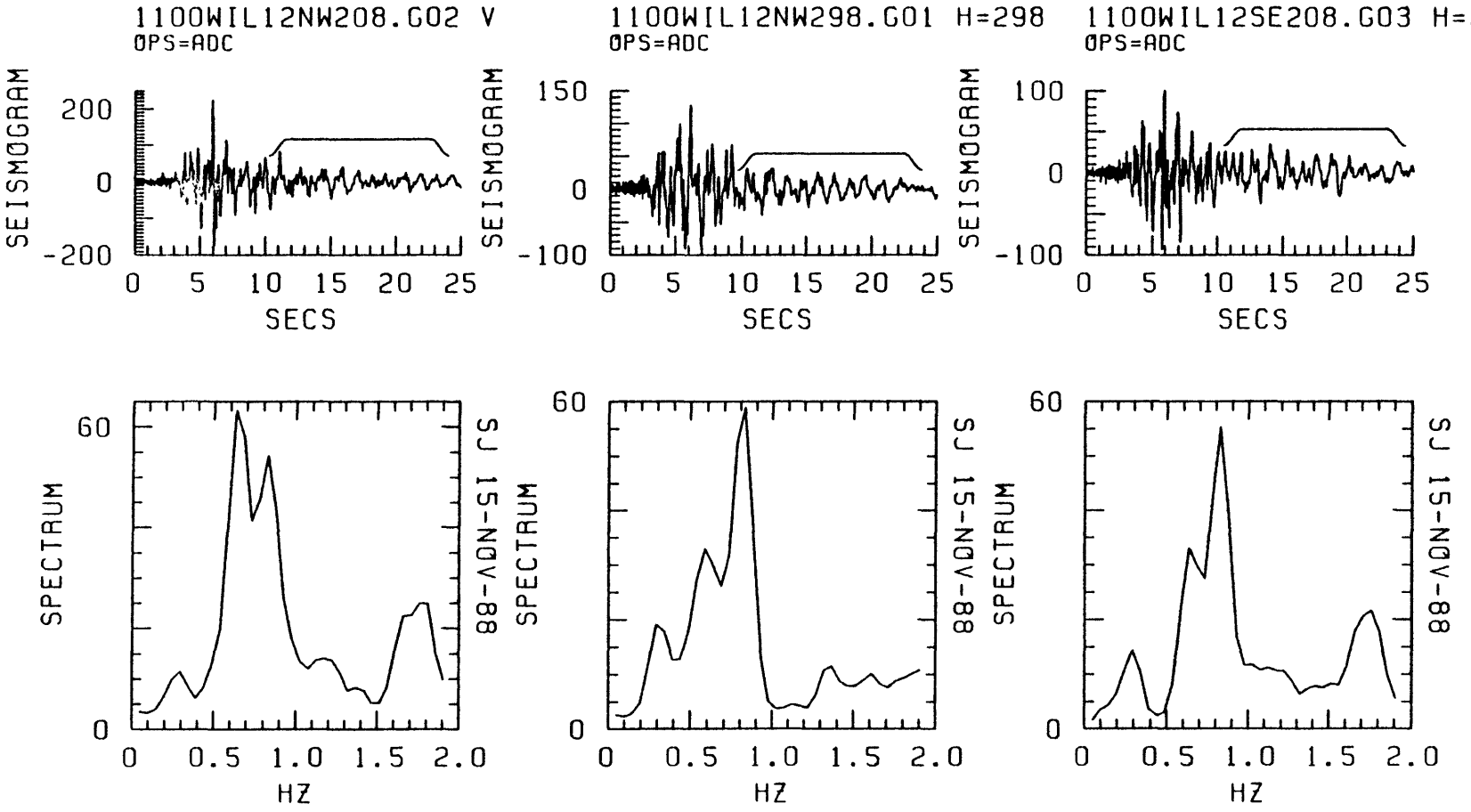

Figure 4.25. Acceleration seismograms with time windows beyond the peaks of the records from the 12th floor (NW208, NW298 and SE208) locations and corresponding Fourier amplitude spectra.

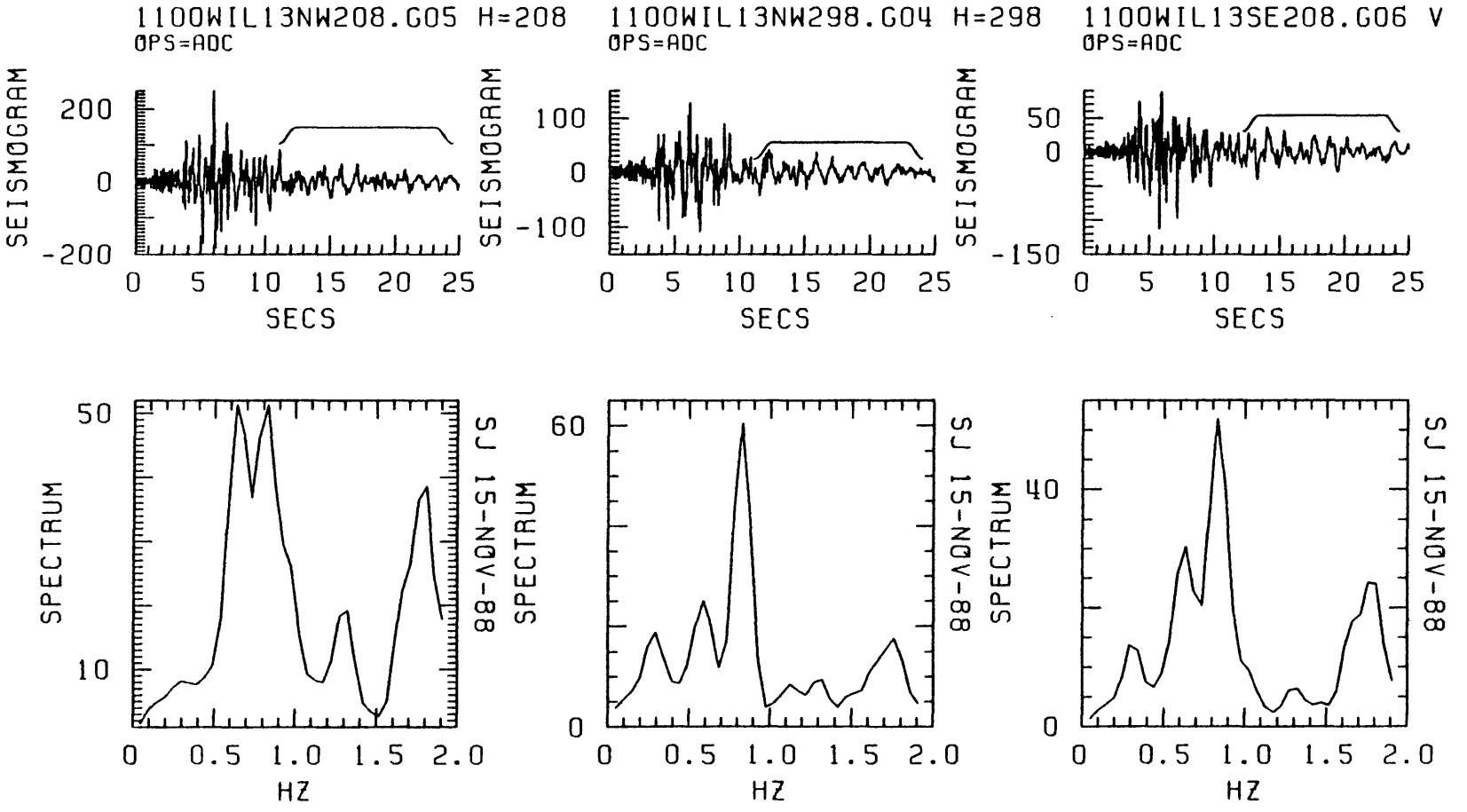

Figure 4.26. Acceleration seismograms with time windows beyond the peaks of the records from the 13th floor (NW208, NW298 and SE208) locations and corresponding Fourier amplitude spectra.

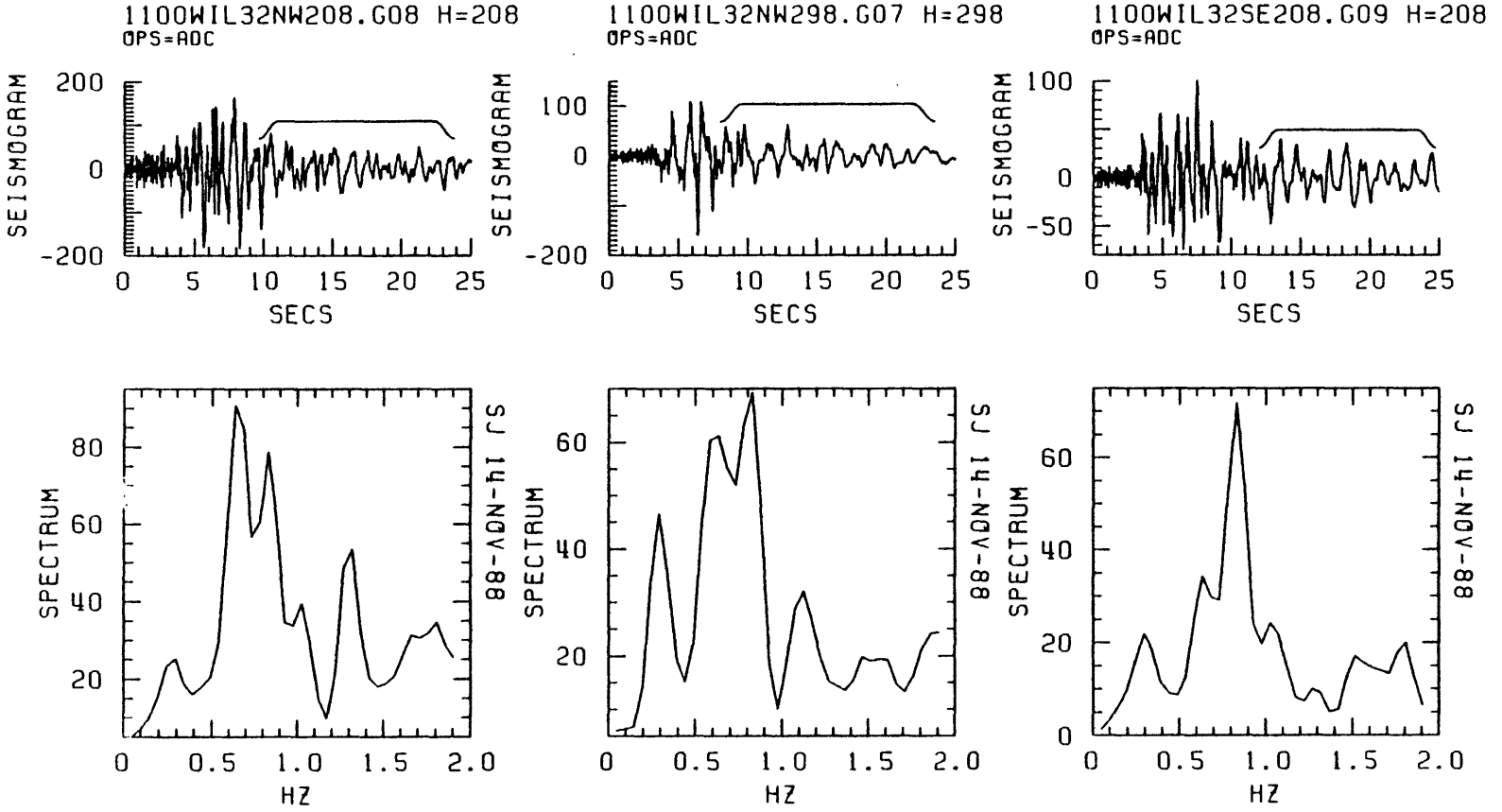

Figure 4.27. Acceleration seismograms with time windows beyond the peaks of the records from the 32nd floor (NW208, NW298 and SE208) locations and corresponding Fourier amplitude spectra.

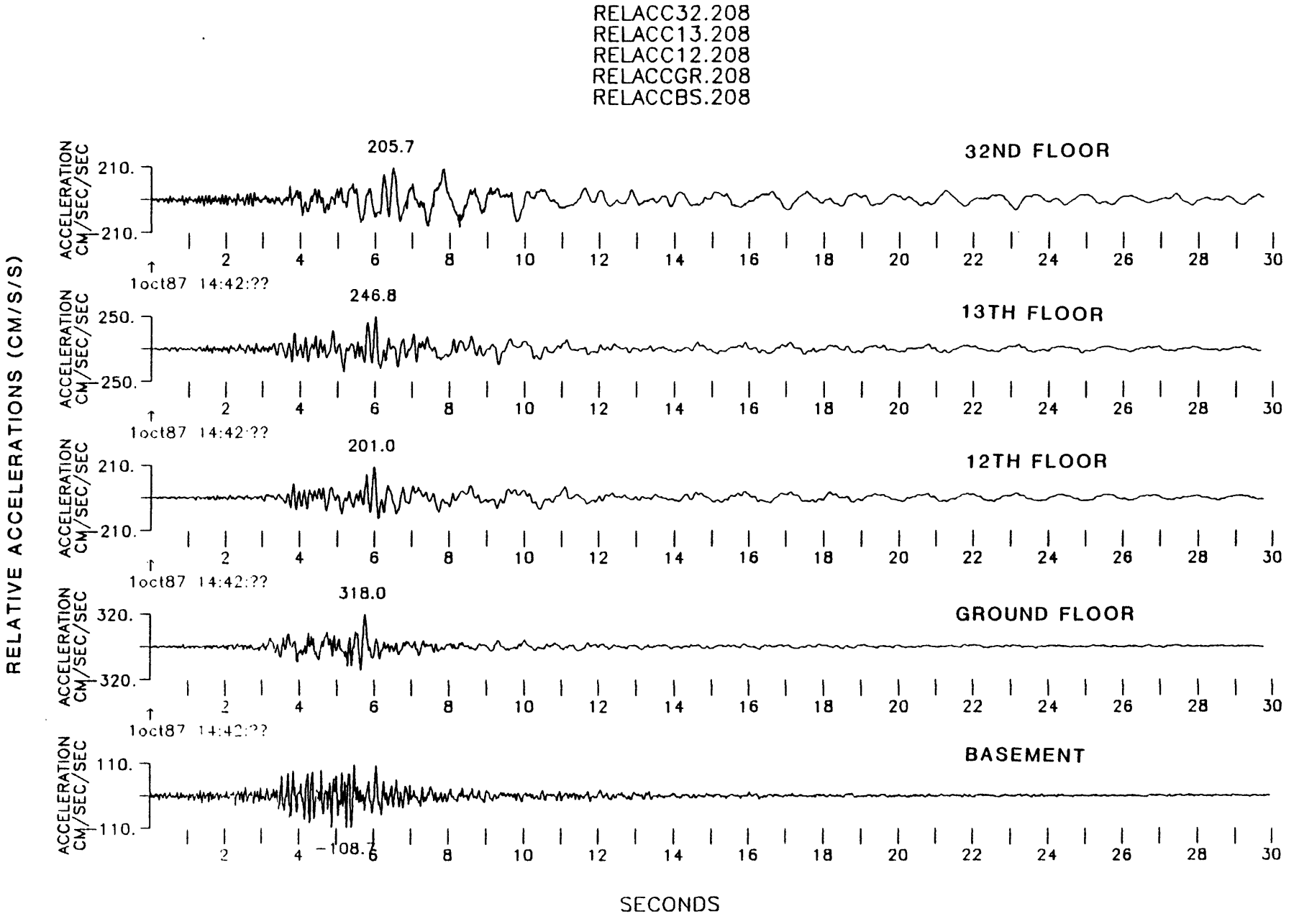

Figure 4.28. Relative accelerations at five instrumented levels of the building.

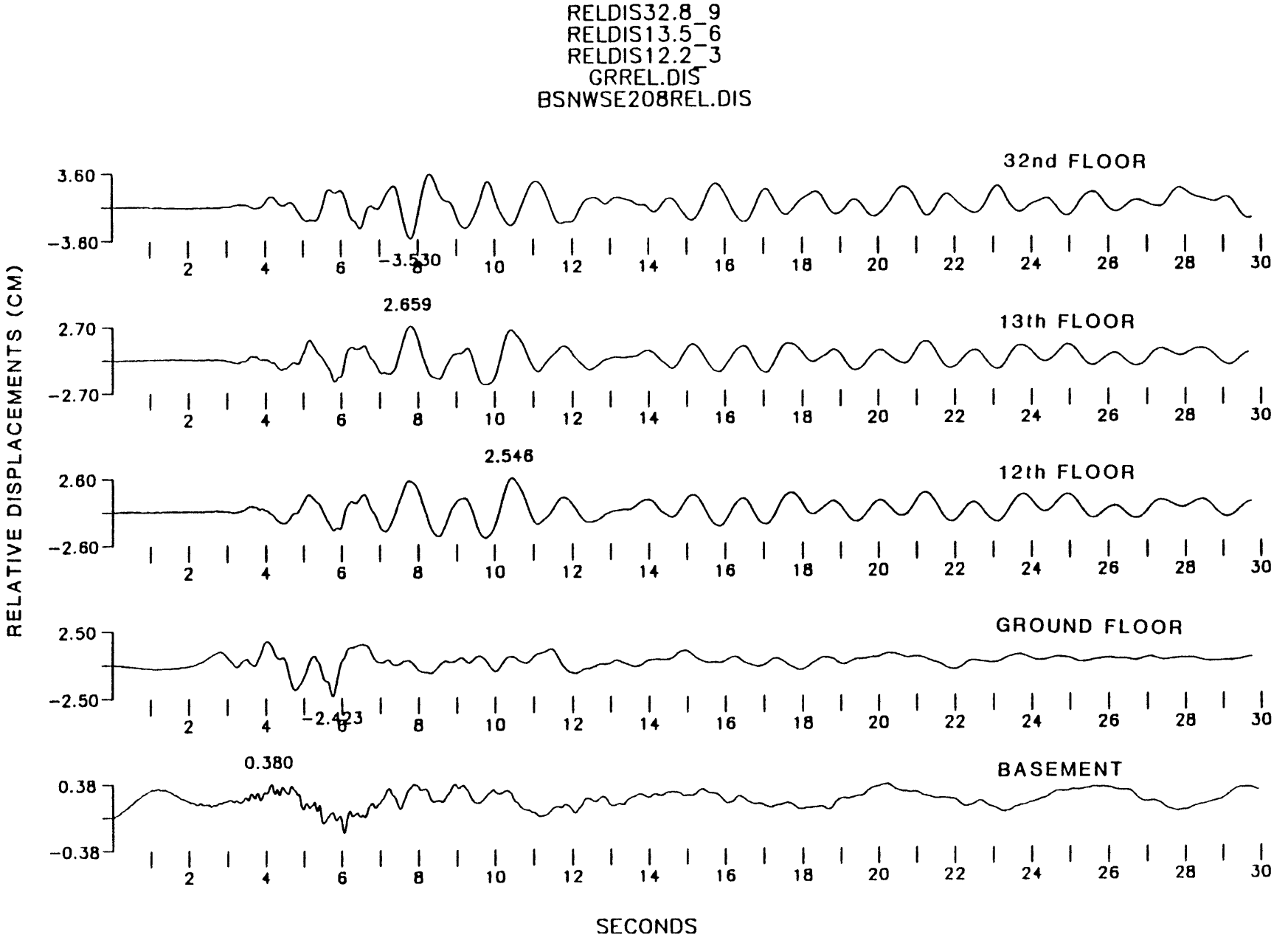

Figure 4.29. Relative displacements at five instrumented levels of the building.

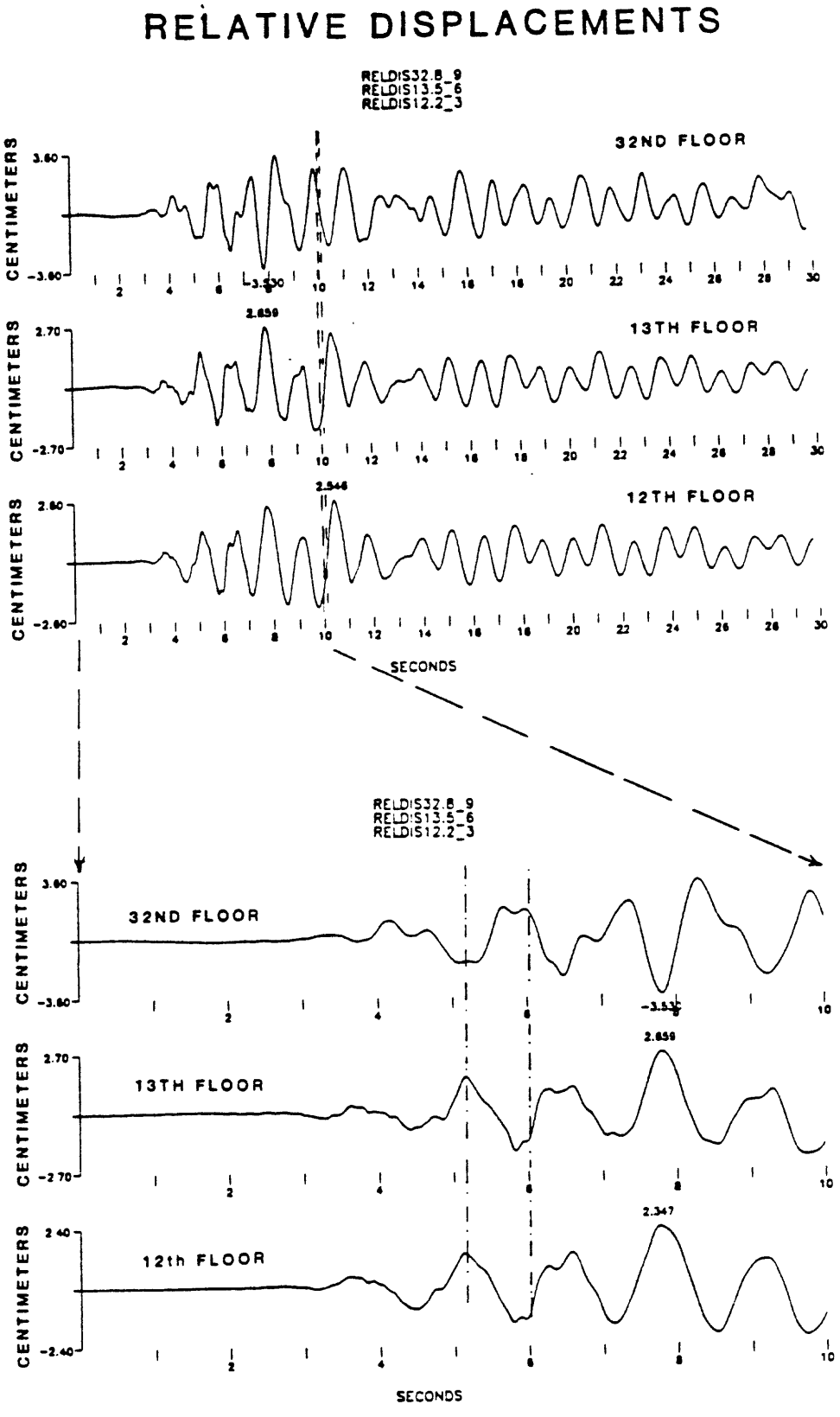

Figure 4.30. Relative displacements showing that the sense of rotation at 32nd floor is different than that of the 13th or 12th floors.

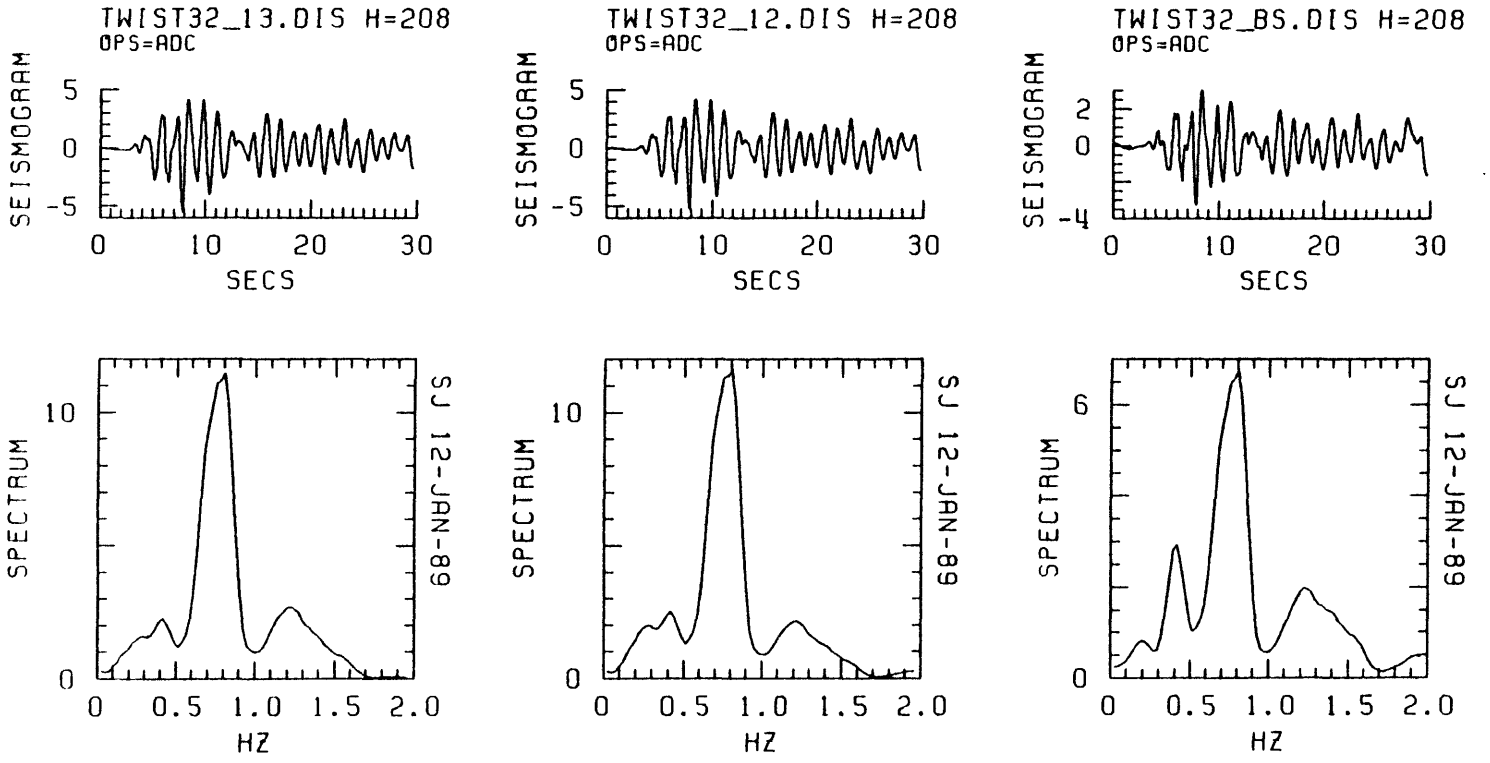

Figure 4.31. Plots representative of angles of twist between 32nd to 13th, 32nd to 12th and 32nd to basement levels and corresponding Fourier amplitude spectra.

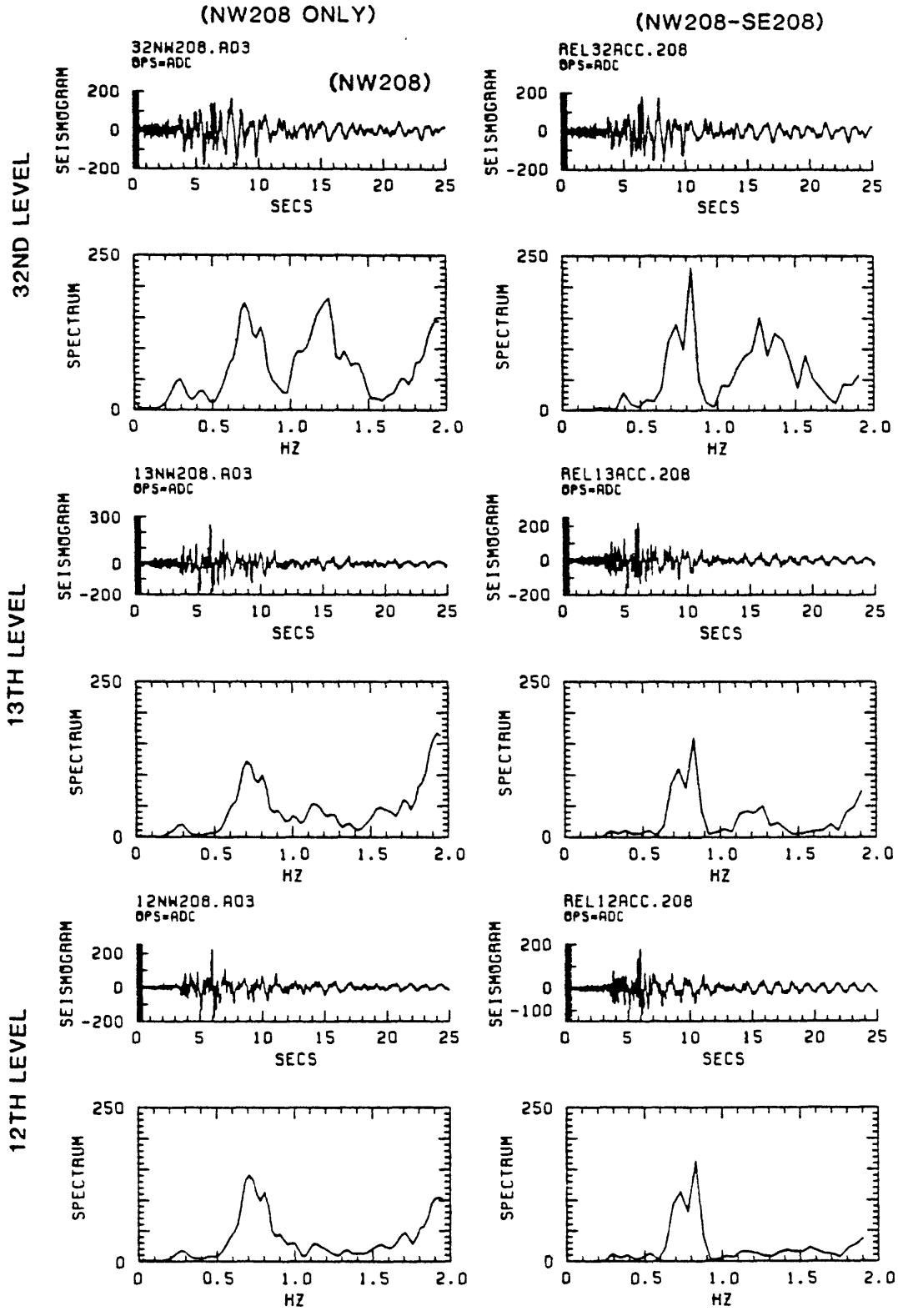

Figure 4.32. NW208 accelerations and NW208–SE208 accelerations at 32nd, 13th and 12th levels. The differences represent torsional accelerations. Corresponding equiscaled Fourier amplitude spectra are shown.

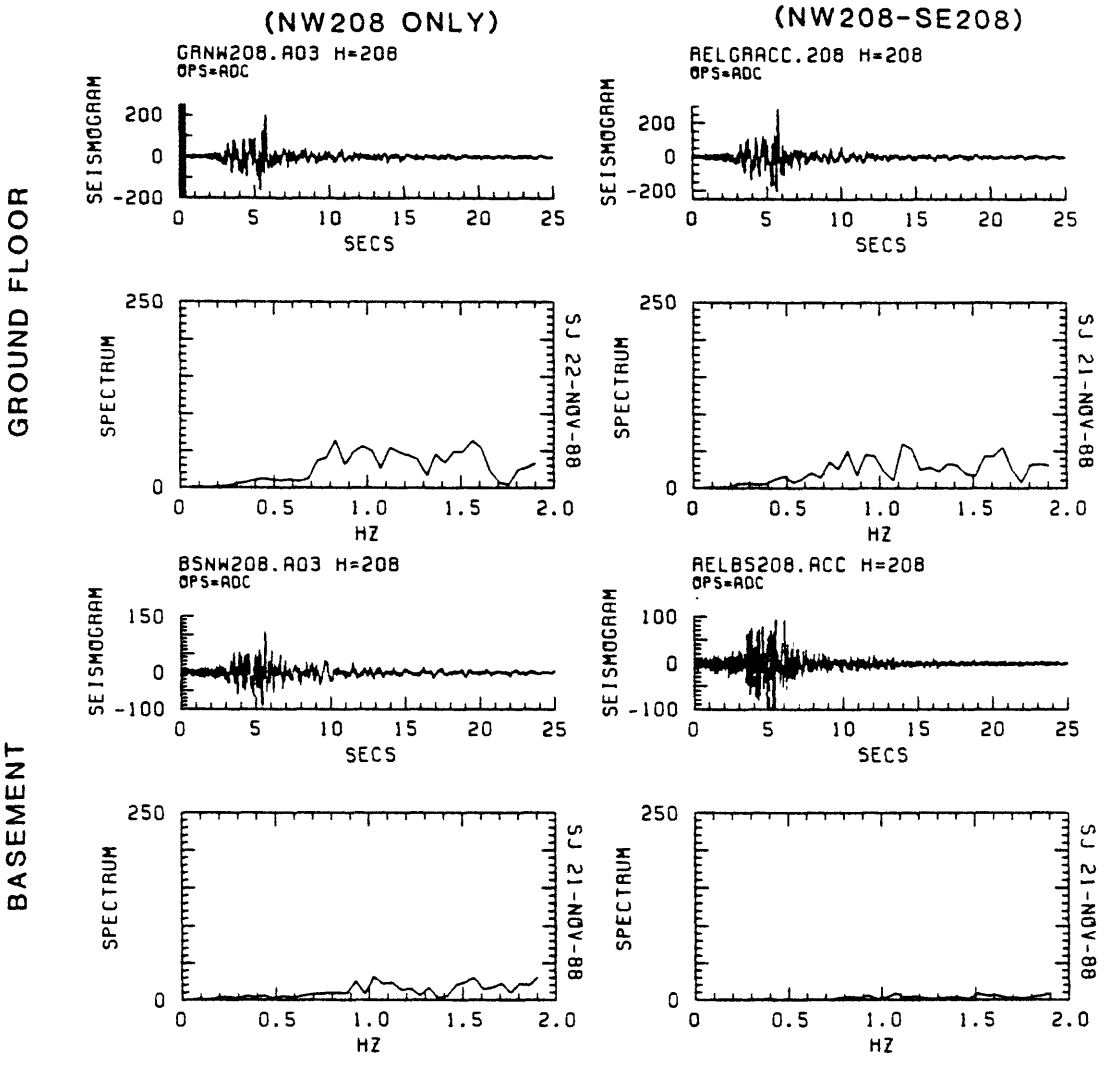

Figure 4.33. NW208 accelerations and NW208–SE208 accelerations at Ground and basement levels. The differences represent torsional accelerations. Corresponding equiscaled Fourier amplitude spectra are shown. The level of torsional input energy at the basement is insignificant.

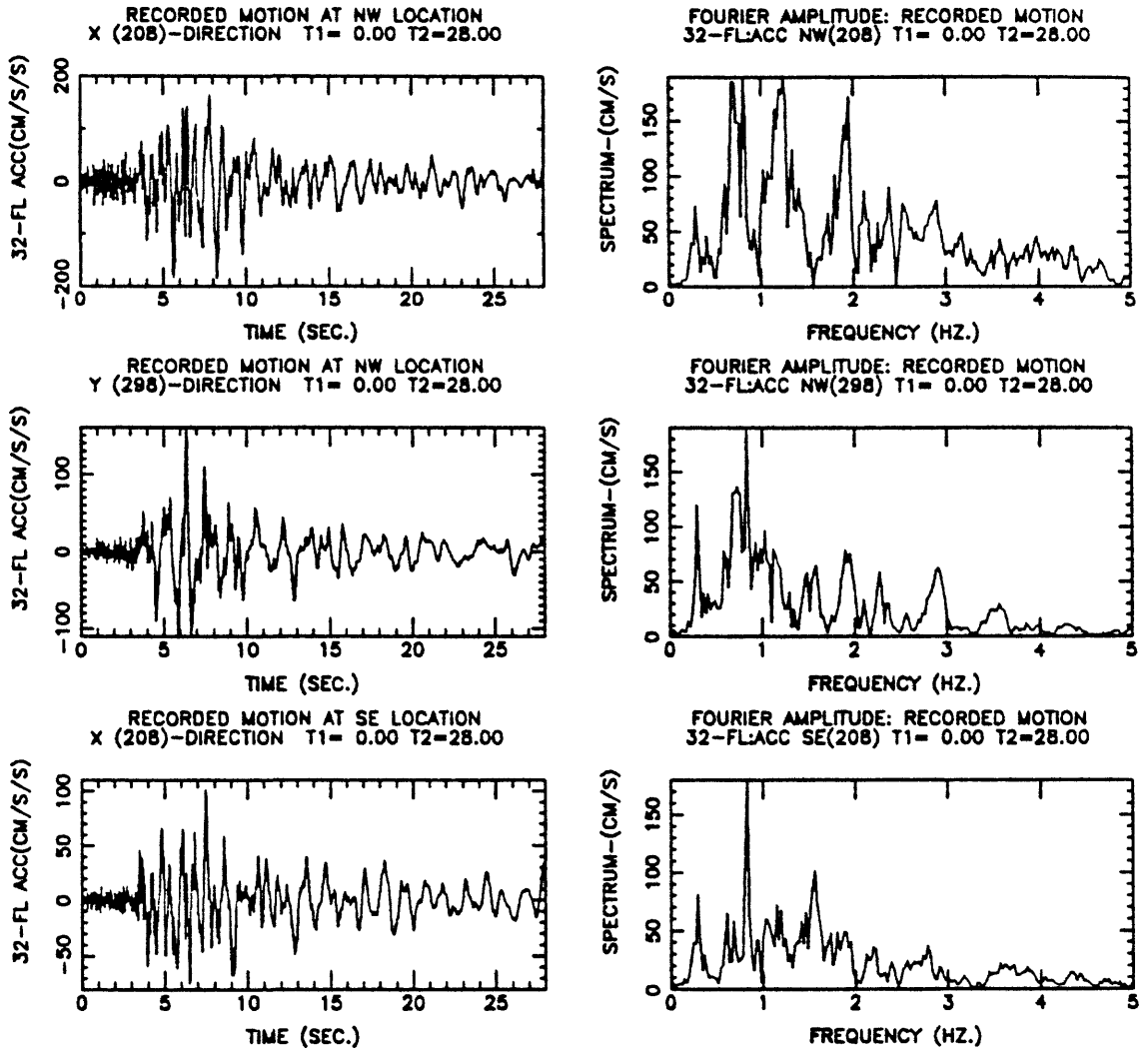

Figure 4.34. Motions recorded at the 32nd floor and corresponding Fourier amplitude spectra.

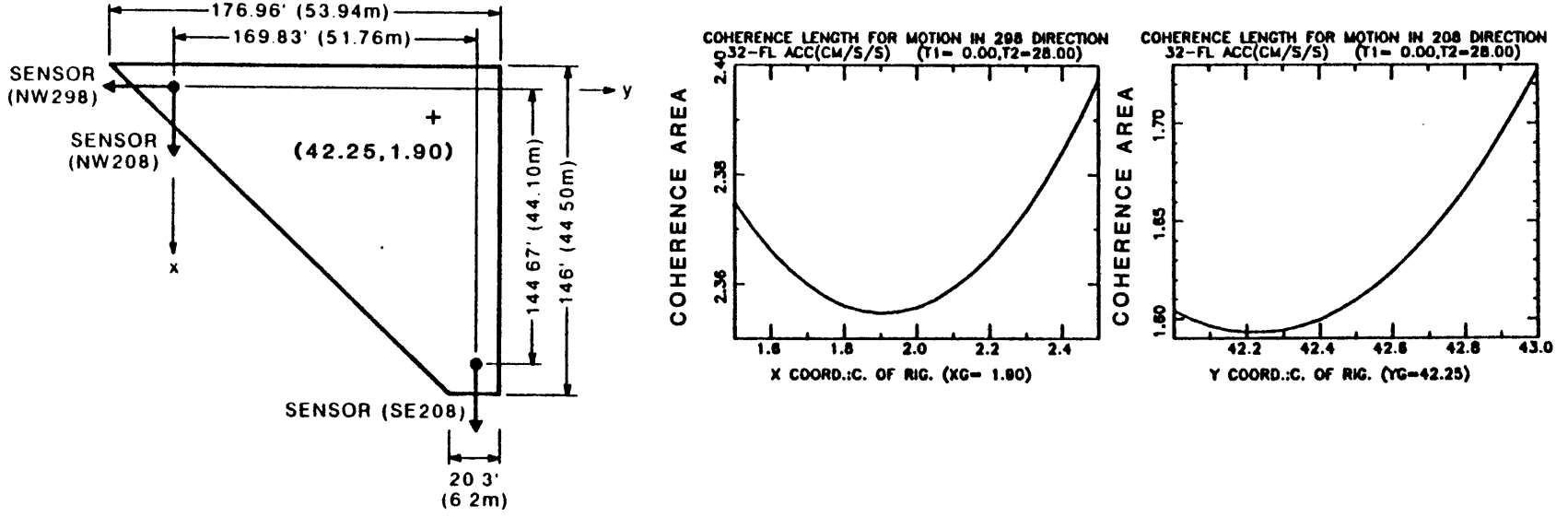

Figure 4.35. Reference axis system and plots of coherence areas versus assumed locations of center of rigidities.

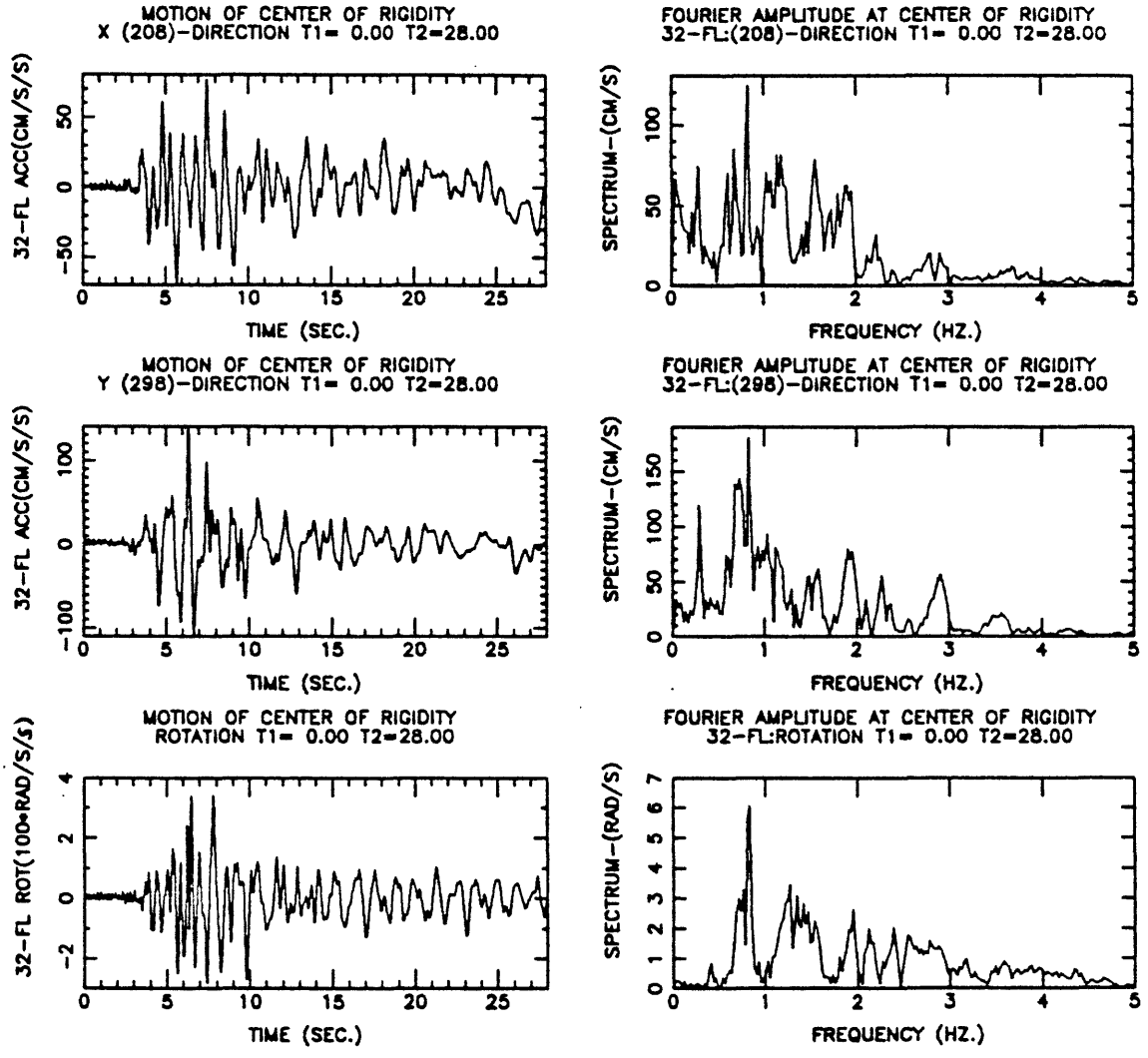

Figure 4.36. Motions (208, 298 linear and rotational) at the estimated center of rigidity of 32nd floor. Corresponding Fourier amplitude spectra are shown on the right.

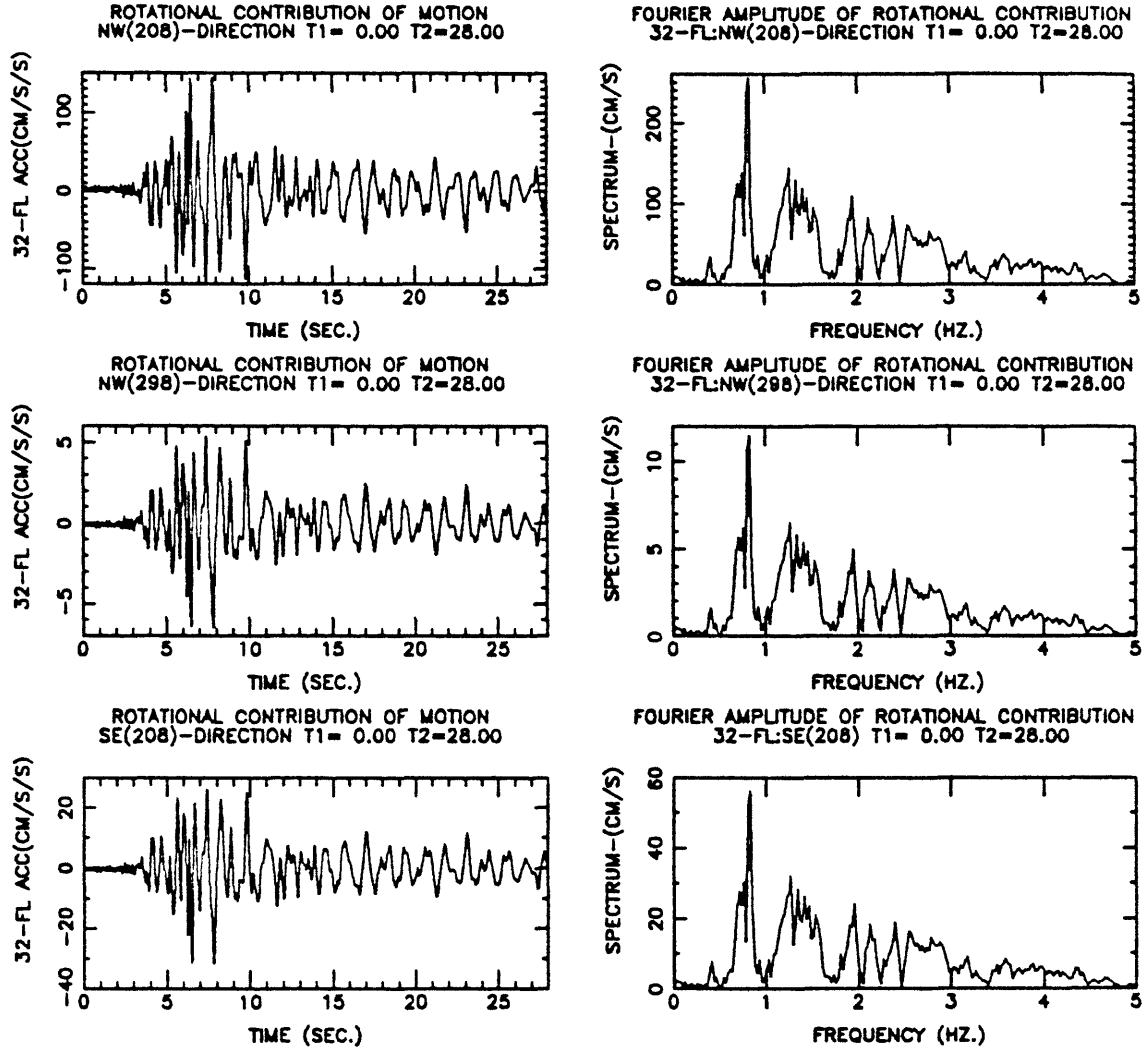

Figure 4.37. Rotational contributions to the motions at 32nd Floor and corresponding Fourier amplitude spectra.

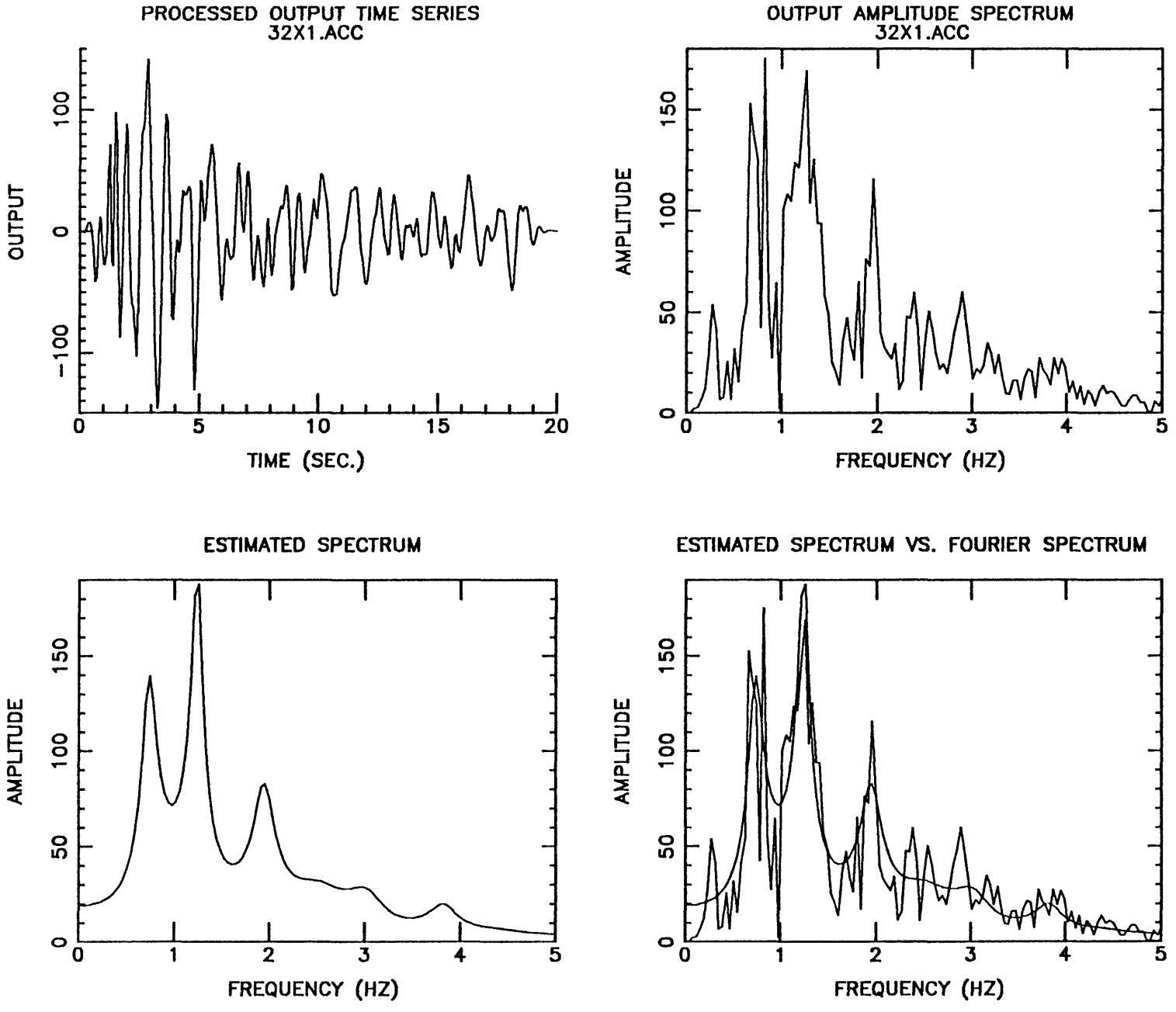

Figure 4.38. Processed NW208 record from the 32nd floor (windowed between 5–25 seconds), corresponding Fourier amplitude spectrum, estimated spectrum by system identification technique and superposition of the two spectra.

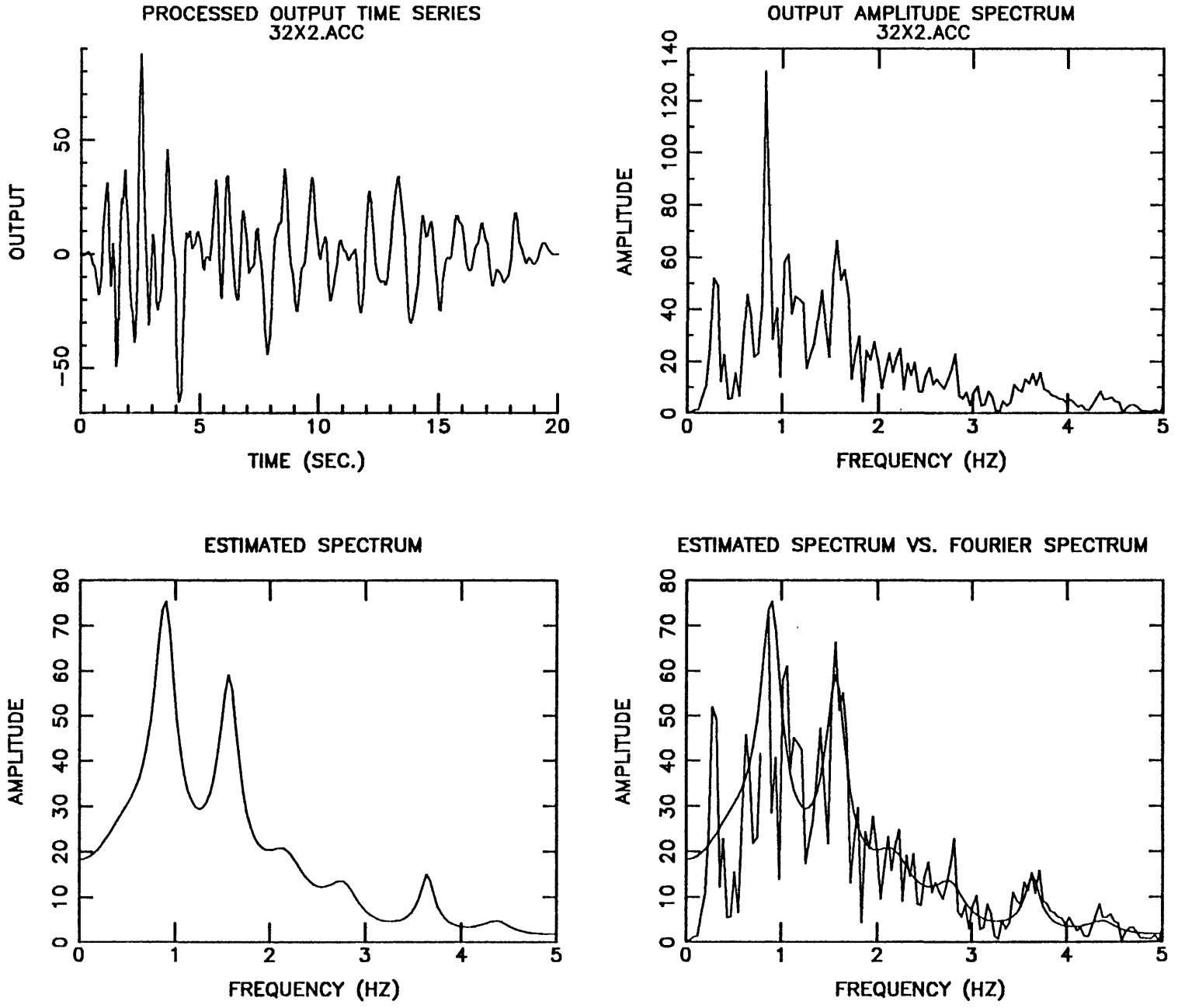

Figure 4.39. Processed SE208 record from the 32nd floor (windowed between 5–25 seconds), corresponding Fourier amplitude spectrum, estimated spectrum by system identification technique and superposition of the two spectra.

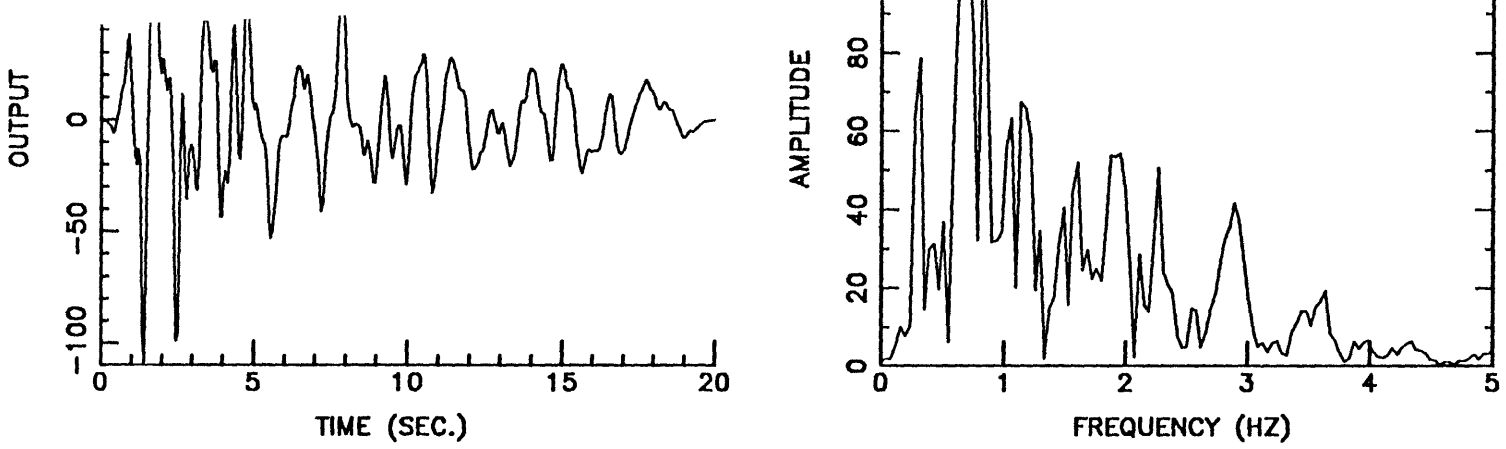

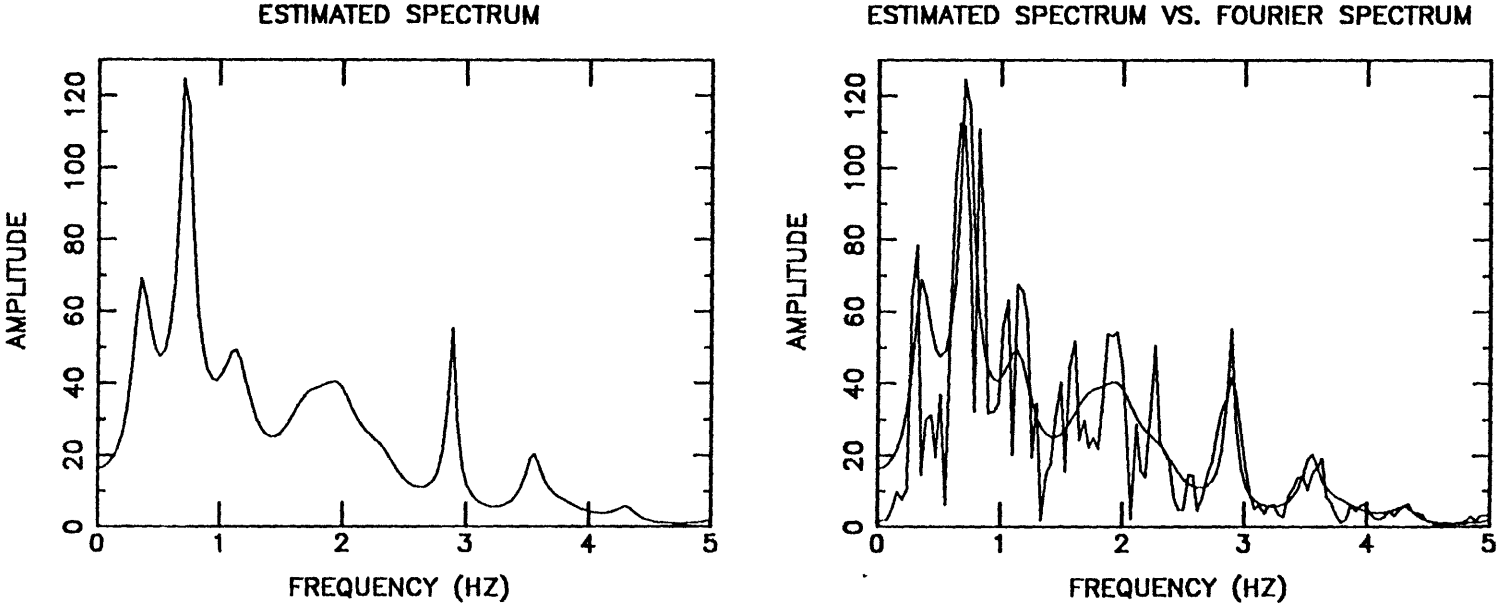

Figure 4.40. Processed NW298 record from the 32nd floor (windowed between 5–25 seconds), corresponding Fourier amplitude spectrum, estimated spectrum by system identification technique and superposition of the two spectra.

Figure 4.43. Processed NW298 record from the 32nd floor (windowed between 5–25 seconds), corresponding Fourier amplitude spectrum, estimated spectrum by system identification technique and superposition of the two spectra.